DRMY1 promotes robust morphogenesis by sustaining the translation of cytokinin signaling inhibitor proteins

Shuyao Kong,[1,2,†] Mingyuan Zhu,[1,2,3,†] M. Regina Scarpin,[4] David Pan,[1,2] Longfei Jia,[5] Ryan E. Martinez,[4] Simon Alamos,[6,7,8] Batthula Vijaya Lakshmi Vadde,[1,2] Hernan G. Garcia,[9,10,11,12,13] Shu-Bing Qian,[5] Jacob O. Brunkard,[4] Adrienne H. K. Roeder [1,2,14,*]

[1] Weill Institute for Cell and Molecular Biology, Cornell University, Ithaca, NY 14853, USA
[2] Section of Plant Biology, School of Integrative Plant Science, Cornell University, Ithaca, NY 14853, USA
[3] Present address: Department of Biology, Duke University, Durham, NC 27708, USA
[4] Laboratory of Genetics, University of Wisconsin, Madison, WI 53706, USA
[5] Division of Nutritional Sciences, Cornell University, Ithaca, NY 14853, USA
[6] Environmental Genomics and Systems Biology Division, Lawrence Berkeley National Laboratory, Berkeley, CA 94720, USA
[7] Feedstocks Division, Joint BioEnergy Institute, Emeryville, CA 94608, USA
[8] Department of Plant and Microbial Biology, University of California at Berkeley, Berkeley, CA 94720, USA
[9] Biophysics Graduate Group, University of California at Berkeley, Berkeley, CA 94720, USA
[10] Department of Physics, University of California at Berkeley, Berkeley, CA 94720, USA
[11] Institute for Quantitative Biosciences-QB3, University of California at Berkeley, Berkeley, CA 94720, USA
[12] Department of Molecular and Cell Biology, University of California at Berkeley, Berkeley, CA 94720, USA
[13] Chan Zuckerberg Biohub-San Francisco, San Francisco, CA 94158, USA
[14] Lead Contact
[†] These authors contributed equally
[*] Correspondence: ahr75@cornell.edu

SUMMARY

Robustness is the invariant development of phenotype despite environmental changes and genetic perturbations. In the Arabidopsis flower bud, four sepals robustly initiate and grow to constant size to enclose and protect the inner floral organs. We previously characterized the mutant *development related myb-like1* (*drmy1*), where 3-5 sepals initiate variably and grow to different sizes, compromising their protective function. The molecular mechanism underlying this loss of robustness was unclear. Here, we show that *drmy1* has reduced TARGET OF RAPAMYCIN (TOR) activity, ribosomal content, and translation. Translation reduction decreases the protein level of ARABIDOPSIS RESPONSE REGULATOR7 (ARR7) and ARABIDOPSIS HISTIDINE PHOSPHOTRANSFER PROTEIN 6 (AHP6), two cytokinin signaling inhibitors that are normally rapidly produced before sepal initiation. The resultant upregulation of cytokinin signaling disrupts robust auxin patterning and sepal initiation. Our work shows that the homeostasis of translation, a ubiquitous cellular process, is crucial for the robust spatiotemporal patterning of organogenesis.

Keywords: Robustness, TOR, translation, cytokinin, auxin, ribosomopathy, Arabidopsis, sepal, morphogenesis

INTRODUCTION

Robustness, or canalization, is the invariant, reproducible development of phenotype, unchanged by environmental fluctuations, genetic perturbations, or gene expression noise[1–4]. Commonly, within an individual, a given number of organs develop at well-defined positions to a robust final size and shape, which is crucial for fitness under stabilizing selection[2]. For example, transplanted eyes, limbs, and kidneys in mammals grow to a mature size similar to their donor, irrespective of the mature size of the same type of organ in the recipient[5–7]. The pairs of wings and halteres in Drosophila develop to robust, precisely coordinated final size and shape, which are required for flight[8–11]. The characteristic cruciform flower in *Brassicaceae* consists of four petals[12], a trait that can contribute to pollinator attraction[13]. The robust positioning of leaves around the shoot apical meristem in plants, or phyllotaxis, ensures optimal light capture[14–16]. While these examples of developmental robustness have been documented for a long time, the underlying molecular mechanisms have just begun to be unveiled.

Earlier studies looking for genes involved in maintaining robustness have found *HEAT SHOCK PROTEIN 90* (*HSP90*). Mutations of *HSP90* cause a diverse array of phenotypic changes in plants, fruit fly, zebrafish, worm, and humans[3,17,18]. Notably, the display and severity of these changes vary between individuals and even between different parts of the same individual, indicating that developmental robustness is disrupted[17,18]. *HSP90* encodes a protein chaperone which has clients from nearly all developmental and signaling pathways[3]. *HSP90*, therefore, is a hub gene that affects numerous other genes within the gene network[2]. Disruption of such a hub gene would therefore trigger many defects in numerous developmental processes. Similarly, genes involved in central cellular processes such as chromatin remodelling[19–21], transcription[19,20], translation[22,23], and protein degradation[24,25] are also hub genes, and they have been found to be important for developmental robustness in various systems including fungi, animals, and plants. How these broad-acting hub genes contribute to the robustness of tissue-specific developmental phenotypes is still largely unclear.

We have developed the *Arabidopsis* sepal as a system to elucidate the mechanisms maintaining robustness in organ size and shape[26–28]. Sepals are the outermost floral organs whose function is to enclose buds and protect the developing inner organs, i.e. petals, stamens, and carpels, before the flower blooms. To fulfill this protective function, each flower robustly develops four sepals of equal length, allowing them to close at the top (Figure 1A, top left); these four sepals are of equal width and positioned 90° from each other, leaving no gap on the sides (Figure 1A, middle left). This robustness in sepal size and shape stems from the robust initiation of the four sepal primordia from the floral meristem with precisely coordinated spatiotemporal patterns[27] (Figure 1A, bottom left). The initiated sepal primordia attain robust final size and shape by spatiotemporal averaging of cellular growth variability during sepal elongation, and synchronous progression of a whole-flower growth termination signal from tip to base[26]. In addition, noise in gene expression must be kept low to ensure sepal size robustness[29]. We previously characterized a mutant in *DEVELOPMENT RELATED MYB-LIKE 1* (*DRMY1*) that

87 develops flowers where the inner organs are exposed due to gaps between sepals[27]. The gaps
88 are caused by variability in sepal development. Specifically, some sepals are shorter than others,
89 leaving gaps on the top (Figure 1A, top right); the arrangement of sepals around the flower deviate
90 from the canonical form such that parts of the flower are not covered by a sepal, leaving gaps on
91 the side (Figure 1A, middle right). This variability in the size, number, and position of the mature
92 sepal originates from the earliest stages of floral development where the spatiotemporal pattern
93 of sepal initiation becomes variable (Figure 1A, bottom right). Variability in sepal initiation, in turn,
94 is driven by the loss of robust patterning of auxin and cytokinin[27], two plant hormones critical for
95 morphogenesis[30–32], in the floral meristem before sepal initiation. However, the molecular
96 mechanism through which DRMY1 maintains robust hormone patterning is still unknown.
97
98 In this study, we elucidate a mechanism through which DRMY1 maintains robust hormone
99 patterning and thus robust sepal initiation. Specifically, we find that DRMY1 maintains proper
100 activity of TARGET OF RAPAMYCIN (TOR), a crucial regulator of ribosome level and mRNA
101 translation[33,34], and thereby sustains translation *in vivo*. When *DRMY1* is mutated, the levels of
102 ARABIDOPSIS RESPONSE REGULATOR7 (ARR7) and ARABIDOPSIS HISTIDINE
103 PHOSPHOTRANSFER PROTEIN 6 (AHP6), two cytokinin inhibitor proteins that are rapidly
104 synthesized during hormone patterning prior to sepal initiation, are drastically reduced in the floral
105 meristem. Consequently, cytokinin signaling uniformly increases in the meristem periphery,
106 causing variability in auxin patterning and sepal initiation. We further propose that the increase in
107 cytokinin signaling may be a survival mechanism to alleviate the translation rate reduction when
108 ribosomal content is limited. In summary, our work shows that the hub processes of TOR signaling
109 and translation, which occur in every cell, have very tissue-specific roles in maintaining robust
110 organogenesis by sustaining the rapid synthesis of hormone signaling proteins.
111
112
113 **RESULTS**
114
115 **The *drmy1* mutant has reduced TOR activity, ribosome content, and translation rate**
116
117 *DRMY1* encodes a MYB/SANT domain protein which may exert transcriptional
118 regulation[27]. To look for differentially expressed genes in *drmy1* which may be candidates
119 underlying variable sepal initiation, we performed RNA-sequencing (RNA-seq) in *drmy1* and wild
120 type (WT) of *apetala1* (*ap1) cauliflower (cal) AP1-GR* background[35,36]. The *ap1 cal AP1-GR*
121 inflorescence produces numerous tightly packed ball-shaped meristems, which, upon induction,
122 synchronously initiate sepal primordia, allowing us to collect large quantities of floral meristems
123 with sepal primordia initiating (Stage 3)[37] (Figure S1A). We crossed *drmy1* into *ap1 cal AP1-GR*
124 and performed RNA-seq on induced inflorescences of WT and *drmy1* in this background. We
125 detected transcripts from a total of 21,496 genes, of which 1,042 (4.8%) were differentially
126 expressed in *drmy1* (Figure S1B; Supplemental Dataset 1). We found that the 443 genes
127 downregulated at the transcript level in *drmy1* were most enriched in the gene ontology (GO) term
128 “Translation”, a fundamental and ubiquitous cellular process that converts genetic information

129 from transcript to protein. Within this term, genes encoding ribosomal components were most
130 downregulated (Figure S1C). The 443 downregulated genes were also enriched in several other
131 ribosome-related GO terms (Figure 1B). We therefore hypothesized that ribosomal abundance
132 and translation are affected in *drmy1*, potentially altering the accumulation of proteins critical to
133 developmental robustness.
134
135 To determine whether and how ribosomal abundance and translation are affected in
136 *drmy1*, we performed polysome profiling in induced inflorescences of WT and *drmy1* in *ap1 cal*
137 *AP1-GR* background. Compared to WT, all peaks corresponding to 40S, 60S, monosomes, and
138 polysomes are drastically reduced in *drmy1* (Figure 1C; Supplemental Dataset 2). To see whether
139 this reduction in ribosomal content affected *de novo* protein synthesis rate *in vivo*, we performed
140 puromycin labeling. Samples were incubated with puromycin, an amino acid-tRNA analog that is
141 incorporated into nascent polypeptide chains and can be detected using an anti-puromycin
142 antibody to infer global translation rate[38,39]. In both young seedlings and induced *ap1 cal AP1-GR*
143 inflorescences, we found that the puromycin level detected in *drmy1* mutant samples was much
144 reduced compared to WT (Figure 1D), indicating a reduction in global translation rate. We
145 hypothesized that reduced global translation rate should likely result in globally decreased protein
146 levels. For this, we looked at a ubiquitously expressed membrane marker *UBQ10::mCherry-*
147 *RCI2A*, and found that it had a small (~25%) but significant decrease in fluorescence intensity in
148 the inflorescence meristem and young floral buds of *drmy1* compared with WT (Figure S1D, E).
149 We also measured its fluorescence intensity in the ribosomal mutant *ul4y* (*rpl4d*)[40] and we found
150 that the decrease in fluorescence intensity in *drmy1* is even greater than in *ul4y* (Figure S1F, G).
151 Overall, these results show that ribosomal content and translation are indeed reduced in the
152 *drmy1* mutant.
153
154 To test how the global repression of translation in *drmy1* impacts its proteome, we
155 extracted total soluble protein from induced inflorescences of WT and *drmy1* in *ap1 cal AP-GR*
156 background and performed mass spectrometry. We identified a total of 5,077 proteins, of which
157 548 (10.8%) were differentially accumulated in *drmy1* (Figure S1B; Supplemental Dataset 1).
158 These differentially accumulated proteins were enriched in GO terms related to translation and
159 ribosomes (Figure 1E). Despite the overall reduction in ribosomes (Figure 1C), relative to other
160 proteins, ribosomal components are more abundant in *drmy1* (Figure S1H; Supplemental Dataset
161 1). This is not true for all proteins involved in translation; poly-A binding proteins and tRNA
162 synthetases, for example, are relatively less abundant in *drmy1* than in WT. Moreover, the 26S
163 proteasome responsible for targeted protein degradation is much more abundant in *drmy1* than
164 in WT (Supplemental Dataset 1). In concert, these results demonstrate that the machinery
165 responsible for maintaining protein homeostasis is substantially dysregulated in *drmy1*.
166
167 A key signaling pathway that regulates protein homeostasis is TARGET OF RAPAMYCIN
168 (TOR)[41,42]. TOR is a hub that integrates information from light, sugars, nutrient availability, etc.,
169 to promote growth-related processes, including ribosome biogenesis and translation, and to
170 repress catabolic processes, including protein degradation by autophagy and the

171 proteasome[33,34,43–45]. TOR directly regulates the translation of specific mRNAs by promoting the
172 phosphorylation of proteins, including LARP1, eIF3h, RISP, eS6, and 4EBPs, that impact
173 translation initiation, reinitiation, or elongation of mRNAs with specific features, such as 5'TOP
174 motifs or short upstream open reading frames (uORFs) in the 5' leaders of mRNAs[34,42,46–52]. TOR
175 also indirectly increases overall protein synthesis rates by globally increasing ribosome levels.
176 We therefore hypothesize that the overall decrease in ribosomal content and protein synthesis in
177 *drmy1* may reflect altered TOR signaling. To test for signatures of transcriptomic changes that
178 have been well defined in seedlings under TOR inhibition[34,53,54], we performed RNA-seq on
179 seedlings of WT, *drmy1*, WT treated with AZD-8055 (a potent TOR inhibitor), and mock-treated
180 WT (Supplemental Dataset 3). We found that the *drmy1* mutation causes transcriptomic changes
181 similar to TOR inhibition (Figure 1F). A significant portion of genes differentially expressed under
182 TOR inhibition vs. mock were also differentially expressed in *drmy1* vs. WT (466/2044 = 22.8%;
183 hypergeometric test, $p = 4.7 \times 10^{-108}$). Not only were these 466 genes differentially expressed in
184 both situations, but also most of them were coherently downregulated or upregulated (439/466 =
185 94.2%, Chi-square test, $p < 2.2 \times 10^{-16}$; Figure 1G, S1I). Genes coherently downregulated in both
186 situations were enriched in GO terms related to translation and ribosomes, and, most strikingly,
187 a quarter of them were under the GO term "translation" (Figure 1F, S1J). These similar
188 transcriptomic changes support our hypothesis that TOR activity is reduced in *drmy1*. To further
189 test this hypothesis, we measured TOR activity in WT and *drmy1* by assaying the phosphorylation
190 of its direct substrate, RIBOSOMAL PROTEIN eS6 KINASE (S6K)[55,56]. While the total protein
191 level of S6K did not change in *drmy1*, we found that S6K phosphorylation drastically decreased,
192 demonstrating reduced TOR activity (Figure 1H, I). Overall, these results are consistent with the
193 idea that *drmy1* has reduced TOR activity—a main pathway controlling ribosomal abundance and
194 translation—which causes reduced ribosomal content and global translation rate.
195
196 **Defects in TOR activity, ribosome, and translation disrupt robust sepal initiation**
197
198 We next asked whether defects in TOR activity, ribosome, or translation have any effects
199 on robust sepal initiation like the *drmy1* mutation does (Figure 2A, 2B; also see Zhu et al.[27]). In a
200 WT bud, initiation is robust in that four sepal primordia of similar size form evenly spaced around
201 the periphery of the floral meristem (Figure 2A, 2H). Angles between them vary little, i.e., they are
202 all at around 90° angles from each other (Figure 2I, 2J). By contrast, in *drmy1* buds, three to five
203 sepal primordia initiate and grow to different sizes (Figure 2B, 2H; also see Zhu et al.[27]). Sepal
204 primordia in *drmy1* buds are generally unevenly spaced, and angles between them have a high
205 coefficient of variation (CV) (Figure 2I, 2J). To determine whether defects in ribosomes can cause
206 the same sepal initiation defects, we imaged three ribosomal mutants, *ul4z* (*rpl4a*), *ul4y*, and *ul18z*
207 (*rpl5a*)[40], each mutated in a gene encoding a ribosomal component that is also downregulated in
208 *drmy1* at the transcript level (Figure S1C). The *ul4z* mutant bud shows reduced size of the inner
209 sepal primordia relative to the outer sepal primordia (Figure 2C), and slightly more variable spatial
210 distribution of sepal primordia (Figure 2J), although it always develops four sepal primordia
211 (Figure 2H). This is a weaker phenotype than *drmy1* but has similar characteristics. The *ul4y* and
212 *ul18z* mutants show great variability in the number and position of sepal primordia (Figure 2D,

2E, 2H, 2J), more similar to *drmy1*. We also crossed these ribosomal mutants with *drmy1* to study sepal variability in the double mutants (Figure S2A-H). In *drmy1 ul4z*, *drmy1 ul4y*, and *drmy1 ul18z/+*, on average, sepal initiation was as variable as in the *drmy1* single mutant (Figure S2I, S2J). However, there were buds with no outgrowth in the adaxial or lateral regions of the bud periphery (Figure S2B, S2E, S2G), buds with six sepal primordia (Figure S2C, S2F, S2H), and buds with two outer sepal primordia (Figure S2D, S2H), which were not seen in the *drmy1* single mutant. Note that we were unable to characterize the homozygous *drmy1 ul18z* double mutant because they were embryo-lethal (Figure S2K), further supporting the idea that ribosomal mutations enhance the phenotypic defects in *drmy1*.

We then imaged mutants with reduced TOR activity to determine whether sepal initiation is also less robust. *lst8-1-1* is a T-DNA insertional mutant of the TOR complex component LST8-1[57] and is weakly hypomorphic in TOR activity. We found that *lst8-1-1* shows variable sepal initiation in a small proportion of buds (4/41, 9.8%) (Figure 2F, 2H, 2J). The *spaghetti-1* mutant defective in TOR complex 1 (TORC1) assembly[58] showed a level of variability comparable to the *drmy1* mutant and the ribosomal mutants *ul4y* and *ul18z* (Figure 2G, 2H, 2J). Mutants with more severe disruption of TOR activity are embryo lethal and could not be analyzed[58,59]. These results show that reduction in TOR activity can cause variability in sepal initiation, similar to *drmy1*.

To corroborate these findings, we directly inhibited translation by *in vitro* culture of dissected WT inflorescences on 2 μM cycloheximide (CHX, a chemical inhibitor of translation) for 9-10 days. This is a low concentration that does not completely block translation, as inflorescences were still alive after 10 days in this condition. Compared with mock, CHX-treated inflorescences develop buds that have 2 to 6 sepal primordia of variable sizes that are unevenly spaced around the bud periphery (Figure 2K, 2M, 2N). These phenotypes are stronger than *drmy1*. Similarly, we directly inhibited TOR activity by application of 2 nmol Torin2 to the growing shoot apex twice a day for 15 days, and we observed variable sepal initiation (Figure 2L, 2M, 2N). Overall, these data show that inhibition of TOR activity and translation can disrupt the robustness of sepal initiation, in terms of sepal primordium number, position, and size.

We previously showed that *drmy1* buds develop sepals of different sizes because of increased differences in the initiation timing of sepals within the same bud. The late-initiating primordia remain smaller throughout development. They end up as smaller sepals relative to those that initiated earlier, leaving gaps that expose the developing inner floral organs[27]. Moreover, different buds have different temporal patterns of sepal initiation, contributing to between-bud variability of sepal phenotype[27]. We asked whether TOR or ribosomal defects similarly disrupt the relative timing of sepal initiation, within-bud and between-bud. We live imaged WT and *ul4y* every six hours during sepal initiation and quantified the amount of time the bud takes to initiate the inner and lateral sepals after it initiates the outer sepal. In WT, after the initiation of the outer sepal, most buds initiate the inner sepal within 6 hours and the lateral sepals within 12 hours (Figure 3A, 3C; also see Zhu et al.[27]). In *ul4y*, the time differences between outer and inner sepal initiation and between outer and lateral sepal initiation are longer (Figure 3B,

255 mean in Figure 3C). Moreover, these time differences are more variable across buds, indicating
256 a loss of robustness in organ initiation timing (SD in Figure 3C). Similarly, we compared the sepal
257 initiation timing in Torin2 vs mock-treated WT buds. While in most mock-treated buds, the inner
258 and lateral sepals initiate within 12 hours after the outer sepal (Figure 3D, 3F), in Torin2-treated
259 buds, sepals within the same bud initiates at vastly different times (Figure 3E, mean in Figure 3F),
260 and the temporal pattern of sepal initiation is more variable across buds than mock (SD in Figure
261 3F). These results show that TOR and ribosomal defects can disrupt the precisely orchestrated
262 initiation timing of sepal primordia.
263
264 Does the variability in initiation timing cause variable sizes and gaps in mature sepals, as
265 in *drmy1* (Figure S3A, B, G, H; also see Zhu et al. [27])? We imaged the mature sepals of the
266 ribosomal mutants *ul4z*, *ul4y*, *ul18z*, as well as the TOR component mutant *lst8-1-1*. Surprisingly,
267 unlike *drmy1*, the sepals in *ul4z*, *ul4y*, *ul18z* enclose the inner floral organs perfectly, leaving no
268 gaps, regardless of sepal number (Figure S3C-E). Small gaps still exist in buds of *lst8-1-1*,
269 although sepal size differences appear greatly reduced (Figure S3F). Further dissection shows
270 that in these mutants, sepals within the same flower are of similar sizes, although sepals from
271 different flowers can be of vastly different sizes, most conspicuously for *lst8-1-1* (Figure S3I-N).
272 This is unlike *drmy1*, where sepal size variability is equally high comparing sepals within the same
273 flower or from different flowers (Figure S3H, S3M-N). Upon closer examination, while sepals
274 initiating late in *drmy1* buds remain small, leaving a gap in the sepal whorl (Figure S3O-P), those
275 in *ul4y* were able to catch up with the other sepals and close the gap (Figure S3Q). Our results
276 suggest that there exists a size-coordinating mechanism independent of TOR or ribosomal
277 functions that allows sepals within the same bud to reach the same mature length, and that this
278 mechanism is disrupted in *drmy1*. Such a mechanism requires further investigation in the future.
279
280 **Inhibition of TOR activity and translation increase cytokinin signaling and disrupts the**
281 **robust spatial pattern of auxin and cytokinin signaling**
282
283 Auxin and cytokinin are two important plant hormones critical to many aspects of plant
284 development[30–32], and there is accumulating evidence that they act synergistically in the shoot
285 apical meristem to promote lateral organ initiation[16,60,61]. We previously showed that, in a WT floral
286 meristem prior to sepal initiation, auxin and cytokinin signaling are concentrated at the four
287 incipient primordia, which is required for robust sepal initiation from these regions (Figure 4A,
288 S4A; Zhu et al.[27]). In the *drmy1* mutant, cytokinin signaling becomes stronger and diffuse around
289 the bud periphery (Figure 4A-B). Auxin signaling also becomes more diffuse, forming irregular
290 auxin maxima that are less focused than those in WT, except at the incipient outer sepal where it
291 remains robust (Figure 4A, S4B; Zhu et al.[27]). These changes in hormone signaling correlate with
292 variable sepal initiation (Figure S4B)[27]. We wondered whether ribosomal mutations have similar
293 effects on auxin and cytokinin signaling. To this end, we imaged the auxin signaling reporter
294 *DR5::3xVENUS-N7* and the cytokinin signaling reporter *TCS::GFP* in floral meristems of the
295 ribosomal mutant *ul4y*. Both reporters lose their robust spatial pattern except in the incipient outer
296 sepal (Figure 4A, S4C). The hormone signaling patterns were quantified by circular histogram

297 analysis (see Methods for details). For each of DR5 and TCS, WT buds showed four clear peaks
298 ~90 degrees apart from each other, with very little signal in between, whereas in *drmy1* and *ul4y*,
299 peaks were barely seen except at the incipient outer sepal (at 45 degrees), and there was greater
300 noise and variation all around the bud (Figure 4C-D). Diffuse bands of auxin signaling that typically
301 occurs in the adaxial or lateral periphery of *drmy1* and *ul4y* buds (Figure S4B and S4C, brackets)
302 can later resolve into several distinct auxin maxima of various intensity and at various positions,
303 correlated with the initiation of sepal primordia of various sizes at these same positions (Figure
304 S4B and S4C, red arrowheads).
305
306 We also tested whether drug treatments that inhibit TOR activity or translation can disrupt
307 the robust hormone patterning. Buds treated *in vitro* with the translation inhibitor CHX (2 μM) for
308 3 days showed a 50% increase in cytokinin signaling, and both auxin and cytokinin signaling
309 became diffuse around the bud periphery (Figure 4E-H). By day 6, cytokinin signaling was still
310 diffuse all around, and increased to more than two-fold relative to mock (Figure 4I, 4J, 4L). Auxin
311 signaling formed maxima of variable number at variable positions (Figure 4I arrowheads, 4K),
312 correlated with the variable initiation of sepal outgrowth at these positions (Figure S4D-E). Similar
313 changes occurred in buds treated *in vitro* with the TOR inhibitor AZD-8055 (2 μM) for 6 days
314 (Figure 4I-L). For both CHX and AZD-8055, the disruptions of hormone signaling are similar to
315 *drmy1*. *In vivo* treatment using another TOR inhibitor Torin2 for 15 days increased cytokinin
316 signaling by 70%, although it did not make auxin and cytokinin signaling more diffuse (Figure
317 S4F-I). Overall, these results show that defects in TOR activity and translation increase cytokinin
318 signaling, and disrupt the precise spatial patterning of cytokinin and auxin signaling required for
319 robust sepal initiation.
320
321 **An increase in cytokinin signaling is necessary and sufficient for variable auxin signaling**
322 **and sepal initiation under translation inhibition**
323
324 Auxin is a critical hormone in organogenesis[62,63]. As shown above, variable patterning of
325 auxin signaling correlates with variable sepal initiation during inhibition of TOR activity and
326 translation. We wondered what caused auxin to lose its robust patterning under such conditions.
327 It was previously reported that the ribosomal mutants *ul4y*, *ul18z*, and *el24y* have reduced protein
328 levels of AUXIN RESPONSE FACTOR (ARF) 3, 5, and 7[64–66], key transcription factors that
329 mediate the auxin signaling response[67]. The transcripts of these ARFs contain upstream open
330 reading frames (uORFs), requiring translation reinitiation to translate their main open reading
331 frames[68,69], a process defective in the ribosomal mutants *ul4y*, *ul18z*, and *el24y*[64–66]. We therefore
332 hypothesized that *drmy1* loses robust auxin signaling pattern because of reduced translation of
333 uORF-containing transcripts, including those of certain ARFs. To begin, we utilized our
334 transcriptomics and proteomics data, and considered that the protein-transcript ratio of a gene
335 should reflect its level of translation, among other factors such as protein stability. Therefore,
336 following our hypothesis, genes containing uORFs should, in general, have a lower protein-
337 transcript ratio in *drmy1* than in WT. We calculated the difference of this ratio between *drmy1* and
338 WT for all 5,086 gene-protein pairs in our inflorescence dataset, and compared the ratio against

339 the number of uORFs in each transcript (Figure S5A; uORF data from von Arnim et al.[69]). We
340 found a small but significant decrease in the protein-transcript ratio in *drmy1* for the 724 genes
341 containing at least 2 uORFs in their transcripts, supporting the hypothesis that *drmy1* has reduced
342 translation reinitiation for uORF-containing transcripts, just like *ul4y*, *ul18z*, and *el24y*[64–66]. Then,
343 we examined whether the translation reinitiation of uORF-containing ARFs are indeed reduced in
344 the *drmy1* mutant. We selected *ARF3/ETTIN*, *ARF5/MONOPTEROS*, and *ARF6*, which have 2,
345 6, and 6 uORFs respectively, and as controls, *ARF8* and *ARF10* which do not contain uORFs.
346 None of these *ARF*s were differentially expressed in *drmy1* at the transcript level, except *ARF10*
347 which was slightly upregulated (Figure S5B). We utilized promoter-fluorescent protein fusion
348 reporters (Figure S5C) which have the same uORFs in the promoter region as the corresponding
349 ARF genes if the genes have them. These reporters reflect transcriptional and uORF-mediated
350 translational regulation. *pARF3::N3xGFP*, *pARF5::ER-EYFP-HDEL*, and *pARF6::N3xGFP*
351 contain uORFs and thus, following our hypothesis, are expected to drastically decrease in
352 fluorescence intensity in *drmy1* compared to WT. *pARF8::N3xGFP* and *pARF10::N3xGFP* do not
353 have uORFs and are thus expected to have comparable or higher fluorescence intensity in *drmy1*.
354 Surprisingly, we saw no correlation between the presence of uORFs and decrease in fluorescent
355 intensity in *drmy1* (Figure S5C-D). While it might arise from additional layers of regulation on
356 these ARFs, this result suggests that the decrease in translation reinitiation of uORF-containing
357 ARFs is not the main factor explaining the loss of robust auxin signaling pattern in *drmy1*.
358
359 It was previously reported that external application of cytokinin increases auxin
360 biosynthesis in actively growing tissue including the shoot apex, young leaves, and roots[70], and
361 cytokinin application also changes the expression and polarity of PIN-FORMED (PIN) polar auxin
362 transport carriers[71,72]. We previously noticed that external application of 6-benzylaminopurine
363 (BAP), a synthetic cytokinin, induced additional convergence points of PIN1 and increased
364 variability in auxin signaling, causing variability in sepal initiation (Zhu et al.[27], in this reference
365 see Fig. 4e, Extended Data Fig. 7e and 7f). Here, we confirmed this observation by circular
366 histogram analysis (Figure 5A-D). While the mock-treated WT buds showed four clear peaks of
367 DR5 signal with very little signal in between (Figure 5A-B), those treated with 5 μM BAP showed
368 a less robust spatial pattern, with less distinguishable peaks and larger variation all around the
369 bud (Figure 5C-D). Thus, excessive cytokinin is sufficient for the variable spatial pattern of auxin
370 signaling.
371
372 We then wondered whether an increase in cytokinin signaling (Figure 4) is the cause of
373 variable pattern of auxin signaling under translation-limited conditions such as *drmy1*. To test this
374 hypothesis, we crossed *drmy1* containing the DR5 reporter with a triple mutant of *ARABIDOPSIS*
375 *RESPONSE REGULATOR* (*ARR*) *1*, *10*, and *12*, the three most highly expressed B-type ARRs
376 in our RNA-seq (Supplementary Dataset 1) which are crucial for the activation of cytokinin-
377 responsive genes[73]. While buds of *arr1,10,12* did not show apparent phenotypic differences from
378 WT, the quadruple mutant *drmy1 arr1,10,12* largely rescued the *drmy1* phenotype, with much
379 less variability in sepal number and position (Figure 5E-G). While mature buds of *drmy1* have
380 sepals of variable sizes, leaving gaps and exposing the inner floral organs (Figure S6D vs. S6A-

C), those of *drmy1 arr1,10,12* have sepals of robust sizes that are able to close (Figure S6E). Likewise, mutation in a cytokinin receptor *WOODEN LEG* (*WOL*)/*ARABIDOPSIS HISTIDINE KINASE 4* (*AHK4*) showed a similar rescue of the *drmy1* sepal phenotype (Figure 5E-G, S6F). While the auxin signaling reporter DR5 was diffuse and variable in *drmy1* except in the incipient outer sepal (Figure 5H-I), in *drmy1 arr1,10,12*, it was focused in all the four incipient sepals that were robustly positioned, although the signal intensity in the incipient outer sepal was much higher than others (Figure 5J-K). These results indicate that cytokinin signaling is required for the increased variability in auxin signaling pattern and sepal initiation in *drmy1*.

Furthermore, we wanted to test whether cytokinin signaling is required for variability in more general conditions where translation is inhibited. The translation inhibitor CHX disrupted robustness in auxin signaling and sepal initiation in WT (Figure 2K, 4E, 4I), and we tested whether these effects are still present in *arr1,10,12* and *wol* mutants. We found that, unlike WT, sepal initiation remained mostly robust in *arr1,10,12* and *wol* after ten days of 2 μM CHX treatment (Figure 5L-N). While DR5 in WT became diffuse and occurred in variable positions after three days of CHX treatment (Figure 5O-P, arrow), DR5 in *arr1,10,12* remained robust and concentrated at the four incipient sepal primordia (Figure 5Q-R). These results suggest that elevated cytokinin signaling level is the primary cause for variability in auxin patterning under translation-inhibited conditions. Thus, in WT, maintaining a low level and focused cytokinin signaling is crucial for robust auxin patterning and sepal initiation.

Upregulation of cytokinin signaling is required to sustain translation and fitness in *drmy1*

Under translation-inhibited conditions, why does the plant upregulate cytokinin signaling at the cost of robust morphogenesis? Previous studies revealed that cytokinin signaling can stimulate translation[74–78], by increasing transcription or protein abundance of ribosomal components or biogenesis factors[79–81] and modification of initiation and elongation factors[82]. We therefore hypothesized that an increase in cytokinin signaling under translation-inhibited conditions (such as *drmy1*) sustains a survivable rate of translation in a feedback loop. We first validated that, under our growth conditions, an increase in cytokinin signaling (*arr1 35S::ARR1*) is sufficient to increase global translation (Figure 6A; also see Karunadasa et al.[74]) in 14-day-old seedlings. We then tested whether cytokinin signaling is required to sustain global translation (Figure 6B-C). Compared to WT, the cytokinin receptor single mutant *wol* has a mild reduction in global translation rate at day 8 and a ~50% reduction at day 14. The *drmy1* single mutant shows drastically reduced global translation rate at day 8, but by day 14, global translation rate in *drmy1* increased and matched WT. In the *drmy1 wol* double mutant, however, translation rate was unable to recover at day 14 and remained lower than *drmy1*. Our data suggest that, in *drmy1* plants which has reduced TOR activity and ribosomal level (Figure 1), the upregulated cytokinin signaling is required to sustain global translation at nearly WT levels.

We then hypothesized that an upregulation of cytokinin signaling in plants with reduced TOR activity and ribosomal content such as *drmy1* and the consequent restoration of global

translation would provide fitness benefits. Thus, we expect that removal of the cytokinin receptor WOL from *drmy1* and the consequent failure to sustain global translation should affect plant vitality and reproduction. We found that at day 14, the *drmy1* single mutant is slightly smaller than WT. In contrast, in the absence of WOL, growth of *drmy1 wol* plants were extremely retarded compared to *wol*, with tiny and chlorotic cotyledons and true leaves (Figure 6D). In older plants, the *drmy1* single mutant has similar rosette size and slightly shorter inflorescences compared to WT. In contrast, in the absence of WOL, *drmy1 wol* produced tiny rosettes and stunted inflorescences with a few chlorotic buds that develop into small, short siliques (Figure 6E, S6F). Similarly, when B-type ARRs are mutated, the growth of the *drmy1 arr1,10,12* quadruple mutant is much retarded compared to *arr1,10,12*. They produced slightly chlorotic and anthocyanin-rich rosettes, a tiny inflorescence composed of very few buds (Figure 6F, S6E) and, in the end, siliques in which all seeds had aborted (Figure 6G). Overall, these results show that *drmy1* requires the cytokinin signaling pathway for normal growth and reproduction. While it remains possible that unknown effects of the cytokinin signaling pathway other than promoting translation are critical for the proper growth of *drmy1*, our results are consistent with our hypothesis that the upregulation of global translation (Figure 6A) by increased cytokinin signaling (Figure 4) maintains a survivable level of protein synthesis in plants with reduced ribosomal content such as *drmy1* (Figure 1C).

TOR and translation inhibition decreases the protein level of cytokinin signaling inhibitors ARR7 and AHP6

What causes cytokinin signaling to increase in plants with reduced TOR activity and translation (Figure 4)? It was previously shown that *cis*-type cytokinins can be synthesized from tRNAs by the tRNA isopentenyltransferases (IPTs), IPT2 and IPT9[83]. We hypothesized that the decrease in global translation may increase the availability of tRNAs as substrates for cytokinin biosynthesis, increasing the level of cytokinins. To test this idea, we extracted cytokinins from induced inflorescences of WT and *drmy1* in *ap1 cal AP1-GR* background (Figure S1A). We measured the level of three cytokinin bases, *trans*-Zeatin (tZ), *cis*-Zeatin (cZ), and isopentenyladenine (iP), and their corresponding nucleosides (tZR, cZR, and iPR), using liquid chromatography-mass spectrometry. Surprisingly, we found no significant difference in their levels between WT and *drmy1*, and notably, the amount of *cis*-Zeatin was barely detectable in all samples (Figure S7A). This suggests that the increase in *cis*-type cytokinin synthesis is not the mechanism underlying the increase in cytokinin signaling under our translation-inhibited conditions.

We then considered the effects that a decrease in translation rate might have on the protein components of the cytokinin signaling pathway. In particular, A-type *ARR*s, which encode inhibitors of cytokinin signaling[84–86], are rapidly induced upon cytokinin application and serve to dampen cytokinin response in the tissue[87–89]. Likewise, *AHP6* is highly expressed in lateral organ primordia downstream of auxin signaling, which non-cell autonomously represses and restricts cytokinin signaling to robust spatial patterns[16]. The rapid synthesis of the A-type ARR and AHP6 proteins may be crucial for maintaining the homeostasis of cytokinin signaling during

465 developmental processes. We therefore hypothesized that, during hormone patterning prior to
466 sepal initiation, translation defects in *drmy1* cause reduced synthesis of these proteins,
467 decreasing them to a level insufficient to repress cytokinin signaling (Figure 7A).
468
469 We started testing the level of protein reporters for a variety of cytokinin signaling
470 components, in *drmy1* vs. WT and/or under translation or TOR inhibition. We reasoned that, given
471 that the transcript level of most cytokinin signaling components do not significantly differ between
472 *drmy1* and WT inflorescence tissue (Figure S7B), any changes in the level of these protein
473 reporters should reflect post-transcriptional regulation, including mRNA translation. For A-type
474 ARRs, we were unable to detect fluorescence in the inflorescence of a published *pARR4::ARR4-*
475 *GFP* line[90]. We reasoned that this was because A-type ARRs have low protein levels (none was
476 detected in our proteomics dataset) and short half-lives[91]. We therefore employed LlamaTagging,
477 a recently developed method to visualize the abundance of nuclear-localized proteins with short
478 half-lives[92]. Rapidly degraded proteins cannot be visualized through fusion with standard
479 fluorescent proteins, because fluorescent proteins take time to mature before they fluoresce, and
480 the protein of interest is degraded before the maturation of the fluorescent protein. On the other
481 hand, the LlamaTag folds immediately. A LlamaTag with a high affinity for GFP can be encoded
482 as a translational fusion with a nuclear-localized protein of interest. Soon after translation, the
483 fusion immediately binds cytoplasm-localized GFP and translocates it to the nucleus. Thus,
484 increased GFP fluorescence in the nucleus indicates higher abundance of the protein of interest
485 (Figure 7B).
486
487 We focused on ARR7, the most highly expressed A-type ARR in our inflorescence RNA-
488 seq (Figure S7B) which was also shown to be nuclear-localized[93,94]. We designed a construct with
489 ARR7 fused with GFP-specific LlamaTag by a short linker, driven by the ARR7 native promoter
490 (*pARR7::ARR7-linker-llama-ARR7ter*; *ARR7-llama* for short). This construct was co-transformed
491 with cytoplasm-localized GFP containing a nuclear exclusion signal (*pUBQ10::sfGFP-nes-*
492 *UBQ3ter*; *GFP-nes* for short; Figure 7C). As a proof of concept, we treated this reporter in WT
493 background with 200 μM BAP. We found that GFP signal became more nuclear-localized within
494 5 hours of the treatment (Figure S7C-D), agreeing with an increased expression and stability of
495 A-type ARR proteins upon cytokinin application as previously reported[91,95].
496
497 We then compared the localization of GFP signal in floral meristems of WT and *drmy1*
498 before sepal initiation. According to the null hypothesis, increased cytokinin signaling in *drmy1*
499 would cause an increase in ARR7 protein level and thus more nuclear-localized GFP signal in
500 *drmy1 ARR7-llama GFP-nes* than its WT counterpart. This is because cytokinin signaling
501 increases the gene expression and protein stability of A-type ARRs[88,91,95,96]. In contrast, according
502 to our hypothesis, insufficient protein synthesis of A-type ARRs contributes at least in part to
503 increased in cytokinin signaling in *drmy1*, so we expect to see reduced ARR7 protein level and
504 thus more cytoplasm-localized GFP signal in *drmy1 ARR7-llama GFP-nes*. We found that WT
505 buds had slightly more nuclear-localized GFP signal than cytoplasm-localized GFP signal, with
506 brighter spots corresponding to the nucleus surrounded by darker grooves in between

507 corresponding to the cytoplasm (Figure 7D,E). In contrast, in the periphery of *drmy1* buds, GFP
508 signal localizes more to the cytoplasm than to the nucleus, with darker spots surrounded by
509 brighter grooves (Figure 7D,E). More nuclear GFP was present near the center of *drmy1* buds.
510 This result indicates nuclear ARR7 protein concentration is reduced in the *drmy1* mutant,
511 particularly in the zone where sepals initiate. To see whether this conclusion holds in other
512 translation-inhibited conditions, we treated WT plants carrying the *ARR7-llama* and *GFP-nes*
513 reporters with the translation inhibitor CHX and the TOR inhibitor AZD-8055. 2 μM CHX treatment
514 for 24 hours drastically reduced the nuclear localization of the GFP signal and increased its
515 cytoplasmic localization (Figure 7F). 2 μM AZD-8055 treatment for 72 hours had a milder but
516 similar effect (Figure 7G). These treatments did not affect the localization of the GFP signal in
517 plants without *ARR7-llama* (Figure S7E-H). These results show that conditions that decrease
518 global protein synthesis greatly decrease the nuclear level of ARR7 protein.
519
520 We also tested whether TOR or translation inhibition alter the protein level of AHP6. To
521 this end, we imaged the *pAHP6::AHP6-VENUS*[16] protein reporter under mock, CHX, or AZD-8055
522 treatment. While mock-treated buds highly accumulate the AHP6 protein in the four incipient sepal
523 primordia, buds treated with CHX or AZD-8055 abolished AHP6 accumulation within 72 hours
524 (Figure 7H). The *pAHP6::GFP-ER*[97] transcriptional reporter does not change under these
525 treatments (Figure 7I), in agreement with our RNA-seq data of WT vs. *drmy1* (Figure S7B),
526 suggesting that the change in AHP6 protein level is due to post-transcriptional regulation such as
527 altered translation.
528
529 It is possible that inhibition of TOR and translation results in a general, uniform reduction
530 in the level of all proteins, not just for the cytokinin signaling inhibitors ARR7 and AHP6, but also
531 for the positive regulators of cytokinin signaling. For this, we tested whether AHP3, a component
532 of the cytokinin phosphorelay[98,99], respond to TOR and translation inhibition. CHX treatment did
533 not affect the level or spatial localization pattern of the *pAHP3::AHP3-GFP* reporter[100], while AZD-
534 8055 treatment only mildly decreased its level (Figure S7I). We also tested how the level of other,
535 more generic proteins respond to TOR and translation inhibition. Unexpectedly, the level of
536 *pUBQ10::mCherry-RCI2A* increased upon 72 hours of CHX or AZD-8055 treatments (Figure
537 S7J). Overall, these results show that TOR and translation inhibition does not result in a uniform
538 reduction in the level of all proteins, but specific proteins such as ARR7 and AHP6 are dramatically
539 decreased. Further, these results are consistent with our hypothesis that depletion of cytokinin
540 signaling inhibitor proteins, including ARR7 and AHP6, may underlie the upregulation of cytokinin
541 signaling when the floral meristem is under TOR or translation inhibition (Figure 4).
542
543 Having shown a reduction in the level of ARR7 and AHP6 greater than other proteins
544 under TOR and translation inhibition, we next tested whether such a reduction contributes to the
545 variability in sepal initiation also seen under such conditions (Figure 2). High-order mutant of A-
546 type *ARR*s (*arr3,4,5,6,7,8,9,15*[101]) shows reduced size of the inner sepal primordium (Figure 7J,K)
547 and a minor but significant increase in the positional variability of sepal primordia compared to
548 WT (Figure 7Q), although sepal primordium number remains robust (Figure 7P). The *ahp6*

549 mutant[16] shows great variability of sepal primordium number, position, and size, although to a
550 lower extent than *drmy1* (Figure 7J,L,P,Q). Similarly, if the reduction of ARR7 level in *drmy1*
551 contributes to variability in sepal initiation, increasing ARR7 expression should restore sepal
552 initiation robustness. While *ARR7-llama GFP-nes* plants phenocopy WT (Figure 7M), introducing
553 the *ARR7-llama GFP-nes* constructs into *drmy1* plants partially restores robustness in sepal
554 initiation, particularly in the position of sepal primordia (Figure 7N-Q). In older buds, while *drmy1*
555 buds show great variability in sepal number and size resulting in gaps, some buds of *drmy1 ARR7-*
556 *llama GFP-nes* have robustly sized sepals that are able to close properly (Figure S7K-N). Overall,
557 these results show that reducing the level of cytokinin signaling inhibitor proteins ARR7 and AHP6
558 create variability in sepal primordium initiation, and increasing their level in *drmy1* partially
559 restores robustness. We propose that, during hormone patterning prior to sepal initiation, the rapid
560 synthesis of these inhibitor proteins in response to auxin and cytokinin signaling is crucial for
561 maintaining the homeostasis of cytokinin signaling and thus the robustness in sepal initiation.
562
563 We also considered other hormone-related proteins that are dynamically regulated during
564 organogenesis and thus may be depleted under translation defects. AUXIN/INDOLE-3-ACETIC
565 ACID INDUCIBLE (Aux/IAA) proteins are auxin signaling inhibitors that are rapidly induced by
566 auxin[102,103]. They bind auxin and are rapidly degraded by the ubiquitin E3 ligase SKP1, CUL1, F-
567 BOX PROTEIN (SCF) complex involving TRANSPORT INHIBITOR RESPONSE1/AUXIN
568 SIGNALING F-BOX (TIR1/AFB)[104–107]. Degradation is dependent on the Short Linear Motif (SLiM)
569 degron contained within Domain II (DII)[106–108]. We hypothesized that the level of DII-containing
570 proteins including Aux/IAAs would be drastically decreased in translation-inhibited conditions
571 such as *drmy1* because they are unable to be rapidly synthesized to keep up with their
572 degradation upon auxin signaling. To test this, we used the R2D2 reporter[109], which contains a
573 DII fused with 3xVENUS (*pUS7Y::DII-n3xVENUS*), and as a control, a mutated non-degraded DII
574 fused with tdTomato (*pUS7Y::mDII-ntdTomato*). We compared this reporter in *drmy1* vs. WT. The
575 ratio of *VENUS* to *tdTomato* was not reduced in *drmy1*, but instead slightly but significantly
576 elevated (Figure S7O-P). In addition, *drmy1* has stochastic patches of DII-VENUS degradation,
577 consistent with its often mislocalized auxin maxima (Figure 4A, S4B), unlike WT which had four
578 patches of degradation corresponding to the four incipient sepal primordia where auxin maxima
579 robustly form (Figure 4A, S4A). Overall, these results suggest that the level of DII-containing
580 Aux/IAA proteins is not reduced in *drmy1*, despite the high requirement for synthesis due to their
581 rapid turnover. They also indicate that not all proteins that are dynamically regulated in response
582 to hormone signaling are equally affected by translation inhibition, which may result in different
583 changes in hormone signaling output under such condition.
584
585
586 **DISCUSSION**
587
588 Robustness, the strikingly reproducible development of phenotype, has fascinated
589 biologists for decades[2]. The Arabidopsis flower robustly develops four sepals of equal size. This
590 stems from the robust initiation of four sepal primordia from the floral meristem, which is in turn

591 dictated by the robust patterning of auxin and cytokinin controlled by DRMY1[27]. Here we
592 elucidated how DRMY1 controls robust hormone patterning and thus robust sepal initiation. We
593 show that DRMY1 sustains TOR activity, ribosomal content, and translation. We further show that
594 inhibition of TOR activity or translation is sufficient to cause variability in the timing, position, and
595 number of sepal primordia, mimicking the *drmy1* phenotype. Our findings are in concert with
596 previous studies that have shown robustness is often maintained by genes involved in central
597 cellular processes[2]. In our case, the rate of translation in wild type maintains proper levels of
598 ARR7 and AHP6, two cytokinin signaling inhibitor proteins, which need to be rapidly synthesized
599 to dampen cytokinin signaling. Homeostasis of cytokinin signaling ensures robustness in auxin
600 signaling patterns, and thus robustness in sepal initiation (Figure 7R, top). In the *drmy1* mutant,
601 the reduced TOR activity, ribosomal content, and translation rate causes inability to rapidly
602 synthesize these inhibitor proteins. Consequently, cytokinin signaling is elevated, disrupting the
603 robust spatial pattern of auxin signaling, leading to variable sepal initiation (Figure 7R, bottom).
604 Blocking cytokinin signaling in *drmy1* is sufficient to restore robust initiation of four sepal
605 primordia, but has severe consequences on the overall fitness of the plant. Our results reveal how
606 defects in hub cellular processes such as TOR signaling and translation can have tissue-specific
607 phenotypic effects.
608
609 Although we propose that reduced TOR activity and mRNA translation affects
610 developmental robustness through reduced synthesis of ARR7 and AHP6, we do not exclude
611 other potential mechanisms that could contribute to the drmy1 phenotype. For example, we
612 observed that several subunits of the 26S proteasome are more abundant in drmy1 than in WT
613 (Supplemental Dataset 1), which could reflect or influence the accumulation of proteotoxic
614 peptides and disrupt protein homeostasis[110–114]. This accumulation of 26S proteasomes could
615 function upstream and/or downstream of the defect in TOR activity that impacts robust
616 organogenesis[34,115–120]. Substantial future research will be needed to comprehensively define
617 how DRMY1 participates in the complex interactions among TOR, mRNA translation, and
618 proteolysis.
619
620 It was discovered long ago that extrinsic cytokinin application to plant tissue or cell-free
621 extracts can promote mRNA translation[75–78]. Recent studies further confirmed that the up-
622 regulation of translation by cytokinin is at least in part mediated by the cytokinin signaling
623 pathway[74,82]. Here, we show that cytokinin signaling in floral buds is upregulated in translation-
624 inhibited conditions, such as *drmy1*, AZD-8055 treatment, or CHX treatment (Figure 4), through
625 reduced level of cytokinin inhibitor proteins (Figure 7; also potentially through other untested
626 mechanisms). The enhanced cytokinin signaling maintains translation rate at a level necessary
627 for the survival and reproduction of the plant (Figure 6). We propose that this represents a
628 homeostasis mechanism where plants leverage increased cytokinin signaling to rescue the
629 translation rate reduction caused by deficient TOR activity and ribosomal content (Figure 7R,
630 bottom). It remains to be tested how widely this mechanism is applicable to other mutants with
631 ribosomal defects, or whether parallel mechanisms operate in other species across kingdoms.
632

While translation-inhibited plants likely upregulate cytokinin signaling to maintain protein synthesis, this upregulation negatively affects developmental robustness. We have previously shown that exogenous cytokinin application to the WT floral meristem increases variability in PIN1 convergence and auxin signaling patterns, and consequently, in sepal initiation. These effects are more pronounced in the *drmy1* mutant, which by itself has increased and diffuse cytokinin signaling[27]. Here, we provide additional evidence that increased and diffuse cytokinin signaling is necessary for such variability. While *drmy1* and CHX-treated WT floral meristems are variable in auxin signaling pattern and sepal initiation (Figure 2, 4), mutations in *wol* and *arr1,10,12*, which decreases cytokinin signaling, largely restore robustness (Figure 5). Robustness is also restored in the mature sepals of *drmy1 wol* and *drmy1 arr1,10,12*, enabling sepal closure (Figure S6). Similar effects in restoring robustness are seen when an extra functional transgene of *ARR7* (*pARR7::ARR7-llama*) is introduced to the *drmy1* mutant (Figure 7J-Q, S7K-N). Our results suggest that cytokinin upregulation is necessary and sufficient for variability in auxin patterning and sepal initiation, indicating that the cytokinin signaling changes are primary defects in *drmy1*, and the auxin signaling changes are secondary. Our results suggest a mechanism different from that previously reported in *ul4y*, *ul18z*, and *el24y*, where ribosomal mutations affect auxin signaling through reduced translation reinitiation of uORF-containing mRNAs, including those of AUXIN RESPONSE FACTOR (ARF) 3, 5, and 7[64–66]. While we found that uORF-containing mRNAs generally have reduced protein-transcript ratio in *drmy1* suggestive of reduced translation, we did not see a consensus reduction in the level of uORF-containing promoter reporters of ARFs (Figure S5). This suggests that the variable auxin signaling pattern in *drmy1* is unlikely to result from changes in uORF-mediated translational regulation of ARFs. Overall, our results suggest that homeostasis in cytokinin signaling is crucial for maintaining robust patterns of auxin signaling and robust morphogenesis in the floral meristem.

Mutations affecting ribosome abundance or translation have long attracted interest due to the surprisingly tissue-specific phenotypes they cause[121]. In humans, these mutations have been associated with diseases collectively known as ribosomopathies, where patients show various abnormalities in blood, skeleton, hair, teeth, and pancreas, as well as intellectual disability and increased risk of cancer[122–127]. Ribosomal protein mutants have been characterized in numerous other species with similarly diverse impacts. They display a range of specific phenotypic changes, such as altered pigmentation and skeletal structure in mouse[128–130] and zebrafish[131], shorter bristles and notched wing margins in fruit fly[23,132], abnormal gonad development in worm[133], and pointed leaves and abnormal vascular patterning in Arabidopsis[64,66,134–136]. Here, we show that the Arabidopsis mutant *drmy1* has reduced TOR activity, ribosomal content, and translation rate, causing variable sepal initiation which phenocopies the ribosomal mutants *ul4y* and *ul18z* and the TORC1 assembly mutant *spaghetti-1* (Figure 2, 3). We therefore propose that *drmy1* is an Arabidopsis ribosomopathy mutant like those previously characterized[135].

Several mechanisms have been proposed to explain why ribosomopathies do not usually cause a general reduction in growth, but rather affect development in tissue-specific ways. These include extra-ribosomal functions of certain ribosomal proteins[137–141], altered translation behavior

675 of ribosomal variants on certain mRNAs[142], different competitiveness of mRNAs for scarce
676 ribosomes[64–66,143–146], and high translation rate requirement for certain proteins[147,148]. For example,
677 neurotransmitter release in animals relies on constant synthesis of the synaptic vesicle protein
678 Syt1[149]. A Drosophila *Minute* mutant, *uS15/+,* shows reduced synthesis of Syt1, which in turn
679 reduces ecdysone secretion in 5-HT neurons, causing delayed larval-to-pupal transition[147].
680 Similarly, the human apoptosis inhibitor Mcl-1 has a half-life of ~30 min and thus requires a high
681 translation rate to maintain its proper level. Under translation inhibition, the synthesis of Mcl-1 is
682 unable to keep up with its degradation, causing apoptosis[148]. Here, we show that the levels of
683 ARR7 and AHP6, which are rapidly induced by cytokinin and auxin signaling, respectively[150,151],
684 are drastically reduced under translation inhibition, which underlies the upregulation of cytokinin
685 signaling and loss of robustness in auxin signaling and morphogenesis (Figure 7R). This
686 mechanism parallels those previously found in animal systems[147,148], highlighting how
687 downregulation of proteins with high translational requirements can underlie the tissue-specificity
688 of ribosomopathy. Outside the floral meristem, the *drmy1* mutant shows other phenotypic changes
689 such as enlarged shoot apical meristem, reduced apical dominance, phyllotaxy defects, and
690 reduced root system, all of which are related to altered cytokinin/auxin signaling activity[27]. Thus,
691 our work highlights how defects in translation, which occurs in every cell, can have tissue-specific
692 effects on how cells robustly arrange into organs.
693
694 In addition, we note that not all proteins are equally reduced under broad translation
695 inhibition. Our data suggest that the cytokinin signaling inhibitor proteins ARR7 and AHP6 are
696 drastically reduced, compared to others such as AHP3, RCI2A, and GFP-nes. This suggests that
697 the observed increase in cytokinin signaling under translation inhibition may be due to an
698 imbalance in the relative levels of activators and inhibitors, which may further suggest that the
699 inhibitor proteins are more temporally dynamic and thus have higher translational requirements
700 during development. These hypotheses remain to be tested in future studies.
701
702

703 **ACKNOWLEDGEMENTS**

704 We thank Bella Burda, Frances Clark, Byron Rusnak, Erich Schwarz, Avilash Yadav, and Maura
705 Zimmermann for comments and suggestions on the manuscript. We thank Frank Wellmer for the
706 *ap1 cal 35S::AP1-GR* (Ler) seeds, Elliot Meyerowitz and Arnavaz Garda for the *DR5::3xVENUS-*
707 *N7/PIN1::GFP* (Ler) seeds, Teva Vernoux and Géraldine Brunoud for the *TCS::GFP*, *TCS-DR5*
708 (Col), *ahp6*, *pAHP6::AHP6-VENUS*, and *pAHP6::GFP-ER* seeds, Jan Smalle for the *arr1-1*
709 *35S::ARR1* seeds, Joseph Kieber and Jamie Winshell for the *arr3,4,5,6,7,8,9,15* and
710 *pARR4::ARR4-GFP* seeds, Thomas Greb and Min-Hao Chiang for the *pARF5::ER-ARF5-HDEL*
711 seeds, and Jianru Zuo for the *pAHP3::AHP3-GFP* plasmid. We thank Georg Jander for advice
712 and protocol for cytokinin extraction. We thank Brian Curtis and Frank Schroeder for help on mass
713 spectrometry, and Sheng Zhang and Qin Fu for help on Xcalibur. We thank Richie Ragas, Yanã
714 Rizzieri, and Ziqing Wei for assistance on experiments and data analysis. We thank Vicky
715 Spencer and Minsung Kim for sharing the *in vivo* Torin2 treatment protocol. We thank Arabidopsis
716 Biological Resource Center for providing seed stocks and plasmids used in this research.

Research reported in this publication was supported by the National Institute of General Medical Sciences of the National Institutes of Health (NIH) under award numbers R01GM134037, DP5OD023072, and R01GM145814; Cornell Graduate School new student fellowship (S.K.); and in part by a Schmittau-Novak Grant from the School of Integrative Plant Science, Cornell University (M.Z.). H.G.G. was supported by NIH Director's New Innovator Award (DP2 OD024541-01) and NSF CAREER Award (1652236), NIH R01 Award (R01GM139913), and the Koret-UC Berkeley-Tel Aviv University Initiative in Computational Biology and Bioinformatics. H.G.G. is also a Chan Zuckerberg Biohub Investigator. We thank the Metabolomics Workbench[152] for providing the data repository for our cytokinin mass spectrometry data, which is funded by NIH under award numbers U2C-DK119886 and OT2-OD030544. We thank the Biotechnology Resource Center (BRC) Genomics Facility (RRID:SCR_021727) of Cornell University for performing RNA-seq on *ap1 cal AP1-GR* inflorescence samples. We thank Novogene for performing seedling RNA-Seq library synthesis and sequencing. We thank the BRC Proteomics Facility (RRID:SCR_021743) of Cornell University for performing mass spectrometry on *ap1 cal AP1-GR* inflorescence samples, and NIH SIG Grant 1S10 OD017992-01 for supporting the Orbitrap Fusion mass spectrometer. The content is solely the responsibility of the authors and does not necessarily represent the official views of the National Institutes of Health.

AUTHOR CONTRIBUTIONS

S.K.: Conceptualization, Investigation, Formal Analysis, Visualization, Writing - Original Draft, Writing - Review & Editing. M.Z.: Conceptualization, Investigation, Formal Analysis, Writing - Review & Editing. M.R.S: Investigation, Visualization. D.P.: Investigation, Formal Analysis, Visualization. L.J.: Investigation. R.E.M.: Investigation, Formal Analysis. S.A.: Methodology, Resources. B.V.L.V.: Methodology, Resources, Writing - Review & Editing. H.G.: Methodology, Resources, Writing - Review & Editing, Supervision. S.B.Q: Writing - Review & Editing, Supervision. J.O.B.: Resources, Writing - Review & Editing, Supervision. A.H.K.R: Conceptualization, Writing - Review & Editing, Supervision, Project administration, Funding acquisition.

DECLARATION OF INTERESTS

The authors declare no competing interests.

750 **FIGURE TITLES AND LEGENDS**

751

752 **Figure 1. *drmy1* has reduced ribosome abundance, translation rate, and TOR activity.**
753 **(A)** Top row, stage 12 buds of WT (left) and *drmy1* (right) viewed from the side. Asterisk shows
754 the gap between sepals with petals and carpels exposed. Middle row, stage 12 buds of WT (left)
755 and *drmy1* (right) viewed from the top. Arrowheads point to sepals. Note that the *drmy1* bud has
756 5 sepals of unequal size and unevenly spaced, exposing the stamens and carpels. Bottom row,
757 stage 5 buds of WT (left) and *drmy1* (right) containing *35S::mCitrine-RCI2A* (plasma membrane
758 marker). Arrowheads point to sepal primordia. Note that the *drmy1* bud has 5 sepal primordia of
759 different sizes. Scale bars are 0.5 mm for stage 12 bud images and 25 μm for stage 5 bud images.
760 **(B)** Gene ontology (GO) enrichment of downregulated genes in *drmy1* compared to WT, in the
761 *ap1 cal AP1-GR* background. Shown are the top 8 GO terms and their enrichment p-values. A
762 complete list can be found in Supplemental Dataset 1. Arrowheads highlight terms related to
763 ribosome biogenesis or translation.
764 **(C)** Polysomal profiles of WT (blue) and *drmy1* (red) in the *ap1 cal AP1-GR* background,
765 representative of 3 biological replicates each. Additional replicates are in Supplemental Dataset
766 2. M, monosomes. P, polysomes.
767 **(D)** Puromycin labeling of WT vs *drmy1*. Left, WT and *drmy1* seedlings. From left to right: WT pre-
768 treated with CHX, two biological replicates of WT pre-treated with mock, and two biological
769 replicates of *drmy1* pre-treated with mock. All groups were then treated with puromycin. For
770 seedlings to match in size, WT seedlings were 8 days old and *drmy1* seedlings were 10 days old.
771 Right, WT and *drmy1* inflorescences of induced *ap1 cal AP1-GR* background. From left to right:
772 WT co-treated with puromycin and CHX, three biological replicates of WT treated with puromycin,
773 and three biological replicates of *drmy1* treated with puromycin. In both experiments, RuBisCO
774 large subunit on Ponceau S-stained membrane is shown as a loading control (bottom). Ratio
775 between puromycin and Ponceau S signals, normalized by the mean of WT, is shown on the
776 bottom (p-values are from two-sided Student's t-test).
777 **(E)** Gene ontology (GO) enrichment of differentially accumulated proteins in *drmy1* compared to
778 WT, in the *ap1 cal AP1-GR* background. Shown are the top 8 GO terms and their enrichment p-
779 values. A complete list can be found in Supplemental Dataset 1. Arrowheads highlight terms
780 related to ribosome biogenesis or translation.
781 **(F-G)** Coherent alteration of gene expression by *drmy1* and AZD-8055 TOR inhibitor treatment.
782 **(F)** Scatterplot of RNA log2 fold change in *drmy1* vs WT (x-axis), and WT+AZD vs WT+Mock (y-
783 axis), in 7-day-old seedlings. Genes are color-coded based on the following categories: genes in
784 "Structural constituents of the ribosome" (GO:0003735) and its offspring terms (magenta); all
785 other genes in "Translation" (GO:0006412) and its offspring terms (orange); all other genes (gray).
786 Blue line shows a linear regression of all points ($R^2 = 0.1446$, $p < 2.2\times10^{-16}$). **(G)** Of the 466 genes
787 that are differentially expressed under both conditions, 439 (94%) are coherently altered by AZD-
788 8055 treatment and the *drmy1* mutation.
789 **(H-I)** Phosphorylation of the direct TOR substrate, S6K-pT449, in WT and *drmy1*. **(H)** A
790 representative blot. Top, S6K-pT449. Middle, total S6K protein. Bottom, Ponceau S staining. Ratio
791 between S6K-pT449 signal and Ponceau S signal is shown above the blots. **(I)** Ratio between

792 S6K-pT449 and Ponceau S signals normalized by WT, quantified across in three experiments,
793 shows that TOR activity decreased by half in *drmy1*. (mean ± SD; *, $p<0.05$).
794

795 **Figure 2. Defects in TOR activity, ribosome, and translation disrupt robust sepal initiation.**
796 **(A-G)** Representative images of stage 5 buds in WT (A), *drmy1* (B), *ul4z* (C), *ul4y* (D), *ul18z* (E),
797 *lst8-1-1* (F), and *spaghetti-1* (G). Tissue morphology is visualized by either propidium iodide (a
798 cell wall-staining dye) or a plasma membrane marker. Arrowheads indicate sepal primordia that
799 are variable in number, position, and size. Note that *ul4z* flowers always develop four sepal
800 primordia, although of different sizes; *lst8-1-1* occasionally (4/41, 9.8%) develops buds with more
801 than four sepal primordia.
802 **(H)** Quantification of sepal primordium number, comparing *drmy1* (n = 67 buds), *ul4z* (n = 52
803 buds), *ul4y* (n = 53 buds), *ul18z* (n = 52 buds), *lst8-1-1* (n = 41 buds), and *spaghetti-1* (n = 84
804 buds) with WT (n = 51 buds). Asterisks indicate statistically significant ($p < 0.05$) differences from
805 WT in Fisher's contingency table tests.
806 **(I)** Illustration of robust versus variable positioning of sepal primordia. Primordia are considered
807 robustly positioned if they are evenly distributed around the edge of the bud. Within each bud,
808 angles between adjacent primordia with respect to the center of the bud are measured, and
809 coefficient of variation (CV) is calculated. A bud with robustly positioned primordia would have
810 similar angular values and a low CV value. A bud with variably positioned primordia would have
811 very different angular values and a high CV value.
812 **(J)** Quantification of variability in primordium positioning (CV) in the same buds as in (H), following
813 illustration in (I). Asterisks indicate statistically significant ($p < 0.05$) differences from WT in
814 Wilcoxon's rank sum tests.
815 **(K)** Representative images of buds from *in vitro*-cultured WT inflorescences treated with mock or
816 2 μM CHX for 9-10 days. Arrowheads indicate sepal primordia that are variable in number,
817 position, and size.
818 **(L)** Representative images of buds from WT plants treated with mock or 2 nmol Torin2 for 15
819 days. Arrowheads indicate sepal primordia that are variable in number, position, and size.
820 **(M-N)** Quantification of sepal primordium number (M) and positional variability (N) similar to (H,J),
821 comparing CHX-treated (n = 31 buds), CHX-mock (n = 42 buds), Torin2-treated (n = 51 buds)
822 and Torin2-mock buds (n = 56 buds). Scale bars in all micrographs, 25 μm.

823 **Figure 3. TOR and ribosomal defects cause variability in the timing of sepal initiation.**
824 **(A-C)** 6h-interval live imaging of the sepal initiation process in WT (A) and *ul4y* (B), which is
825 quantified in (C). n = 48 buds for WT; n = 40 buds for *ul4y*.
826 **(D-F)** 6h-interval live imaging of the sepal initiation process in buds from WT plants treated with
827 mock or 2 nmol Torin2 twice a day for 15 days, which is quantified in (F). n = 31 buds for mock; n
828 = 15 buds for Torin2.
829 In **(A,B,D,E)**, top rows show the *35S::mCitrine-RCI2A* membrane marker, and bottom rows show
830 Gaussian curvature heatmaps of the same image stacks. Asterisks indicate sepal initiation
831 events, defined as a dark red band (primordium with positive curvature) separated from the floral
832 meristem by a dark blue band (boundary with negative curvature) in the heatmap. Scale bars, 25
833 µm.
834 In **(C,F)**, the amount of time between outer and inner sepal initiation (left) and between outer and
835 lateral sepal initiation (right) were calculated for each bud. Bar plot shows mean ± SD which is
836 also shown on top of each plot. Asterisks indicate statistically significant differences ($p < 0.05$) in
837 Wilcoxon's rank sum test (for mean) or Levene's test (for SD).
838

839 **Figure 4. Inhibition of TOR activity and translation cause variability in auxin and cytokinin**
840 **signaling.**
841 **(A-D)** The ribosomal mutant *ul4y* loses robustness in auxin and cytokinin signaling. (A)
842 Representative images of late stage 2 buds of WT, *drmy1*, and *ul4y*, showing the auxin signaling
843 reporter *DR5::3xVENUS-N7* in yellow, the cytokinin signaling reporter *TCS::GFP* in cyan, and
844 both merged with Chlorophyll (in WT) or *UBQ10::mCherry-RCI2A* (in *drmy1* and *ul4y*) in magenta.
845 (B) Quantification of TCS intensity (integrated density divided by area) from maximum intensity
846 projection images, normalized to mean of WT. Shown are mean ± SD. Asterisks show statistically
847 significant differences from WT in two-tailed Student's t-tests (*drmy1*, $p = 2.1\times10^{-6}$; *ul4y*, $p =$
848 3.4×10^{-5}). (C) Circular histogram of DR5 signal distribution. Each bud was divided into 360 sectors
849 of 1° each. Within each sector, DR5 signal measured in pixel intensity units (0-255 range) was
850 summed. This sum was plotted along the x-axis starting from the sector at 1:30 position (between
851 the incipient outer sepal and incipient right sepal) going counterclockwise. I.e., in WT, the outer
852 sepal is near 45°, the inner sepal near 225°, and the lateral sepals near 45° and 135° (vertical
853 dotted lines). The mean was plotted as a solid line, and mean ± SD was plotted as a shaded area.
854 (D) Circular histogram of TCS signal distribution. Sample size for (A-D): WT, n = 12 buds; *drmy1*,
855 n = 15 buds; *ul4y*, n = 10 buds.
856 **(E-H)** 3 days of translation inhibition causes increased and diffuse cytokinin signaling, and diffuse
857 auxin signaling. (E) Representative images of late stage 2 WT buds treated *in vitro* with mock or
858 2 μM CHX for 3 days. Shown are *DR5::3xVENUS-N7* in yellow, *TCS::GFP* in cyan, and both
859 merged with Chlorophyll in magenta. (F) Quantification of TCS intensity from maximum intensity
860 projection images, normalized to mean of WT mock day 3. Shown are mean ± SD. Asterisk shows
861 statistically significant difference in a two-tailed Student's t-test ($p = 2.0\times10^{-4}$). (G) Circular
862 histogram of DR5 signal distribution. (H) Circular histogram of TCS signal distribution. Sample
863 size for (E-H): WT mock day 3, n = 10 buds; WT CHX day 3, n = 12 buds.
864 **(I-L)** 6 days of TOR or translation inhibition causes increased and diffuse cytokinin signaling, and
865 randomly positioned auxin signaling maxima. (I) Representative images of late stage 2 WT buds
866 treated *in vitro* with mock, 2 μM CHX, or 2 μM AZD for 6 days. Shown are *DR5::3xVENUS-N7* in
867 yellow, *TCS::GFP* in cyan, and both merged with Chlorophyll in magenta. Arrowheads point to
868 randomly positioned auxin maxima. (J) Quantification of TCS intensity from maximum intensity
869 projection images, normalized to mean of WT mock day 6. Shown are mean ± SD. Asterisks show
870 statistically significant differences from mock in two-tailed Student's t-tests (CHX, $p = 1.0\times10^{-3}$;
871 AZD, $p = 1.2\times10^{-4}$). (K) Circular histogram of DR5 signal distribution. (L) Circular histogram of
872 TCS signal distribution. Sample size for (I-L): WT mock day 6, n = 12 buds; WT CHX day 6, n =
873 11 buds; WT AZD day 6, n = 10 buds. Scale bars in all micrographs, 25 μm.

874 **Figure 5. Cytokinin signaling is required for increased variability in auxin signaling and**
875 **sepal initiation under translation inhibition.**
876 **(A-D)** Cytokinin treatment makes auxin signaling diffuse. Shown are late stage 2 WT buds under
877 mock (A,B) or 5 μM cytokinin (BAP) treatment (C,D) for 4 days. (A,C) Auxin signaling reporter
878 *DR5* in yellow, and *DR5* merged with Chlorophyll in magenta. (B,D) Circular histograms of the
879 *DR5* signal, showing mean (solid line) and mean ± SD (shaded area). Arrows point to DR5 signal
880 in variable positions. Sample size: WT Mock n = 10, WT BAP n = 10. Also see Zhu et al. (2020),
881 in this reference see Extended Data Figure 7e.
882 **(E-G)** Cytokinin signaling is required for variable sepal initiation in *drmy1*. (E) Stage 5 buds. Sepal
883 primordia in *drmy1* are variable (arrowheads), which does not occur in *drmy1 arr1,10,12* and
884 *drmy1 wol* mutants. (F,G) Quantification of sepal primordium number (F) and positional variability
885 (G), comparing WT (n = 58) with *drmy1* (n = 31), *arr1,10,12* (n = 24) with *drmy1 arr1,10,12* (n =
886 20), and *wol* (n = 36) with *drmy1 wol* (n = 39). Asterisks indicate statistically significant ($p < 0.05$)
887 differences in Fisher's contingency table tests (F) and Wilcoxon's rank sum tests (G) respectively.
888 **(H-K)** Cytokinin signaling is required for variable patterning of auxin signaling in *drmy1*. Shown
889 are late stage 2 buds of WT vs *drmy1* (H,I), and *arr1,10,12* vs *drmy1 arr1,10,12* (J,K). (H,J) Auxin
890 signaling reporter *DR5* in yellow, and *DR5* merged with propidium iodide in magenta. Arrows point
891 to diffuse DR5 signal in variable positions of the *drmy1* bud. Arrowheads show four robust DR5
892 maxima in the *drmy1 arr1,10,12* bud. (I,K) Circular histograms of the *DR5* signal, showing mean
893 (solid line) and mean ± SD (shaded area). For ease of visualization, circular histograms of *drmy1*
894 and *drmy1 arr1,10,12* between 90 and 360 degrees are enlarged and shown as insets (y-axis
895 range 0-0.4). Note the presence of DR5 signal in inter-sepal regions in *drmy1* (black arrow) which
896 is largely suppressed in *drmy1 arr1,10,12*. Sample size: WT n = 19, *drmy1* n = 16, *arr1,10,12* n =
897 13, *drmy1 arr1,10,12* n = 9.
898 **(L-N)** Cytokinin signaling is required for variable sepal initiation under translation inhibition. (L)
899 Stage 6 buds of WT, *arr1,10,12*, and *wol*, treated with Mock or 2 μM CHX for 10 days. WT initiates
900 sepal primordia at variable positions when treated with CHX (arrowheads), which does not occur
901 in *arr1,10,12* and *wol*. (M,N) Quantification of sepal primordium number (M) and positional
902 variability (N), comparing mock and CHX within each genotype. Sample size: WT Mock n = 29,
903 WT CHX n = 19, *arr1,10,12* Mock n = 18, *arr1,10,12* CHX n = 19, *wol* Mock n = 15, *wol* CHX n =
904 19. Asterisks indicate statistically significant ($p < 0.05$) differences in Fisher's contingency table
905 tests (M) and Wilcoxon's rank sum tests (N) respectively.
906 **(O-R)** Cytokinin signaling is required for diffuse auxin signaling under translation inhibition. Shown
907 are late stage 2 buds of WT (O,P) and *arr1,10,12* (Q,R), treated with Mock or 2 μM CHX for 3
908 days. (O,Q) Auxin signaling reporter *DR5* in yellow, and *DR5* merged with Chlorophyll in magenta.
909 Arrows point to diffuse DR5 signal in variable positions in CHX-treated WT. Arrowheads show
910 four robust DR5 maxima in CHX-treated *arr1,10,12*. (P,R) Circular histograms of the *DR5* signal,
911 showing mean (solid line) and mean ± SD (shaded area). Sample size: WT Mock n = 17, WT CHX
912 n = 18, *arr1,10,12* Mock n = 7, *arr1,10,12* CHX n = 7. Scale bars in all micrographs, 25 μm.
913

914 **Figure 6. Upregulation of cytokinin signaling is required to maintain translation and fitness**
915 **in *drmy1*.**
916 **(A)** Puromycin labeling of WT seedlings with 4 h CHX pre-treatment (control), and three biological
917 replicates each of WT and *arr1 35S::ARR1* seedlings with 4 h mock pre-treatment. All seedlings
918 are 14 days old. RuBisCO large subunit in Ponceau S-stained membrane is shown as a loading
919 control. Signal ratio between puromycin and Ponceau S, normalized to mean of WT, is show on
920 the bottom. P-value is from a two-sided Student's t-test. Also see Karunadasa et al. (2020).
921 **(B,C)** Puromycin labeling of WT seedlings with 4 h CHX pre-treatment (control), and two biological
922 replicates of WT, *drmy1*, *wol*, and *drmy1 wol* seedlings with 4 h mock pre-treatment. Seedlings
923 are 8 days old in (B) and 14 days old in (C). RuBisCO large subunit in Ponceau S-stained
924 membrane is shown as a loading control. Letters show compact letter display of a Tukey's all-pair
925 comparison in a one-way ANOVA model.
926 **(D)** Representative 14 days old seedling images of WT, *drmy1*, *wol*, and *drmy1 wol* used in (C).
927 Notice that *drmy1 wol* is very small and pale. Scale bars, 5 mm.
928 **(E)** Representative aerial part images of 42 days old plants of WT, *drmy1*, *wol*, and *drmy1 wol*.
929 Inset shows the zoomed-in *drmy1 wol* plant, which has a tiny rosette and a short inflorescence.
930 Scale bars, 5 cm. See also Figure S6F.
931 **(F)** Representative aerial part images of 74 days old plants of WT, *drmy1*, *arr1*,*10*,*12*, and *drmy1*
932 *arr1*,*10*,*12*. Inset shows the zoomed-in *drmy1 arr1*,*10*,*12* plant, which has pale leaves
933 accumulating anthocyanin and a short inflorescence. Scale bars, 5 cm. See also Figure S6E.
934 **(G)** Dissected siliques of *arr1,10,12* (left) and *drmy1 arr1,10,12* (right) showing developing
935 seeds. Notice that while *arr1,10,12* occasionally have aborted seeds, all seeds in the *drmy1*
936 *arr1,10,12* silique were aborted. Scale bars, 0.2 mm.

937 **Figure 7. ARR7 and AHP6 protein levels are reduced upon inhibition of TOR and**
938 **translation.**
939 **(A)** The hypothesis. During hormone patterning prior to sepal initiation in the WT floral meristem,
940 A-type ARR and AHP6 proteins are rapidly produced to dampen cytokinin signaling to a normal
941 level. In *drmy1*, reduced protein synthesis causes reduced levels of these cytokinin signaling
942 inhibitor proteins, resulting in an upregulation of cytokinin signaling.
943 **(B)** Illustration of Llama Tag. Plants were co-transformed with *ARR7-llama* (*pARR7::ARR7-linker-*
944 *llama-ARR7ter*) and *GFP-nes* (*pUBQ10::sfGFP-nes-UBQ3ter*). Without ARR7-llama, GFP
945 localizes to the cytosol due to the nuclear export sequence (nes). ARR7-llama is produced in the
946 cytoplasm, C, and translocates into the nucleus, N. The Llama Tag on ARR7-llama binds to GFP
947 and drags GFP into the nucleus (note that from our observation it is excluded from the nucleolus,
948 NL). Thus, at low ARR7-llama levels, GFP signal is mainly in the cytoplasm. At intermediate
949 ARR7-llama levels, GFP is at comparable levels between the cytoplasm and the nucleus, and no
950 clear pattern can be seen. At high ARR7-llama levels, GFP is mainly seen in the nucleus.
951 **(C)** A *GFP-nes* bud showing localization of the GFP signal to the cytoplasm.
952 **(D,E)** GFP images of buds from two independent transgenic lines of *ARR7-llama GFP-nes*, 7-4
953 (D) and 7-6 (E), of WT (top) vs *drmy1* (bottom) genotypes. Images are representative of n = 17
954 (line 7-4, WT), n = 40 (line 7-4, *drmy1*), n = 9 (line 7-6, WT), and n = 6 (line 7-6, *drmy1*) buds.
955 Note that GFP is more cytoplasm-localized in *drmy1* than WT, indicating reduced ARR7-llama
956 protein level.
957 **(F)** GFP images of WT *ARR7-llama GFP-nes* buds treated with mock (top) or 2 μM CHX (bottom)
958 for 24 hours. The mock image is representative of n = 20 buds from three independent lines. The
959 CHX image is representative of n = 19 buds from these same lines.
960 **(G)** GFP images of WT *ARR7-llama GFP-nes* buds treated with mock (top) or 2 μM AZD-8055
961 (bottom) for 72 hours. The mock image is representative of n = 13 buds from two independent
962 lines. The AZD-8055 image is representative of n = 11 buds from these same lines. For (C-G),
963 each image was brightened to reveal subcellular localization patterns of GFP. A square region
964 taken from the image containing 5-10 cells is enlarged and shown on the top right. Within the
965 square, GFP intensity was quantified along the dotted line and plotted on the bottom right. X-axis,
966 pixels (range 0-238). Y-axis, GFP intensity (smoothened by taking the average intensity of 11-
967 pixel neighborhoods; range 90-210 in gray value).
968 **(H-I)** Response of the AHP6 protein reporter (H) and transcriptional reporter (I) to mock, CHX,
969 and AZD-8055 treatments for 72 hours. For (H), images are representative of n = 29 (mock), n =
970 29 (CHX), and n = 34 (AZD-8055) buds in three experiments. For (I), images are representative
971 of n = 11 (mock), n = 9 (CHX), and n = 12 (AZD-8055) buds in two experiments.
972 **(J-Q)** Reduction of A-type ARR and AHP6 protein levels contribute to the variability in sepal
973 initiation. (J-O) Stage 5-6 buds of indicated genotype stained with propidium iodide. Arrowheads
974 indicate sepal primordia that are variable in number, position, and/or size. Note that the
975 *arr3,4,5,6,7,8,9,15* bud has an inner sepal that is slightly smaller than its outer sepal and
976 positioned slightly right-skewed (K). The *ahp6* bud develops five sepal primordia of variable sizes
977 and unevenly positioned (L). The *ARR7-llama GFP-nes* constructs partially rescue the *drmy1*
978 phenotype in some buds (O, left) but not others (O, right). (P) Quantification of sepal primordium

979 number. Asterisk indicates statistically significance difference in a Fisher's exact test (WT vs
980 *ahp6*, p = 3.026×10^{-7}; *drmy1* vs *drmy1 ARR7-llama GFP-nes*, p = 0.4389). (Q) Quantification of
981 variability in sepal primordium position. Asterisk indicates statistically significant difference in a
982 Wilcoxon rank sum test (WT vs. arr3,4,5,6,7,8,9,15, p = 2.948×10^{-4}; WT vs *ahp6*, p = $2.137\times10^{-}$
983 ^{11}; WT vs *ARR7-llama GFPnes*, p = 1; *drmy1* vs *drmy1 ARR7-llama GFPnes*, p = 1.538×10^{-7}).
984 Data for *drmy1* were reused from Figure 2H, 2J. Data for *ARR7-llama GFP-nes* and *drmy1 ARR7-*
985 *llama GFP-nes* were pooled from two independent lines (7-4 and 7-6). Sample size: WT, n = 78;
986 *arr3,4,5,6,7,8,9,15*, n = 28; *ahp6*, n = 106; *ARR7-llama GFPnes*, n = 16; *drmy1*, n = 67; *drmy1*
987 *ARR7-llama GFP-nes*, n = 20.
988 **(R)** Working model. In WT, DRMY1 maintains TOR activity and translation, which sustains the
989 rapid production of cytokinin signaling inhibitors (ARR7 and AHP6) in response to cytokinin
990 signaling. These inhibitors maintain cytokinin signaling at a normal level, allowing auxin and
991 cytokinin signaling to interact and form robust spatial patterns. Robust patterning of auxin and
992 cytokinin signaling gives rise to robustly initiated sepal primordia. In *drmy1*, due to decreased
993 TOR signaling and translation rate, the meristem cannot rapidly produce cytokinin signaling
994 inhibitor proteins in response to cytokinin signaling. As a result, cytokinin signaling is upregulated,
995 which rescues the translation rate reduction in a homeostatic mechanism. This upregulation of
996 cytokinin signaling disrupts the robust spatial pattern of both cytokinin and auxin signaling, which
997 in turn causes variability in sepal initiation. Scale bars in all micrographs, 25 μm.
998

999 **MATERIALS AND METHODS**

1000

1001 **Plant material**

1002 Most Arabidopsis plants were in Col-0 background (WT). *ap1 cal 35S::AP1-GR* was in Ler
1003 background. *drmy1* (Col-0) was backcrossed to Ler twice and then crossed with *ap1 cal*
1004 *35S::AP1-GR* to obtain *drmy1 ap1 cal 35S::AP1-GR*. R2D2 was originally in Col-Utrecht
1005 background and was backcrossed twice into WT (Col-0) and *drmy1* (Col-0). The following mutants
1006 and reporters were previously described: *drmy1-2*[27], *wol-1*[153], *spaghetti-1* (*tpr5-1*)[154], *ahp6*[16],
1007 *arr3,4,5,6,7,8,9,15*[101], *ap1 cal 35S::AP1-GR* (Ler)[35,36], *arr1-1 35S::ARR1*[74], *DR5::3xVENUS-*
1008 *N7*[155], *TCS::GFP*[156], *pARF5::ER-EYFP-HDEL*[157], *pUS7Y-mDII-NtdTomato-pUS7Y-DII-*
1009 *N3xVENUS* (R2D2)[109], *35S::mCirtine-RCI2A*[27], *UBQ10::mCherry-RCI2A*[27], *pAHP3::AHP3-*
1010 *GFP*[100], *pAHP6::AHP6-VENUS*[16], and *pAHP6::GFP-ER*[16,97]. The following mutants and reporter
1011 lines were obtained from Arabidopsis Biological Resource Center (ABRC): *ul4z* (SALK_130595),
1012 *ul4y* (SALK_029203), *ul18z* (SALK_089798), *arr1-3 arr10-5 arr12-1*[158] (CS39992), *lst8-1-1*
1013 (SALK_002459), *pARF3::N3xGFP*[159] (CS67072), *pARF6::N3xGFP*[159] (CS67078),
1014 *pARF8::N3xGFP*[159] (CS67082), *pARF10::N3xGFP*[159] (CS67086).

1015

1016 **Llama-tagged ARR7 construct**

1017 For the LlamaTag system, we first generated plasmid *pVV13* containing linker-llama. We
1018 amplified the LlamaTag (from a plasmid containing vhhGFP4[160]) and added a linker sequence of
1019 tccggagcagctgcggctgccgctgcggcagcggccactagt at its 5' end by two rounds of overlap PCRs.
1020 Primers for the first round were oVV64 and oVV53, and primers for the second round were oVV35
1021 and oVV53. After the second round, we A-tailed the PCR product according to the Promega
1022 manufacturer's protocol. A-tailed product was ligated to the pGEMTeasy vector according to the
1023 Promega ligation protocol, to create the plasmid *pVV13*.

1024 To make *pARR7::ARR7-llama*, a genomic fragment of *pARR7::ARR7* minus the stop
1025 codon and terminator was amplified from the Arabidopsis (Col-0) genome using the primers
1026 oSK197 and oSK198. The linker-llama fragment was PCR-amplified from *pVV13* using the
1027 primers oSK199 and oSK200. The *ARR7* stop codon, 3' UTR, and terminator was amplified from
1028 the Arabidopsis (Col-0) genome using the primers oSK201 and oSK202. *pMLBART* backbone
1029 was digested with NotI, and all fragments were assembled into *pMLBART* using NEBuilder
1030 according to the manufacturer's protocol.

1031 To make *pUBQ10::sfGFP-NES:UBQ3ter*, sfGFP sequence was amplified from the *35S-*
1032 *sfGFP-nosT* plasmid[161] (Addgene # 80129) using primers UsfGM-F1 and UsfGnes-R1. The
1033 UBQ10 promoter was amplified from the *UPG* plasmid[162] (Addgene # 161003) using primers
1034 OutALFd and UsfGM-R1. The UBQ3 terminator was amplified from the *UPG* plasmid[162] (Addgene
1035 # 161003) using primers UsfGnes-F1 and OutALRb. Primer overhangs spanning the junction
1036 between sfGFP and the UBQ3 terminator contain the sequence of the mouse PKIα NES.
1037 *pCambia1300* backbone was digested with BamHI and KpnI, and all fragments were Gibson-
1038 assembled into the backbone. Sequences of primers, *pARR7::ARR7-llama*, and *pUBQ10::sfGFP-*
1039 *NES:UBQ3ter* can be found in Supplemental Dataset 5.

1040 Col-0 plants were co-transformed with *pARR7::ARR7-llama* and *pUBQ10::sfGFP-*
1041 *NES:UBQ3ter*, and selected with Basta (for *pARR7::ARR7-llama*) + Hygromycin (for
1042 *pUBQ10::sfGFP-NES:UBQ3ter*). Surviving T1 plants were screened for clear nuclear signal in the
1043 inflorescence, and 5 independent T1 plants were selected and crossed into *drmy1*. F2 plants from
1044 each line were again selected with Basta + Hygromycin and genotyped. One line showed co-
1045 segregation with the *DRMY1* locus. Two lines showed severe silencing in the F2 and could not
1046 be used. Two lines (7-4 and 7-6), though with minor silencing in F2, were used for imaging and
1047 image analysis. F3 plants of 7-4 and 7-6 had severe silencing, and therefore only F2 were imaged.
1048

1049 **Plant growth conditions**

1050 For most experiments, seeds were sown in wetted Lamber Mix LM-111 soil and stratified
1051 at 4°C for 3-5 days. For experiments including *drmy1 wol* and *drmy1 arr1,10,12*, all seeds were
1052 sown onto ½ MS plates with 0.05% (w/v) MES, 1% (w/v) sucrose, 1.2% (w/v) agar, pH 5.7, and
1053 stratified at 4°C for a week. They were grown for 7-10 days before being transplanted to soil (for
1054 imaging of inflorescence or aerial part of the plant) or left on the plates until desired time of the
1055 experiment (for seedling imaging or puromycin labeling).

1056 Most plants were grown under 16 h – 8 h light-dark cycles (fluorescent light, ~100 μmol
1057 m^{-1} s^{-1}) at 22°C in a Percival walk-in growth chamber. We found that the *drmy1* phenotype is more
1058 pronounced in this condition than under continuous light. The *ap1 cal 35S::AP1-GR* and *drmy1*
1059 *ap1 cal 35S::AP1-GR* plants were grown in soil under continuous light at 16°C to prevent
1060 premature floral induction.
1061

1062 **Flower staging**

1063 Flower buds were staged as previously described[37]. Briefly, stage 1 is when the floral
1064 meristem emerges, but not yet separated, from the inflorescence meristem. Stage 2 is when the
1065 floral meristem separates from the inflorescence meristem but with no floral organs initiated.
1066 Stage 3 is when sepal primordia initiate. Stage 4 is when sepal primordia bend to cover part of
1067 the floral meristem. Stage 5 is when stamen primordia initiate. Stage 6 is when sepal primordia
1068 completely cover the floral meristem.
1069

1070 **RNA-seq data collection and analysis**

1071 For RNA-seq in the inflorescence, bolting *ap1 cal 35S::AP1-GR* and *drmy1 ap1 cal*
1072 *35S::AP1-GR* plants were induced daily with an aqueous solution containing 10 μM
1073 dexamethasone (Sigma-Aldrich), 0.01% (v/v) ethanol, and 0.015% (v/v) Silwet L-77
1074 (Rosecare.com). When sepals initiated from the floral meristems, usually on the fourth day after
1075 three daily inductions, three inflorescence samples per genotype (including inflorescence
1076 meristems and buds under stage 6) were collected and immediately put into liquid nitrogen. RNA
1077 extraction, library preparation, RNA-seq, and data analysis for inflorescence samples were done
1078 as previously described[27] with a few changes. After read mapping, genes with at least two raw
1079 reads in at least two biological replicates in either WT or *drmy1* were kept for downstream
1080 analysis. For differentially expressed genes, we set a log2 fold change threshold of ±1 and a BH-
1081 adjusted p-value threshold of 0.05. For GO term enrichment, gene-GO mapping data was

1082 obtained from TAIR (https://www.arabidopsis.org
1083 /download_files/GO_and_PO_Annotations/Gene_Ontology_Annotations/ATH_GO_GOSLIM.txt)
1084 . The R package "topGO"[163] (version 2.38.1) was used for the enrichment, with statistic "fisher",
1085 algorithm "weight01", annotation function "annFUN.gene2GO", and minimum node size 10. The
1086 results were ranked by their p-value, and the first 8 terms were plotted.
1087 For RNA-seq in seedlings, WT and *drmy1* seedlings were grown to quiescence (7 days)
1088 in ½ MS liquid media as previously described[34]. After 7 days, the media was replaced with ½ MS
1089 liquid media containing 15 mM glucose and incubated for 24 hours to activate TOR. Seedlings
1090 were then incubated with or without AZD-8055 in addition to 15 mM glucose in ½ MS liquid media
1091 for 2 hours before collecting tissue. RNA was extracted from 100 mg pooled seedlings using the
1092 Spectrum Plant Total RNA Kit (Sigma). This RNA was used as a template for RNA-Seq library
1093 synthesis and sequencing, which was performed by Novogene. RNA-seq data for AZD-8055
1094 treated WT and *drmy1* seedlings were preprocessed with fastp (v. 0.22.0) using default
1095 parameters. Preprocessed reads were then mapped to the TAIR10 reference genome using
1096 STAR (v. 2.7.10z_alpha_220314). Following alignment, BAM output files from STAR were used
1097 to generate feature counts for transcripts using subread-featureCounts (v. 2.0.3) and the
1098 Araport11 transcriptome. TPMs were generated using TPMCalculator (v. 0.0.3). Differential
1099 expression analysis was performed using feature count data and DESeq2 (v. 1.36.0).
1100 A list of genes with uORFs based on gene models of the TAIR10 Arabidopsis genome
1101 assembly were downloaded from von Arnim et al.[69]. For each gene, within each genotype, protein-
1102 transcript ratio was calculated as the ratio between mean protein abundance and mean transcript
1103 TPM across all bio-reps in our proteomics and RNA-seq datasets, respectively. This was log2-
1104 transformed, and the difference between *drmy1* and WT was calculated. This was used as an
1105 indicator of translation rate difference between *drmy1* and WT, although we acknowledge that
1106 other factors such as protein stability may affect this number. This was plotted against the number
1107 of uORFs in each gene model (0, 1, or ≥ 2).
1108
1109 **Proteomics**
1110 Five induced inflorescence samples of WT and *drmy1* in *ap1 cal AP1-GR* background
1111 were collected as described above. Samples were ground in liquid nitrogen. Total soluble proteins
1112 were extracted in ice-cold extraction buffer (50 mM PBS-HCl (pH 8.0) buffer with 150 mM NaCl,
1113 2% NP-40, 1 mM PMSF, 1x Roche cOmplete protease inhibitor cocktail (Sigma 11697498001),
1114 and 1x Halt TM Phosphatase inhibitor cocktail (ThermoFisher 78420)) and filtered through
1115 Pierce™ Micro-Spin Columns (30 µm pore size; Thermo Scientific 89879). Extracts were
1116 RuBisCO-depleted using Seppro Bubisco Kit (Sigma SEP070-1KT), concentrated, denatured,
1117 reduced, cysteine blocked, trypsin-digested, and TMT 10-plex labeled. Then, mass spectrometry
1118 was done using an UltiMate 3000 RSLCnano / Orbitrap Fusion system (Thermo Scientific). Raw
1119 data was searched against the NCBI protein database using PD 2.3 (Thermo Scientific) with
1120 Sequest HT searching engine. Precursor-based protein identification and relative quantification
1121 was done using the standard processing workflow in PD 2.3, with an additional node of Minora
1122 Feature Detector. Proteins with at least 2 supporting peptides were kept for downstream analysis.
1123 For each protein, data was fit with an ANOVA model and a p-value was calculated. Proteins with

1124 a p-value < 0.05 were considered differentially accumulated in *drmy1*. GO term enrichment was
1125 done as above, using genes corresponding to the differentially accumulated proteins.
1126
1127 **Polysome extraction and profiling**
1128 Three induced inflorescence samples of WT and *drmy1* in *ap1 cal AP1-GR* background
1129 were collected as described above, and polysomes were extracted as previously described[164].
1130 Briefly, samples were ground in liquid nitrogen, mixed with an extraction buffer twice the volume
1131 of pulverized tissue (0.2 M Tris pH 9.0, 0.2 M KCl, 0.025 M EGTA, 0.035 M $MgCl_2$, 1% (w/v) Brij-
1132 35, 1% (v/v) Triton X-100, 1% (v/v) Igepal CA-630, 1% (v/v) Tween-20, 1% (w/v) Sodium
1133 deoxycholate, 1% (v/v) Polyoxyethylene 10 tridecyl ether, 5 mM Dithiothreitol, 1 mM
1134 Phenylmethylsulfonyl fluoride, 100 µg/ml cycloheximide, 100 µg/ml chloramphenicol, 40 U/ml
1135 RNasin, 10 U/ml DNase I), and let sit on ice for 10 min. Samples were centrifuged at 4°C 4,000 g
1136 for 5 min, supernatant was transferred to a new tube, centrifuged at 4°C 16,000 g for 15 min, and
1137 supernatant was filtered through Miracloth.
1138 Polysome extracts were profiled as previously described[165]. Briefly, 600 µl of each sample
1139 were loaded onto a 15%-45% sucrose density gradient and centrifuged at 4°C 32,000 rpm in a
1140 SW41 rotor. Separated samples were fractionated at a rate of 0.375 mL/min in an Isco
1141 fractionation system, and absorbance at 254 nm was recorded.
1142
1143 **Puromycin labeling**
1144 Puromycin labeling was done as previously described[39], with slight modifications.
1145 In seedlings, when comparing WT and *drmy1*, in order to control for plant size, WT
1146 seedlings were grown for 8 days and *drmy1* seedlings were grown for 10 days (Figure 1E). When
1147 comparing WT, *drmy1*, *wol*, and *drmy1 wol*, we were unable to control for plant size because
1148 *drmy1 wol* seedlings were too small. We therefore controlled for plant age, and seedlings were
1149 grown to specified age (8 days for Figure 6B and 14 days for Figure 6C). Seedlings were
1150 harvested from plates and incubated with an incubation buffer (½ MS, 0.05% (w/v) MES, 1% (w/v)
1151 sucrose, 0.1% (v/v) Tween-20, 0.1% (v/v) DMSO, 1x Gamborg vitamin mix, pH 5.7), with or
1152 without 50 µM CHX, for 4 hours in an illuminated growth chamber. Then, the buffer was replaced
1153 with a fresh incubation buffer (which is same as above, but contains 50 µM puromycin (GoldBio
1154 P-600-100)), and incubation continued for another 45 min.
1155 In inflorescences of WT and *drmy1* in *ap1 cal AP1-GR* background, inflorescences were
1156 DEX-induced as described above. Inflorescence samples were collected and put in an incubation
1157 buffer (½ MS, 1% (w/v) sucrose, 0.02% (v/v) Silwet L-77, 0.1% (v/v) DMSO, 50 µM puromycin,
1158 1x Gamborg vitamin mix, pH 5.7), with or without 100 µM CHX. Samples were vacuum infiltrated
1159 for 15 minutes and then put on a rocking shaker in an illuminated growth chamber for 45 minutes.
1160 In both cases, at the end of the incubation, samples were washed three times with water,
1161 blot dry, weighed, and frozen in liquid nitrogen. Soluble proteins were extracted as described
1162 above. Puromycin incorporated into the proteins were detected in a Western blot using a mouse-
1163 origin anti-puromycin monoclonal antibody (12D10, Sigma MABE343, lot # 3484967) and a goat-
1164 anti-mouse HRP-conjugated secondary antibody (Abcam ab6789, lot # 3436981). RuBisCO large
1165 subunit in Ponceau S-stained membrane was used as a loading control. Quantification was done

1166 in ImageJ. A background signal was determined using blank regions, and subtracted from all
1167 quantified signals (separately for puromycin and Ponceau S).
1168
1169 **TOR activity assay**
1170 WT and *drmy1* seedlings were grown in a six-well plate containing ½ MS liquid media.
1171 After seven days, the media were replaced with half-strength MS liquid media plus 15 mM glucose
1172 and incubated for 24 hours. At least 120 quiescent seedlings per sample were collected and
1173 frozen in liquid nitrogen. Protein was then extracted from the plant tissue in 100 mM MOPS (pH
1174 7.6), 100 mM NaCl, 5% SDS, 0.5% b-mercaptoethanol, 10% glycerin, 2 mM PMSF, and 1x
1175 PhosSTOP phosphatase inhibitor (Sigma). S6K-pT449 was detected by Western blot using a
1176 phosphospecific antibody (Abcam ab207399) and an HRP-conjugated goat anti-rabbit IgG
1177 secondary antibody (Jackson Immuno Research 111-035-003). Total S6K was detected using a
1178 custom monoclonal antibody described by Busche et al.[166]. Total protein visualized in Ponceau
1179 S-stained membrane was used as a loading control.
1180
1181 **Confocal microscopy**
1182 Confocal imaging of reporter lines in the inflorescence were done as previously
1183 described[27]. Briefly, main inflorescences (not side branches) were cut and dissected with a
1184 Dumont tweezer (Electron Microscopy Sciences, style 5, no. 72701-D) to remove buds older than
1185 stage 9 or 10. The inflorescences were then inserted upright into a small petri dish (VWR, 60 x
1186 15 mm) containing inflorescence culture medium (1/2 MS, 1% (w/v) sucrose, 1x Gamborg vitamin
1187 mixture, 0.1% (v/v) plant preservative mixture (Plant Cell Technology) 1% (w/v) agarose, pH 5.8),
1188 leaving most of the stem inside the medium and the buds outside. They were then further
1189 dissected to reveal stage 6 and younger buds, immersed with water, and imaged under a
1190 Zeiss710 upright confocal microscope with a 20x Plan-Apochromat water-dipping lens (1.0 NA).
1191 For live imaging experiments, inflorescence samples were put in a continuous-light growth
1192 chamber between time points. To prevent bacterial growth, samples were transferred onto fresh
1193 media every 2 to 3 days, and for live imaging experiments lasting longer than 6 days, once in the
1194 middle, plants were incubated with an aqueous solution of 100 µg/ml Carbenicillin (GoldBio, C-
1195 103-5, lot # 0129.091814A) for 30 minutes.
1196 To visualize tissue morphology of inflorescence samples without a reporter, samples were
1197 stained for 5 minutes with an aqueous solution of 0.1 mg/ml propidium iodide (PI) and 0.1% (v/v)
1198 Tween-20, washed three times with water, and imaged.
1199 The following laser and wavelength were used in confocal imaging. Chlorophyll, excitation
1200 488 nm, emission 647-721 nm. PI, excitation 514 nm, emission 566-659 nm. mCherry, excitation
1201 594 nm, emission 600-659 nm. tdTomato, excitation 561 nm, emission 566-595 nm. For
1202 EYFP/VENUS/mCitrine, in *35S::mCirtine-RCI2A*, excitation 514 nm, emission 519-580 nm; in
1203 *DR5::3xVENUS-N7*, excitation 514 nm, emission 519-569 nm; in *pARF5::ER-EYFP-HDEL*,
1204 excitation 514 nm, emission 519-550 nm; in *R2D2*, excitation 488 nm, emission 493-551 nm. For
1205 GFP/sfGFP, in *pARR7::ARR7-llama UBQ10::sfGFP-NES*, excitation 488 nm, emission 493-569
1206 nm; in *pARF3::N3xGFP*, *pARF6::*N3xGFP, *pARF8::N3xGFP*, and *pARF10::N3xGFP*, excitation
1207 488 nm, emission 493-564 nm; in *TCS::GFP*, excitation 488 nm, emission 493-513 nm.

1208
1209 **Visualization of tissue morphology**
1210 For single-channel image stacks intended for the visualization of tissue morphology
1211 (*35S::mCitrine-RCI2A* or PI), stacks were 3D-rendered using the ZEN confocal software
1212 (Processing -> 3D). Parameters were set to best visualize tissue morphology, typically, minimum
1213 5-10, ramp 60-80, maximum 100. Buds were rotated to desired orientation, and screenshots were
1214 taken using the "Create Image" button. For fluorophores that are dimmer, less sharp, or have a
1215 noisy background (*UBQ10::mCherry-RCI2A* or Chlorophyll), stacks were converted from LSM to
1216 TIF using ImageJ[167,168], loaded into MorphoGraphX[169], and screenshots were taken using the
1217 built-in screenshot function in MorphoGraphX.
1218 To aid visualizing tissue morphology and determine the timing of sepal initiation, each
1219 stack was fitted with a surface, and a Gaussian curvature heatmap was calculated from the
1220 surface (see below). We consider a sepal primordium as initiated when we see a dark red band
1221 of positive Gaussian curvature (primordium) separated from the center of the floral meristem by
1222 a dark blue band of negative Gaussian curvature (boundary)[27].
1223 Gaussian curvature heatmaps were calculated as previously described[27], with slight
1224 modifications. Briefly, stacks underwent the following processes in MorphoGraphX: Gaussian blur
1225 (3 times; X/Y/Z sigma = 1 μm for the first 2 times, and 2 μm for the third time), edge detection
1226 (threshold = 2000-8000 depending on the brightness of the stack, multiplier = 2.0, adapt factor =
1227 0.3, fill value = 30000), marching cube surface (cube size = 8 μm, threshold = 20000), subdivide
1228 mesh, smooth mesh (passes = 5), subdivide mesh, smooth mesh (passes = 5), project mesh
1229 curvature (type = Gaussian, neighborhood = 10 μm, autoscale = no, min curv = -0.0015, max curv
1230 = 0.0015). For ease of visualization, the lookup table "jet" was applied to the mesh.
1231
1232 **Quantification of sepal initiation robustness**
1233 For sepal primordium number, screenshots were taken of stage 3-6 buds of indicated
1234 genotypes, in either ZEN or MorphoGraphX. The number of sepal primordia initiated were
1235 counted from these screenshots.
1236 For variability in sepal primordium positioning, within each bud, an angular distance was
1237 measured between each pair of adjacent sepal primordia (with vertex at the center of the bud),
1238 using ImageJ. Note that the last pair was not measured – the angular distance was calculated as
1239 the sum of all other angular distances subtracted from 360°. A CV value (standard deviation
1240 divided by mean) was calculated from all the measured or calculated angular distances. Buds
1241 with sepal primordia evenly distributed around the bud periphery should have a small CV value,
1242 i.e. all angles are around 90° for four-sepal buds (or 72° for five-sepal buds, etc.). Buds whose
1243 sepal primordia distributed variably or randomly around the bud periphery will have widely varying
1244 angular distances between adjacent sepal primordia, and thus large CV values.
1245 Relative sepal initiation timing was quantified as previously described[27]. Briefly, dissected
1246 inflorescence samples were live-imaged every 6 hours. A Gaussian curvature heatmap was
1247 generated for each sample at each time point and was used to determine the time point at which
1248 a sepal primordium initiates. A sepal primordium is considered initiated at time point Tn if it is
1249 absent at time point T(n-1) but becomes present at time point Tn. Within the same bud, we

counted the number of time points between outer and inner sepal initiation, and between outer and lateral sepal initiation, and multiplied them by 6 hours to get the relative initiation timing of these sepals.

Quantification of fluorescent reporters

For *TCS::GFP*, *pARF3::N3xGFP*, *pARF5::ER-YFP-HDEL*, *pARF6::N3xGFP*, *pARF8::N3xGFP*, *pARF10::N3xGFP*, *pUS7Y::mDII-NtdTomato, pUS7Y::DII-N3xVENUS*, and *UBQ10::mCherry-RCI2A*, total signal (integrated density) was quantified from maximum intensity projection images using ImageJ[167,168]. Fluorescence intensity was measured in pixel intensity units (0-255 range). Signal intensity was calculated as total signal divided by area.

For both *TCS::GFP* and *DR5:3xVENUS-N7*, circular histogram analysis was done as previously described[27]. Briefly, individual buds were cropped out of image stacks, channels were split using FIJI and saved in TIF format, and TIF stacks were imported into MorphoGraphX. Signal from outside the buds (e.g. inflorescence meristem, parts of other buds within the same image) was manually removed using the Voxel Edit function. Buds were positioned so that the incipient sepal primordia are in the XY plane: the incipient outer sepal is at 45°, the incipient inner sepal and the inflorescence meristem are at 225°, and the incipient lateral sepals are at 135° and 315°, respectively. Fluorescence intensity was measured in pixel intensity units (0-255 range). A circular histogram of bin width 1° centered around the Z axis was exported for each replicate expressing DR5 and/or TCS. Multiple circular histograms of the same reporter and genotype were pooled and mean ± SD were plotted.

For GFP signal in plants carrying *pUBQ10::sfGFP-nes-UBQ3ter* and *pARR7::ARR7-linker-llama-ARR7ter* reporters, screenshots were taken in MorphoGraphX as described above. Screenshots were subtracted of a background determined using blank regions with no tissue, and brightened to the same level to reveal differences in GFP distribution patterns. A square region containing 5-10 cells were taken from each screenshot, and GFP intensity (in gray value ranging from 0 to 255) along a straight line of 239 pixels in length was quantified using ImageJ[167,168] (Analyze -> Plot profile). For ease of visualization, the curves were smoothed by taking the average of the gray value of 11 neighboring pixels (including itself) as the value of each pixel.

For VENUS or GFP signal in *pAHP6::AHP6-VENUS*, *pAHP6::GFP-ER*, *pAHP3::AHP3-GFP*, and *pUBQ10::mCherry-RCI2A* under mock, CHX, or AZD-8055 treatment, total signal at 24 hours (for CHX) or 72 hours (AZD-8055) was normalized by bud area in the 2D projection to get the signal intensity. To account for bud-to-bud differences in signal intensity prior to treatment, the signal intensity was normalized to the 0-hour time point (pre-treatment). Relative level between treatment and mock was calculated by normalizing this value to the mean of mock.

***In vitro* drug treatments on inflorescence samples**

For cycloheximide (CHX) treatment, a stock solution of 10 mM CHX was made from powder (Sigma C1988) in pH 4.0 water. The stock was filter-sterilized and stored in -20°C, and added to autoclaved inflorescence culture medium to a final concentration of 2 μM just before use. For AZD-8055 treatment, a stock solution of 16 mM AZD-8055 was prepared from powder (Cayman Chemical 16978) in DMSO within days of use, and stored in -80°C. The stock was

1292 added to autoclaved inflorescence culture medium to a final concentration of 2 μM. 0.0125% (v/v)
1293 DMSO was added to the mock medium. For 6-benzylaminopurine (BAP) treatment, a stock
1294 solution of 50 mM BAP was prepared from powder (Alfa Aesar A14678) in DMSO, and stored in
1295 -80°C. The stock was added to autoclaved inflorescence culture medium to a final concentration
1296 of 5 μM. 0.01% (v/v) DMSO was added to the mock medium.
1297 Inflorescences were dissected and inserted into regular inflorescence culture medium
1298 without drugs, and pre-treatment image stacks were captured. Then, they were transferred into
1299 specified treatment or mock media, and imaged at the specified time points. For live imaging,
1300 inflorescence samples were transferred onto new medium after each imaging session.
1301
1302 ***In vivo* Torin2 treatment**
1303 Starting at 14 days after germination, twice each day for 15 days, 2 nmol of Torin2
1304 (Cayman Chemical 14185) in 20 μl of aqueous solution containing 0.5% DMSO and 0.5% Tween-
1305 20 was applied to the center of the rosette using a pipette. For mock, 20 μl aqueous solution
1306 containing 0.5% DMSO and 0.5% Tween-20 was applied. At the end of the 15-day treatment
1307 period, inflorescences were dissected and put in the inflorescence culture medium for imaging.
1308 To prevent Torin2 degradation, throughout the duration of this experiment, the Torin2
1309 stock solution in DMSO was kept in -80°C and replaced each week, and the treatment and mock
1310 solutions were kept in 4°C and replaced each day.
1311
1312 **Imaging of whole plant, whole inflorescence, silique, and mature sepals**
1313 For whole-plant imaging, aerial parts of the plants were removed from the pots, flattened,
1314 put on a dark cloth, and imaged with a cell phone (iPhone 12, iOS 16.2).
1315 For whole-inflorescence imaging, inflorescences consisting of open flowers and unopened
1316 buds were removed from the plant and held with forceps. Images were taken under a Zeiss Stemi
1317 2000-C Stereo Microscope with a cell phone (iPhone 12, iOS 16.2).
1318 For silique imaging, siliques on inflorescences sufficiently distant from the shoot apex that
1319 were developed and started to ripen were picked with forceps, opened with a razor blade, and
1320 imaged under a Zeiss Stemi 2000-C Stereo Microscope with a cell phone (iPhone 12, iOS 16.2).
1321 Mature sepal imaging was done as previously described[26,27]. Briefly, mature sepals from
1322 stage 15 flowers (10th to 25th flower on the inflorescence) were dissected and sandwiched
1323 between two slides to flatten. Images were taken using a Canon Powershot A640 camera
1324 attached to a Zeiss Stemi 2000-C Stereo Microscope. Minor damages were manually fixed, and
1325 undesired objects such as pollen grains were manually removed from these images. Sepals with
1326 major damages were discarded. Then, a contour was extracted from each sepal using custom
1327 python scripts[26]. This gave us measurements such as length, width, area, etc. of each sepal. To
1328 measure between-flower variability of length, within each genotype and for each of outer, inner,
1329 and lateral positions, a CV (standard deviation divided by mean) of all sepals was calculated (for
1330 example, a CV of length of all outer sepals in WT). To determine statistical significance, genotypes
1331 were compared pairwise using permutation tests. To measure within-flower variability of length,
1332 a CV was calculated for all sepals within each flower (for example, a CV of length of outer, inner,
1333 and two lateral sepals in WT bud #10). For accurate calculation of CV, flowers with length data of

1334 at least four sepals were included in the analysis. To determine statistical significance, genotypes
1335 were compared pairwise using Wilcoxon rank sum tests.
1336
1337 **Cytokinin extraction and measurement**
1338 Cytokinin extraction was based on a previously published protocol[170] with modifications.
1339 Briefly, five inflorescence samples of induced *ap1 cal 35S::AP1-GR*, and six inflorescence
1340 samples of induced *drmy1 ap1 cal 35S::AP1-GR* were collected as described above. Samples
1341 were ground in liquid nitrogen and twice extracted in methanol : water : formic acid (15:4:1). 200
1342 pg of BAP per sample was added as an internal control. Extracts were centrifuged at 14,650 rpm
1343 in -4°C for 30 min, and supernatant was evaporated of methanol and reconstituted in 1% (v/v)
1344 acetic acid. Samples were passed through an Oasis MCX SPE column (Waters 186000252),
1345 washed with 1% acetic acid, washed with methanol, and eluted with 0.35 M ammonia in 70%
1346 methanol. Eluents were evaporated to complete dryness, reconstituted in 5% acetonitrile, and
1347 sent for LC-MS.
1348 LC-MS was done as previously described[171], with modifications. Briefly, 1 µl of each
1349 sample was injected into a Thermo Fisher Scientific Vanquish Horizon UHPLC System coupled
1350 with a Thermo Q Exactive HF hybrid quadropole-orbitrap high-resolution mass spectrometer
1351 equipped with a HESI ion source. Samples were separated on a C18 ODS column (AQUITY
1352 UPLC BEH C18, 1.7 µm, 2.1 × 100 mm, Waters), at a flow rate of 0.3 ml/min, with linear gradients
1353 of solvent A (0.1% formic acid) and solvent B (0.1% formic acid in methanol) according to the
1354 following profile: 0 min, 99.0% A + 1.0% B; 4.0 min, 55.0% A + 45.0% B; 7 min, 30.0% A + 70.0%
1355 B; and then with isocratic conditions: 8 min, 1.0% A + 99.0% B; 12 min, 99.0% A + 1.0% B.
1356 Cytokinins were detected using the positive ion mode.
1357 For tZ, tZR, iP, iPR, and the internal control BAP, peaks were identified from an external
1358 standard mix composed of 0.1 µg/ml each of BAP (Alfa Aesar A14678), tZ (Sigma Z0876), tZR
1359 (Sigma Z3541), iP (Cayman Chemical 17906), and iPR (Cayman chemical 20522) in 5%
1360 acetonitrile. For cZ and cZR, peaks were identified based on previously reported precursor m/z
1361 and retention time[172]. Using Xcalibur (Thermo Scientific), peak area was quantified for each
1362 cytokinin in each sample, normalized against the peak area of BAP (internal control) and sample
1363 fresh weight, and then normalized against the average abundance of tZ in WT samples.
1364
1365 **Software**
1366 Image processing was done in ImageJ (version 2.9.0/1.53t, build a33148d777)[167,168] and
1367 MorphoGraphX (version 2.0, revision 1-294, CUDA version 11.40)[169].
1368 Data processing was done in RStudio (R version 4.0.5 “Shake and Throw” (2021-03-
1369 31))[173]. Graphs were made using the package ggplot2 (version 3.3.3)[174]. Fisher’s contingency
1370 table tests were done using the function fisher.test in R. Wilcoxon rank sum tests were done using
1371 the function wilcox.test in R. Hypergeometric tests were done using the function phyper in R. Data
1372 fitting with ANOVA was done using the function aov in R.
1373 Figures were assembled in Adobe Illustrator (version 25.4.1). An RGB color profile “Image
1374 P3” was used for all the figures.
1375

1376 **Accession numbers**

1377 RNA-seq data for *ap1 cal AP1-GR* and *drmy1 ap1 cal AP1-GR* inflorescence tissue were
1378 deposited in Gene Expression Omnibus (GEO) under accession number GSE230100. RNA-seq
1379 data for WT and *drmy1* seedlings treated with mock or AZD-8055 were deposited in NIH
1380 BioProject under accession number PRJNA961813. Mass spectrometry data for proteomics were
1381 deposited in the ProteomeXchange Consortium via the PRIDE[175] partner repository under
1382 accession number PXD041723 (reviewer username: reviewer_pxd041723@ebi.ac.uk, and
1383 password: 8pl3ZD1l). Mass spectrometry data for cytokinins were deposited in NIH's National
1384 Metabolomics Data Repository (NMDR) website, the Metabolomics Workbench[152], under
1385 accession number ST002571.
1386

1387 **SUPPLEMENTAL INFORMATION TITLES AND LEGENDS**
1388
1389 **Supplemental Figure 1. Evidence that the *drmy1* mutant has ribosomal and translation**
1390 **defects, associated with Figure 1.**
1391 **(A)** The *drmy1* phenotype is reproduced in the *ap1 cal AP1-GR* system (Ler background). Shown
1392 are representative buds of *ap1 cal AP1-GR* (top row) *and drmy1 ap1 cal AP1-GR* (bottom row) at
1393 day 0 (before DEX induction), day 3 (after 3 DEX inductions, when tissue is collected for RNA,
1394 protein, or cytokinin extraction), and day 5 (after 5 DEX inductions). Arrowheads show sepal
1395 primordia that are of variable number, position, and sizes. Asterisks indicate periphery of the floral
1396 meristem that has limited or no sepal outgrowth. Scale bars, 25 μm.
1397 **(B)** Summary of the inflorescence RNA-seq and proteomics datasets. Shown are numbers of
1398 genes in each category. Down, downregulated in *drmy1*; NS, not significantly changed between
1399 *drmy1* and WT; Up, upregulated in *drmy1*; NA, not available. Note that in the combined dataset
1400 (gene-protein pairs), different genes encoding for the same protein were separately counted, so
1401 were different proteins encoded by the same gene. See also Supplemental Dataset 1.
1402 **(C)** Violin and box plots of log2 fold change in RNA between *drmy1* and WT in induced *ap1 cal*
1403 *AP1-GR* inflorescence, for genes encoding ribosomal components ("Structural constituents of the
1404 ribosome" GO:0003735, and its offspring terms) and all other genes involved in translation
1405 ("Translation" GO:0006412, and its offspring terms). The following genes are labeled on the
1406 graph: *UL4Z* (AT3G09630), log2FC = -0.492; *UL4Y* (AT5G02870), log2FC = -0.509; *UL18Z*
1407 (AT3G25520), log2FC = -0.459.
1408 **(D-G)** Fluorescence of a constitutively expressed marker supports the hypothesis that *drmy1* has
1409 reduced translation rate. (D-F) Representative confocal images of *UBQ10::mCherry-RCI2A* in
1410 dissected inflorescences of WT (D), *drmy1* (E), and *ul4y* (F). Numbers show how the signal is
1411 divided based on the stage of floral meristem when quantified (IM+1, inflorescence meristem plus
1412 stage 1; 2, stage 2; 3, stage 3). Scale bars, 25μm. (G) Signal intensity (i.e. integrated density
1413 divided by area) in all images divided as in (D-F). Mean $\pm$ SD are shown. Data was fit using a
1414 two-way ANOVA model with genotype and stage as two additive factors. Asterisks show
1415 statistically significant pairwise contrasts between WT and *drmy1* ($p < 2\times10^{-16}$) and between WT
1416 and *ul4y* ($p = 2.1\times10^{-15}$). Sample sizes: WT IM+1, n = 30; *drmy1* IM+1, n = 22; *ul4y* IM+1, n = 18;
1417 WT stage 2, n = 99; *drmy1* stage 2, n = 100; *ul4y* stage 2, n = 52; WT stage 3, n = 39; *drmy1*
1418 stage 3, n = 27; *ul4y* stage 3, n = 26.
1419 **(H)** Violin and box plots of log2 fold change in protein level between *drmy1* and WT in induced
1420 *ap1 cal AP1-GR* inflorescence, for genes in the same categories as in (C). The following genes
1421 are labeled on the graph: *UL4Z* (AT3G09630), log2FC = 0.352; *UL4Y* (AT5G02870), log2FC =
1422 0.811; *UL18Z* (AT3G25520), log2FC = 0.742.
1423 **(I)** Coherent regulation of gene expression by *drmy1* and AZD-8055. Shown is a contingency
1424 table of genes downregulated (Down), not significantly changed (NS), and upregulated (Up) in
1425 *drmy1* vs WT (columns), and in AZD-8055-treated WT vs mock-treated WT (rows). Bold font
1426 shows the number of genes in each category, and gray font shows the expected number of genes
1427 if there were no correlation between two conditions (calculated as row margin × column margin /
1428 total number of genes). Categories where the number of genes is above expectation are

1429 highlighted blue, and categories where the number of genes is below expectation are highlighted
1430 red. Chi-square test $p < 2.2\times10^{-16}$.
1431 **(J)** Gene ontology enrichment of genes coherently downregulated by both *drmy1* and AZD-8055.
1432 Shown are the top 8 terms and their enrichment p-values. Note that the first 7 terms are all related
1433 to ribosome and translation. A complete list can be found in Supplementary Dataset 3.
1434

1435 **Supplemental Figure 2. Ribosomal mutations enhance the *drmy1* phenotype, associated**
1436 **with Figure 2.**
1437 **(A-H)** Examples of stage 5 buds from *drmy1* (A), *drmy1 ul4z* (B-D), *drmy1 ul4y* (E-F), and *drmy1*
1438 *ul18z/+* (G-H). In (B,E,G) sepal primordia within each bud have bigger size differences than typical
1439 *drmy1* single mutant buds; asterisks show giant outer sepal primordia and brackets show bud
1440 peripheral regions with little or no primordium outgrowth. In (C,F,H), arrowheads show 6 sepal
1441 primordia within each bud, which does not occur in *drmy1*. In (D,H), asterisks show the presence
1442 of two outer sepal primordia within a bud, instead of one in *drmy1*. Scale bars, 25μm.
1443 **(I-J)** Quantification of sepal primordium number (I) and positional variability (J), comparing each
1444 of *drmy1 ul4z* (n = 60), *drmy1 ul4y* (n = 61), and *drmy1 ul18z/+* (n = 69) with *drmy1* (n = 67). "ns"
1445 indicates no significant difference in Fisher's contingency table tests (I) and Wilcoxon's rank sum
1446 tests (J) respectively. Data for *drmy1* is reused from Figure 2H, 2J.
1447 **(K)** Dissected young silique of a *drmy1 ul18z/+* plant. Arrowheads point to aborted ovules. Scale
1448 bar, 200 μm.
1449

1450 **Supplemental Figure 3. Sepal primordia in ribosome and TOR mutants catch up in growth**
1451 **to form uniformly sized mature sepals within the bud, associated with Figure 3.**
1452 **(A-F)** Inflorescences (left) of WT (A), *drmy1* (B), *ul4z* (C), *ul4y* (D), *ul18z* (E), and *lst8-1-1* (F), with
1453 boxed regions enlarged (right). Blue arrowheads show sepals of regular length, and red
1454 arrowheads show sepals shorter than others. Note that sepals in *drmy1* were unable to close due
1455 to unequal lengths, while sepals in *ul4z*, *ul4y*, and *ul18z*, and close like in WT. Sepals in *lst8-1-1*
1456 were unable to close although there is no apparent variation in length. Scale bars, 0.5 mm.
1457 **(G-L)** Dissected sepals from a bud of WT (G), *drmy1* (H), *ul4z* (I), *ul4y* (J), *ul18z* (K), and two
1458 buds of *lst8-1-1* (L). Note that sepals in the *drmy1* bud are of different sizes. Sepals within each
1459 bud of *ul4z*, *ul4y*, *ul18z*, and *lst8-1-1* are of similar sizes, although there can be variation between
1460 different buds of the same genotype. O, outer sepal. I, inner sepal. L, lateral sepal. Scale bars,
1461 200 μm.
1462 **(M)** Quantification of between-flower variability of sepal length. Length was measured from all
1463 imaged sepals of each genotype and each position (outer, inner, lateral), and coefficient of
1464 variation (CV) was calculated. A two-sided permutation test (100,000 permutations) for CV
1465 difference not equating to zero was done for each pair of genotypes, and results were represented
1466 by letters. Sample size: Outer sepal, WT n = 35, *drmy1* n = 43, *ul4z* n = 37, *ul4y* n = 42, *ul18z* n
1467 = 39, *lst8-1-1* n = 43. Inner sepal, WT n = 34, *drmy1* n = 46, *ul4z* n = 38, *ul4y* n = 44, *ul18z* n =
1468 37, *lst8-1-1* n = 44. Lateral sepal, WT n = 65, *drmy1* n = 84, *ul4z* n = 81, *ul4y* n = 89, *ul18z* n =
1469 76, *lst8-1-1* n = 82.
1470 **(N)** Quantification of within-flower variability of length. Flowers with length data from at least four
1471 sepals were analyzed. A CV of length from all sepals within each flower was calculated, and mean
1472 ± SD was plotted, grouped by genotype. A Wilcoxon rank sum test was done for each pair of
1473 genotypes, and results were represented by letters. Sample size: WT n = 31 buds, *drmy1* n = 38
1474 buds, *ul4z* n = 33 buds, *ul4y* n = 36 buds, *ul18z* n = 32 buds, *lst8-1-1* n = 39 buds.
1475 **(O-Q)** Live imaging of sepal development from stage 3 to 6 in WT (O), *drmy1* (P), and *ul4y* (Q),
1476 showing chlorophyll or propidium iodide channel, and Gaussian curvature of the surface. Note
1477 that both *drmy1* and *ul4y* have inner sepals that initiate late (day 2, asterisk). The *drmy1* inner
1478 sepal develops slowly, and leaves the bud open at day 3 (red arrowhead). The *ul4y* inner sepal
1479 catches up with the rest of the sepals and closes the bud (blue arrowhead). Scale bars, 25 μm.
1480

1481 **Supplemental Figure 4. Inhibition of TOR activity and translation causes auxin maxima**
1482 **formation at variable positions, correlated with variable positions of sepal primordia,**
1483 **associated with Figure 4.**
1484 **(A-E)** Variable patterning of auxin signaling in *drmy1*, *ul4y*, and CHX-treated WT buds
1485 corresponds to variable sepal initiation. During the time course, top rows show *DR5::3xVENUS-*
1486 *N7* (yellow), middle rows show composites of *DR5* (yellow) and Chlorophyll (magenta), and
1487 bottom rows show Gaussian curvature of the Chlorophyll channel. In the last time point, buds
1488 were stained with propidium iodide (top), and Gaussian curvature of the propidium iodide channel
1489 is shown on the bottom.
1490 (A) In WT, four robustly positioned auxin maxima at day 1 correlates with four robustly positioned
1491 sepal primordia at day 4 (blue arrowheads). (B) In *drmy1*, at day 1 there are three robustly
1492 positioned auxin maxima (blue arrowheads). At day 2, a diffuse band of auxin signaling occurs in
1493 the adaxial periphery of the bud, joining with one of the lateral auxin maxima (red bracket). At day
1494 3, this diffuse band splits into three auxin maxima (red arrowheads), making a total of 5. The
1495 maxima correlate with the five sepal primordia at day 4, three at robust positions (blue
1496 arrowheads) and two at irregular positions (red arrowheads). (C) In *ul4y*, at day 1 there are two
1497 auxin maxima at robust positions (blue arrowheads), one at robust lateral position but much
1498 weaker (red arrowhead), and a band of weak auxin signaling in the adaxial periphery of the bud
1499 (red bracket). At day 2, the weak auxin maxima at the lateral position got stronger, and the weak
1500 band at the adaxial position split into two auxin maxima (red arrowheads). These five auxin
1501 maxima correspond to the five sepal primordia at day 3, three in robust positions (blue
1502 arrowheads) and two in irregular positions (red arrowheads). (D) In a mock-treated WT bud, four
1503 robust auxin maxima at day 6 of the treatment grow into four robust sepal primordia at day 9 (blue
1504 arrowheads). (E) In a CHX-treated WT bud, at day 6 there are three stronger auxin maxima (blue
1505 arrowheads) and two weaker ones (red arrowheads), corresponding to three bigger regions of
1506 outgrowth (blue arrowheads) and two smaller ones (red arrowheads) at day 9. For ease of display,
1507 the DR5 channel in CHX-treated WT was brightened three times relative to mock.
1508 **(F-I)** TOR inhibition using Torin2 causes increased cytokinin signaling, and occasional spatial
1509 variability in auxin and cytokinin signaling. (F) Late stage 2 buds of WT treated *in vivo* with mock
1510 or 2 nmol Torin2 twice a day for 15 days. Shown are *DR5::3xVENUS-N7* in yellow, *TCS::GFP* in
1511 cyan, and both merged with propidium iodide in magenta. Note that 3/16 (19%) buds had variable
1512 number and position of DR5 and TCS maxima, and 13/16 (81%) had robust DR5 and TCS
1513 maxima, although TCS intensity is higher than mock in both cases. (G) Quantification of TCS
1514 intensity from maximum intensity projection images, normalized to the mean of WT mock. Shown
1515 are mean ± SD. Asterisk shows statistical significance in a two-tailed Student's t-test ($p = 1.2\times10^{-}$
1516 ^{4}). (H) Circular histograms of DR5 signal distribution (mean ± SD). (I) Circular histograms of TCS
1517 signal distribution (mean ± SD). For calculation of circular histograms, please see Figure 4
1518 legends and Materials and Methods. Sample size: WT mock, n = 11 buds; WT Torin2, n = 16
1519 buds. Scale bars in all micrographs, 25 µm.

1520 **Supplemental Figure 5. Translation of uORF-containing ARFs is not universally**
1521 **downregulated in *drmy1*, associated with Figure 5.**
1522 **(A)** *drmy1* has a lower protein-transcript ratio than WT for genes with at least 2 uORFs. 5,086
1523 transcript-protein pairs in our inflorescence dataset were grouped according to the maximum
1524 number of uORFs in all transcript isoforms (0, n = 3,485; 1, n = 874; ≥ 2, n = 724) (von Arnim et
1525 al., 2014). For each pair, protein-transcript ratio was calculated, log-transformed, and the
1526 difference between *drmy1* and WT was plotted. A negative value means this gene has less protein
1527 per transcript in *drmy1* than WT, and could indicate reduced translation or protein stability.
1528 Medians for each group: 0 uORF, -0.00367; 1 uORF, -0.00808; ≥ 2 uORFs, -0.0243. Asterisk
1529 show statistically significant difference from Group 0 in a Wilcoxon rank sum test ($p = 3.167\times10^{-}$
1530 ^{4}), while ns means no significant difference from Group 0 (p = 0.167).
1531 **(B-D)** There is no universal decrease in the expression of uORF-containing ARF reporters. (B)
1532 Transcript level of three activator *ARF*s (*ARF5*, *ARF6*, *ARF8*) and two repressor *ARF*s (*ARF3*,
1533 *ARF10*) in inflorescence RNA-seq (n = 3 per genotype). *ARF3*, *ARF5*, and *ARF6* contain
1534 uORFs before the main ORF, and *ARF8* and *ARF10* do not. Asterisk indicates statistically
1535 significant differences between WT and *drmy1* from DESeq2 output. p values: *ARF3*, p = 0.583;
1536 *ARF5*, p = 0.497; *ARF6*, p = 0.603; *ARF8*, p = 0.058; *ARF10* p = 0.019. (C) Transcriptional
1537 reporters for these ARFs in stage 2 buds of WT and *drmy1* (cyan, GFP or YFP; magenta,
1538 propidium iodide). Note that the *pARF3*, *pARF5*, and *pARF6* reporters contain the same uORFs
1539 as the genes, reflecting a combination of transcriptional and uORF regulations. Scale bars, 20
1540 µm. (D) Quantification of GFP intensity. Sample size: *pARF3* WT, n = 22; *pARF3 drmy1*, n = 25;
1541 *pARF5* WT, n = 22; *pARF5 drmy1*, n = 22; *pARF6* WT, n = 19; *pARF6 drmy1*, n = 28; *pARF8*
1542 WT, n = 25; *pARF8 drmy1*, n = 31; *pARF10* WT, n = 20; *pARF10 drmy1*, n = 29. Asterisks show
1543 statistically significant differences between WT and *drmy1* in Wilcoxon rank sum tests. p values:
1544 *pARF3*, p = 0.3797; *pARF5*, $p = 6.22\times10^{-5}$; *pARF6*, $p = 2.868\times10^{-13}$; *pARF8*, p = 0.5127;
1545 *pARF10* $p = 7.073\times10^{-14}$.

1546 **Supplemental Figure 6. Cytokinin signaling causes variability in mature sepal number and**
1547 **size in *drmy1*, associated with Figure 5.**
1548 Shown are top-view inflorescence images of WT (A), *arr1,10,12* (B), *wol* (C), *drmy1* (D), *drmy1*
1549 *arr1,10,12* (E), and *drmy1 wol* (F), with boxed areas of individual buds enlarged and shown on
1550 the right. In the enlarged views, blue arrowheads point to sepals of regular size, and red
1551 arrowheads point to sepals that are much smaller. Scale bars, 0.5 mm.
1552

1553 **Supplemental Figure 7. Investigating other mechanisms that may explain the observed**
1554 **changes in hormone signaling.**
1555 **(A)** Cytokinin abundance does not significantly change in *drmy1*. Shown is mean ± SD of levels
1556 of trans-zeatin (tZ), cis-Zeatin (cZ), N^6-(Δ^2-Isopentenyl)adenine (iP), trans-Zeatin riboside (tZR),
1557 cis-Zeatin riboside (cZR), and N^6-(Δ^2-Isopentenyl)adenosine (iPR) quantified by LC-MS in
1558 induced WT and *drmy1* inflorescences of *ap1 cal AP1-GR* background. Levels are normalized to
1559 the mean tZ level in WT. Sample size: n = 5 for WT; n = 6 for *drmy1*. ns, no significant difference
1560 between WT and *drmy1* in two-sided Wilcoxon rank sum tests. P-values: tZ, p = 0.2468; cZ, p =
1561 0.7922; iP, p = 0.2468; tZR, p = 0.1775; cZR, p = 0.6623; iPR, p = 0.6623.
1562 **(B)** Expression of cytokinin signaling components in WT vs *drmy1* inflorescences of *ap1 cal AP1-*
1563 *GR* background (from Supplemental Dataset 1).
1564 **(C-D)** The *ARR7-llama GFP-nes* reporter responds to externally applied cytokinin. Shown are
1565 GFP images of the same bud before (C) or after (D) 5 hours of 200 μM BAP treatment. Images
1566 are representative of n = 9 buds from two independent lines.
1567 **(E-H)** CHX (E-F) or AZD-8055 (G-H) treatments do not change the subcellular localization of GFP-
1568 nes. Images are representative of n = 10 buds (E), n = 9 buds (F), n = 10 buds (G), and n = 11
1569 buds (H). For (C-H), each image was brightened to reveal patterns of GFP distribution. A square
1570 region taken from the image containing 5-10 cells is enlarged and shown on the top right. Within
1571 the square, GFP intensity was quantified along the dotted line and plotted on the bottom right. X-
1572 axis, pixels (range 0-238). Y-axis, GFP intensity (smoothened by taking the average intensity of
1573 11-pixel neighborhoods; range 90-175 in gray value). Scale bars, 25 μm.
1574 **(I-J)** Response of *pAHP3::AHP3-GFP* (I) and *pUBQ10::mCherry-RCI2A* (J) to mock, CHX, and
1575 AZD-8055 treatments for 72 hours. Scale bars, 25 μm. For (I), images are representative of n =
1576 13 (mock), n = 15 (CHX), and n = 16 (AZD-8055) buds in two experiments. For (J), images are
1577 representative of n = 12 (mock), n = 9 (CHX), and n = 10 (AZD-8055) buds in two experiments.
1578 **(K-N)** The *ARR7-llama GFP-nes* construct partially rescues the mature sepal variability in *drmy1*.
1579 Shown are inflorescence images of WT (K), *ARR7-llama GFP-nes* (L), *drmy1* (M), and *drmy1*
1580 *ARR7-llama GFP-nes* (N). The boxed regions were enlarged and shown on the right of each
1581 panel. Note that while *drmy1* buds have normal-sized (blue arrowheads) and smaller (red
1582 arrowheads) sepals, some buds in *drmy1 ARR7-llama GFP-nes* have robustly sized sepals (N,
1583 middle) while others still show variability (N, right). Scale bars, 0.5 mm.
1584 **(O-P)** *drmy1* has decreased and disrupted pattern of DII degradation. **(O)** Representative images
1585 of WT and *drmy1* showing *DII-n3xVENUS* (cyan), *mDII-ntdTomato* (magenta), and merge. For
1586 ease of display, the *VENUS* channel was brightened 3 times relative to the *tdTomato* channel.
1587 Scale bars, 25 μm. **(P)** Quantification of VENUS/tdTomato ratio. A background of 6 gray value
1588 per pixel (determined in blank regions) were subtracted before calculation of ratios. Sample size:
1589 WT, n = 8 buds; *drmy1*, n = 19 buds. Asterisk shows statistically significant difference in a
1590 Wilcoxon rank sum test (p = 0.01335).
1591

1592 **Supplemental Dataset 1. Inflorescence RNA-seq and proteomics.**
1593
1594 **Supplemental Dataset 2. Unprocessed ribosome profiles.**
1595
1596 **Supplemental Dataset 3. Seedling RNA-seq.**
1597
1598 **Supplemental Dataset 4. Data used in graphs.**
1599
1600 **Supplemental Dataset 5. DNA sequences.**
1601

1602 **REFERENCES**

1603 1. Kaneko, K. (2007). Evolution of robustness to noise and mutation in gene expression
1604 dynamics. PLoS One *2*, e434. 10.1371/journal.pone.0000434.
1605 2. Lachowiec, J., Queitsch, C., and Kliebenstein, D.J. (2016). Molecular mechanisms
1606 governing differential robustness of development and environmental responses in plants.
1607 Ann. Bot. *117*, 795–809. 10.1093/aob/mcv151.
1608 3. Zabinsky, R.A., Mason, G.A., Queitsch, C., and Jarosz, D.F. (2019). It's not magic –
1609 Hsp90 and its effects on genetic and epigenetic variation. Semin. Cell Dev. Biol. *88*, 21–
1610 35. 10.1016/j.semcdb.2018.05.015.
1611 4. Waddington, C.H. (1942). Canalization of Development and the Inheritance of Acquired
1612 Characters. Nature *150*, 563–656.
1613 5. Twitty, V.C., and Schwind, J.L. (1931). The growth of eyes and limbs transplanted
1614 heteroplastically between two species of Amblystoma. J. Exp. Zool. *59*, 61–86.
1615 10.1002/jez.1400590105.
1616 6. Silber, S.J. (1976). Growth of Baby Kidneys Transplanted Into Adults. Arch. Surg. *111*,
1617 75–77. 10.1001/archsurg.1976.01360190077014.
1618 7. Summerbell, D., and Lewis, J.H. (1975). Time, place and positional value in the chick
1619 limb bud. J. Embryol. Exp. Morphol. *33*, 621–643. 10.1242/dev.33.3.621.
1620 8. Parker, J., and Struhl, G. (2020). Control of *Drosophila* wing size by morphogen range
1621 and hormonal gating. Proc. Natl. Acad. Sci. U. S. A. *117*, 31935–31944.
1622 10.1073/pnas.2018196117.
1623 9. Garelli, A., Gontijo, A.M., Miguela, V., Caparros, E., and Dominguez, M. (2012). Imaginal
1624 discs secrete insulin-like peptide 8 to mediate plasticity of growth and maturation.
1625 Science *336*, 579–582. 10.1126/science.1216735.
1626 10. Crickmore, M.A., and Mann, R.S. (2006). Hox control of organ size by regulation of
1627 morphogen production and mobility. Science *313*, 63–68. 10.1126/science.1128650.
1628 11. Recasens-Alvarez, C., Ferreira, A., and Milán, M. (2017). JAK/STAT controls organ size
1629 and fate specification by regulating morphogen production and signalling. Nat. Commun.
1630 *8*, 10–12. 10.1038/ncomms13815.
1631 12. Irish, V.F. (2008). The Arabidopsis petal: a model for plant organogenesis. Trends Plant
1632 Sci. *13*, 430–436. 10.1016/j.tplants.2008.05.006.
1633 13. Fenster, C.B., Armbruster, W.S., Wilson, P., Dudash, M.R., and Thomson, J.D. (2004).
1634 Pollination syndromes and floral specialization. Annu. Rev. Ecol. Evol. Syst. *35*, 375–403.
1635 10.1146/annurev.ecolsys.34.011802.132347.
1636 14. King, S., Beck, F., and Lüttge, U. (2004). On the mystery of the golden angle in
1637 phyllotaxis. Plant, Cell Environ. *27*, 685–695. 10.1111/j.1365-3040.2004.01185.x.
1638 15. Smith, R.S., Guyomarc'h, S., Mandel, T., Reinhardt, D., Kuhlemeier, C., and
1639 Prusinkiewicz, P. (2006). A plausible model of phyllotaxis. Proc. Natl. Acad. Sci. U. S. A.
1640 *103*, 1301–1306. 10.1073/pnas.0510457103.
1641 16. Besnard, F., Refahi, Y., Morin, V., Marteaux, B., Brunoud, G., Chambrier, P., Rozier, F.,
1642 Mirabet, V., Legrand, J., Lainé, S., et al. (2014). Cytokinin signalling inhibitory fields
1643 provide robustness to phyllotaxis. Nature *505*, 417–421. 10.1038/nature12791.
1644 17. Queitsch, C., Sangster, T.A., and Lindquist, S. (2002). Hsp90 as a capacitor of
1645 phenotypic variation. Nature *417*, 618–624. 10.1038/nature749.
1646 18. Rutherford, S.L., and Lindquist, S. (1998). Hsp90 as a capacitor for morphological
1647 evolution. Nature *396*, 336–342. 10.1038/24550.
1648 19. Lehner, B., Crombie, C., Tischler, J., Fortunato, A., and Fraser, A.G. (2006). Systematic
1649 mapping of genetic interactions in *Caenorhabditis elegans* identifies common modifiers of
1650 diverse signaling pathways. Nat. Genet. *38*, 896–903. 10.1038/ng1844.
1651 20. Levy, S.F., and Siegal, M.L. (2008). Network hubs buffer environmental variation in

1652 *Saccharomyces cerevisiae*. PLoS Biol. *6*, 2588–2604. 10.1371/journal.pbio.0060264.
1653 21. Folta, A., Severing, E.I., Krauskopf, J., van de Geest, H., Verver, J., Nap, J.P., and
1654 Mlynarova, L. (2014). Over-expression of Arabidopsis AtCHR23 chromatin remodeling
1655 ATPase results in increased variability of growth and gene expression. BMC Plant Biol.
1656 *14*, 76. 10.1186/1471-2229-14-76.
1657 22. Hintze, M., Katsanos, D., Shahrezaei, V., and Barkoulas, M. (2021). Phenotypic
1658 Robustness of Epidermal Stem Cell Number in *C. elegans* Is Modulated by the Activity of
1659 the Conserved N-acetyltransferase nath-10/NAT10. Front. Cell Dev. Biol. *9*, 640856.
1660 10.3389/fcell.2021.640856.
1661 23. Marygold, S.J., Roote, J., Reuter, G., Lambertsson, A., Ashburner, M., Millburn, G.H.,
1662 Harrison, P.M., Yu, Z., Kenmochi, N., Kaufman, T.C., et al. (2007). The ribosomal protein
1663 genes and Minute loci of *Drosophila melanogaster*. Genome Biol. *8*, R216. 10.1186/gb-
1664 2007-8-10-r216.
1665 24. Wang, S., Kurepa, J., and Smalle, J.A. (2009). The *Arabidopsis* 26S proteasome subunit
1666 RPN1a is required for optimal plant growth and stress responses. Plant Cell Physiol. *50*,
1667 1721–1725. 10.1093/pcp/pcp105.
1668 25. Gallois, J.L., Guyon-Debast, A., Lecureuil, A., Vezon, D., Carpentier, V., Bonhomme, S.,
1669 and Guerche, P. (2009). The *Arabidopsis* proteasome RPT5 subunits are essential for
1670 gametophyte development and show accession-dependent redundancy. Plant Cell *21*,
1671 442–459. 10.1105/tpc.108.062372.
1672 26. Hong, L., Dumond, M., Tsugawa, S., Sapala, A., Routier-Kierzkowska, A.L., Zhou, Y.,
1673 Chen, C., Kiss, A., Zhu, M., Hamant, O., et al. (2016). Variable Cell Growth Yields
1674 Reproducible Organ Development through Spatiotemporal Averaging. Dev. Cell *38*, 15–
1675 32. 10.1016/j.devcel.2016.06.016.
1676 27. Zhu, M., Chen, W., Mirabet, V., Hong, L., Bovio, S., Strauss, S., Schwarz, E.M.,
1677 Tsugawa, S., Wang, Z., Smith, R.S., et al. (2020). Robust organ size requires robust
1678 timing of initiation orchestrated by focused auxin and cytokinin signalling. Nat. Plants *6*,
1679 686–698. 10.1038/s41477-020-0666-7.
1680 28. Roeder, A.H.K. (2021). Arabidopsis sepals: A model system for the emergent process of
1681 morphogenesis. Quant. Plant Biol. *2*, e14. 10.1017/qpb.2021.12.
1682 29. Trinh, D.-C., Martin, M., Bald, L., Maizel, A., Trehin, C., and Hamant, O. (2023).
1683 Increased gene expression variability hinders the formation of regional mechanical
1684 conflicts leading to reduced organ shape robustness. Proc. Natl. Acad. Sci. *120*,
1685 e2302441120. 10.1073/pnas.2302441120.
1686 30. Jing, H., and Strader, L.C. (2019). Interplay of auxin and cytokinin in lateral root
1687 development. Int. J. Mol. Sci. *20*, 486. 10.3390/ijms20030486.
1688 31. Hussain, S., Nanda, S., Zhang, J., Rehmani, M.I.A., Suleman, M., Li, G., and Hou, H.
1689 (2021). Auxin and Cytokinin Interplay during Leaf Morphogenesis and Phyllotaxy. Plants
1690 *10*, 1732. 10.3390/plants10081732.
1691 32. Schaller, G.E., Bishopp, A., and Kieber, J.J. (2015). The yin-yang of hormones: Cytokinin
1692 and auxin interactions in plant development. Plant Cell *27*, 44–63.
1693 10.1105/tpc.114.133595.
1694 33. Ingargiola, C., Duarte, G.T., Robaglia, C., Leprince, A.S., and Meyer, C. (2020). The plant
1695 target of rapamycin: A conduc TOR of nutrition and metabolism in photosynthetic
1696 organisms. Genes (Basel). *11*, 1285. 10.3390/genes11111285.
1697 34. Scarpin, M.R., Leiboff, S., and Brunkard, J.O. (2020). Parallel global profiling of plant tor
1698 dynamics reveals a conserved role for LARP1 in translation. eLife *9*, e58795.
1699 10.7554/eLife.58795.
1700 35. Yu, H., Ito, T., Wellmer, F., and Meyerowitz, E.M. (2004). Repression of AGAMOUS-LIKE
1701 24 is a crucial step in promoting flower development. Nat. Genet. *36*, 157–161.
1702 10.1038/ng1286.

1703 36. Wellmer, F., Alves-Ferreira, M., Dubois, A., Riechmann, J.L., and Meyerowitz, E.M.
1704 (2006). Genome-wide analysis of gene expression during early *Arabidopsis* flower
1705 development. PLoS Genet. *2*, 1012–1024. 10.1371/journal.pgen.0020117.
1706 37. Smyth, D.R., Bowman, J.L., and Meyerowitz, E.M. (1990). Early flower development in
1707 Arabidopsis. Plant Cell *2*, 755–767. 10.1105/tpc.2.8.755.
1708 38. Goodman, C.A., and Hornberger, T.A. (2013). Measuring protein synthesis with SUnSET:
1709 A valid alternative to traditional techniques? Exerc. Sport Sci. Rev. *41*, 107–115.
1710 10.1097/JES.0b013e3182798a95.
1711 39. Van Hoewyk, D. (2016). Use of the non-radioactive SUnSET method to detect decreased
1712 protein synthesis in proteasome inhibited Arabidopsis roots. Plant Methods *12*, 20.
1713 10.1186/S13007-016-0120-Z.
1714 40. Scarpin, M.R., Busche, M., Martinez, R.E., Harper, L.C., Reiser, L., Szakonyi, D.,
1715 Merchante, C., Lan, T., Xiong, W., Mo, B., et al. (2023). An updated nomenclature for
1716 plant ribosomal protein genes. Plant Cell *35*, 640–643. 10.1093/plcell/koac333.
1717 41. Schepetilnikov, M., and Ryabova, L.A. (2018). Recent discoveries on the role of tor
1718 (Target of rapamycin) signaling in translation in plants. Plant Physiol. *176*, 1095–1105.
1719 10.1104/pp.17.01243.
1720 42. Scarpin, M.R., Simmons, C.H., and Brunkard, J.O. (2022). Translating across kingdoms:
1721 target of rapamycin promotes protein synthesis through conserved and divergent
1722 pathways in plants. J. Exp. Bot. *73*, 7016–7025. 10.1093/jxb/erac267.
1723 43. Brunkard, J.O. (2020). Exaptive Evolution of Target of Rapamycin Signaling in
1724 Multicellular Eukaryotes. Dev. Cell *54*, 142–155. 10.1016/j.devcel.2020.06.022.
1725 44. Battaglioni, S., Benjamin, D., Wälchli, M., Maier, T., and Hall, M.N. (2022). mTOR
1726 substrate phosphorylation in growth control. Cell *185*, 1814–1836.
1727 10.1016/j.cell.2022.04.013.
1728 45. Valvezan, A.J., and Manning, B.D. (2019). Molecular logic of mTORC1 signalling as a
1729 metabolic rheostat. Nat. Metab. *1*, 321–333. 10.1038/s42255-019-0038-7.
1730 46. Schepetilnikov, M., Kobayashi, K., Geldreich, A., Caranta, C., Robaglia, C., Keller, M.,
1731 and Ryabova, L.A. (2011). Viral factor TAV recruits TOR/S6K1 signalling to activate
1732 reinitiation after long ORF translation. EMBO J. *30*, 1343–1356. 10.1038/emboj.2011.39.
1733 47. Schepetilnikov, M., Dimitrova, M., Mancera-Martínez, E., Geldreich, A., Keller, M., and
1734 Ryabova, L.A. (2013). TOR and S6K1 promote translation reinitiation of uORF-containing
1735 mRNAs via phosphorylation of eIF3h. EMBO J. *32*, 1087–1102. 10.1038/emboj.2013.61.
1736 48. Schepetilnikov, M., Makarian, J., Srour, O., Geldreich, A., Yang, Z., Chicher, J.,
1737 Hammann, P., and Ryabova, L.A. (2017). GTPase ROP2 binds and promotes activation
1738 of target of rapamycin, TOR, in response to auxin. EMBO J. *36*, 886–903.
1739 10.15252/embj.201694816.
1740 49. Chen, G.H., Liu, M.J., Xiong, Y., Sheen, J., and Wu, S.H. (2018). TOR and RPS6
1741 transmit light signals to enhance protein translation in deetiolating Arabidopsis seedlings.
1742 Proc. Natl. Acad. Sci. U. S. A. *115*, 12823–12828. 10.1073/pnas.1809526115.
1743 50. Mancera-Martínez, E., Dong, Y., Makarian, J., Srour, O., Thiébeauld, O., Jamsheer, M.,
1744 Chicher, J., Hammann, P., Schepetilnikov, M., and Ryabova, L.A. (2021).
1745 Phosphorylation of a reinitiation supporting protein, RISP, determines its function in
1746 translation reinitiation. Nucleic Acids Res. *49*, 6908–6924. 10.1093/nar/gkab501.
1747 51. Dong, Y., Srour, O., Lukhovitskaya, N., Makarian, J., Baumberger, N., Galzitskaya, O.,
1748 Elser, D., Schepetilnikov, M., and Ryabova, L.A. (2023). Functional analogs of
1749 mammalian 4E-BPs reveal a role for TOR in global plant translation. Cell Rep. *42*,
1750 112892. 10.1016/j.celrep.2023.112892.
1751 52. Dasgupta, A., Camacho, R.A.U., Enganti, R., Cho, S.K., Tucker, L.L., Torreverde, J.S.,
1752 Abraham, P.E., and Arnim, A.G. von (2024). A phosphorylation-deficient ribosomal
1753 protein eS6 is largely functional in Arabidopsis thaliana, rescuing mutant defects from

1754 global translation and gene expression to photosynthesis and growth. Plant Direct *8*,
1755 e566. 10.1002/pld3.566.
1756 53. Xiong, Y., McCormack, M., Li, L., Hall, Q., Xiang, C., and Sheen, J. (2013). Glucose-TOR
1757 signalling reprograms the transcriptome and activates meristems. Nature *496*, 181–186.
1758 10.1038/nature12030.
1759 54. Riegler, S., Servi, L., Scarpin, M.R., Godoy Herz, M.A., Kubaczka, M.G., Venhuizen, P.,
1760 Meyer, C., Brunkard, J.O., Kalyna, M., Barta, A., et al. (2021). Light regulates alternative
1761 splicing outcomes via the TOR kinase pathway. Cell Rep. *36*, 109676.
1762 10.1016/j.celrep.2021.109676.
1763 55. Obomighie, I., Lapenas, K., Murphy, B.E., Bowles, A.M.C., Bechtold, U., and Prischi, F.
1764 (2021). The Role of Ribosomal Protein S6 Kinases in Plant Homeostasis. Front. Mol.
1765 Biosci. *8*, 636560. 10.3389/fmolb.2021.636560.
1766 56. Xiong, Y., and Sheen, J. (2012). Rapamycin and glucose-target of rapamycin (TOR)
1767 protein signaling in plants. J. Biol. Chem. *287*, 2836–2842. 10.1074/jbc.M111.300749.
1768 57. Moreau, M., Azzopardi, M., Clé ment, G., Dobrenel, T., Marchive, C., Renne, C., Martin-
1769 Magniette, M.L., Taconnat, L., Renou, J.P., Robaglia, C., et al. (2012). Mutations in the
1770 *Arabidopsis* homolog of LST8/GβL, a partner of the target of Rapamycin kinase, impair
1771 plant growth, flowering, and metabolic adaptation to long days. Plant Cell *24*, 463–481.
1772 10.1105/tpc.111.091306.
1773 58. Brunkard, J.O., Xu, M., Regina Scarpin, M., Chatterjee, S., Shemyakina, E.A., Goodman,
1774 H.M., and Zambryski, P. (2020). TOR dynamically regulates plant cell-cell transport. Proc.
1775 Natl. Acad. Sci. U. S. A. *117*, 5049–5058. 10.1073/pnas.1919196117.
1776 59. Menand, B., Desnos, T., Nussaume, L., Bergert, F., Bouchez, D., Meyer, C., and
1777 Robaglia, C. (2002). Expression and disruption of the *Arabidopsis TOR* (target of
1778 rapamycin) gene. Proc. Natl. Acad. Sci. U. S. A. *99*, 6422–6427.
1779 10.1073/pnas.092141899.
1780 60. Zhao, Z., Andersen, S.U., Ljung, K., Dolezal, K., Miotk, A., Schultheiss, S.J., and
1781 Lohmann, J.U. (2010). Hormonal control of the shoot stem-cell niche. Nature *465*, 1089–
1782 1092. 10.1038/nature09126.
1783 61. Yoshida, S., Mandel, T., and Kuhlemeier, C. (2011). Stem cell activation by light guides
1784 plant organogenesis. Genes Dev. *25*, 1439–1450. 10.1101/gad.631211.
1785 62. Du, F., Guan, C., and Jiao, Y. (2018). Molecular Mechanisms of Leaf Morphogenesis.
1786 Mol. Plant *11*, 1117–1134. 10.1016/j.molp.2018.06.006.
1787 63. Taylor-Teeples, M., Lanctot, A., and Nemhauser, J.L. (2016). As above, so below:
1788 Auxin's role in lateral organ development. Dev. Biol. *419*, 156–164.
1789 10.1016/j.ydbio.2016.03.020.
1790 64. Nishimura, T., Wada, T., Yamamoto, K.T., and Okada, K. (2005). The *Arabidopsis* STV1
1791 protein, responsible for translation reinitiation, is required for auxin-mediated gynoecium
1792 patterning. Plant Cell *17*, 2940–2953. 10.1105/tpc.105.036533.
1793 65. Zhou, F., Roy, B., and von Arnim, A.G. (2010). Translation reinitiation and development
1794 are compromised in similar ways by mutations in translation initiation factor eIF3h and the
1795 ribosomal protein RPL24. BMC Plant Biol. *10*, 193. 10.1186/1471-2229-10-193.
1796 66. Rosado, A., Li, R., Van De Ven, W., Hsu, E., and Raikhel, N. V. (2012). *Arabidopsis*
1797 ribosomal proteins control developmental programs through translational regulation of
1798 auxin response factors. Proc. Natl. Acad. Sci. U. S. A. *109*, 19537–19544.
1799 10.1073/pnas.1214774109.
1800 67. Cancé, C., Martin-Arevalillo, R., Boubekeur, K., and Dumas, R. (2022). Auxin response
1801 factors are keys to the many auxin doors. New Phytol. *235*, 402–419.
1802 10.1111/nph.18159.
1803 68. Kim, B.H., Cai, X., Vaughn, J.N., and Von Arnim, A.G. (2007). On the functions of the h
1804 subunit of eukaryotic initiation factor 3 in late stages of translation initiation. Genome Biol.

1805 *8*, R60. 10.1186/gb-2007-8-4-r60.
1806 69. Von Arnim, A.G., Jia, Q., and Vaughn, J.N. (2014). Regulation of plant translation by
1807 upstream open reading frames. Plant Sci. *214*, 1–12. 10.1016/j.plantsci.2013.09.006.
1808 70. Jones, B., Ljung, K., Gunnerås, S.A., Petersson, S. V., Tarkowski, P., Graham, N., May,
1809 S., Dolezal, K., and Sandberg, G. (2010). Cytokinin regulation of auxin synthesis in
1810 Arabidopsis involves a homeostatic feedback loop regulated via auxin and cytokinin
1811 signal transduction. Plant Cell *22*, 2956–2969. 10.1105/tpc.110.074856.
1812 71. Marhavý, P., Duclercq, J., Weller, B., Feraru, E., Bielach, A., Offringa, R., Friml, J.,
1813 Schwechheimer, C., Murphy, A., and Benková, E. (2014). Cytokinin controls polarity of
1814 PIN1-dependent Auxin transport during lateral root organogenesis. Curr. Biol. *24*, 1031–
1815 1037. 10.1016/j.cub.2014.04.002.
1816 72. Růzĭčka, K., Šimášková, M., Duclercq, J., Petrášek, J., Zažímalová, E., Simon, S., Friml,
1817 J., Van Montagu, M.C.E., and Benková, E. (2009). Cytokinin regulates root meristem
1818 activity via modulation of the polar auxin transport. Proc. Natl. Acad. Sci. U. S. A. *106*,
1819 4284–4289. 10.1073/pnas.0900060106.
1820 73. Müller, B., and Sheen, J. (2007). Advances in cytokinin signaling. Science *318*, 68–69.
1821 10.1126/science.1145461.
1822 74. Karunadasa, S.S., Kurepa, J., Shull, T.E., and Smalle, J.A. (2020). Cytokinin-induced
1823 protein synthesis suppresses growth and osmotic stress tolerance. New Phytol. *227*, 50–
1824 64. 10.1111/nph.16519.
1825 75. Szweykowska, A., Gwoidi, E., and Spychala, M. (1980). The Cytokinin Control of Protein
1826 Synthesis in Plants. In Metabolism and Molecular Activities of Cytokinins, J. Guern and C.
1827 Peaud-Lenoel, eds. (Springer-Verlag Berlin Heidelberg), pp. 212–217. 10.1007/978-3-
1828 642-68035-9.
1829 76. Woźny, A., and Gwóźdź, E.A. (1980). The effect of cytokinin on the polyribosome
1830 formation in cucumber cotyledons. Biochem. und Physiol. der Pflanz. *175*, 476–480.
1831 10.1016/s0015-3796(80)80032-1.
1832 77. Klyachko, N.L., Yakovleva, L.A., Shakirova, F.M., and Kulaeva, O.N. (1982). Cell-free
1833 translation of polyribosomes from detached pumpkin cotyledons: Effects of starvation and
1834 cytokinin. Biol. Plant. *24*, 374–380. 10.1007/BF02909106.
1835 78. Short, K.C., Tepfer, D.A., and Fosket, D.E. (1974). Regulation of polyribosome formation
1836 and cell division in cultured soybean cells by cytokinin. J. Cell Sci. *15*, 75–87.
1837 79. Brenner, W.G., and Schmülling, T. (2012). Transcript profiling of cytokinin action in
1838 *Arabidopsis* roots and shoots discovers largely similar but also organ-specific responses.
1839 BMC Plant Biol. *12*, 112. 10.1186/1471-2229-12-112.
1840 80. Kiba, T., Naitou, T., Koizumi, N., Yamashino, T., Sakakibara, H., and Mizuno, T. (2005).
1841 Combinatorial microarray analysis revealing Arabidopsis genes implicated in cytokinin
1842 responses through the His→Asp phosphorelay circuitry. Plant Cell Physiol. *46*, 339–355.
1843 10.1093/pcp/pci033.
1844 81. Černý, M., Kuklová, A., Hoehenwarter, W., Fragner, L., Novák, O., Rotková, G., Jedelský,
1845 P.L., Žáková, K., Šmehilová, M., Strnad, M., et al. (2013). Proteome and metabolome
1846 profiling of cytokinin action in Arabidopsis identifying both distinct and similar responses
1847 to cytokinin down- and up-regulation. J. Exp. Bot. *64*, 4193–4206. 10.1093/jxb/ert227.
1848 82. Cerný, M., Dycka, F., Bobál'Ová, J., and Brzobohatý, B. (2011). Early cytokinin response
1849 proteins and phosphoproteins of Arabidopsis thaliana identified by proteome and
1850 phosphoproteome profiling. J. Exp. Bot. *62*, 921–937. 10.1093/jxb/erq322.
1851 83. Miyawaki, K., Tarkowski, P., Matsumoto-Kitano, M., Kato, T., Sato, S., Tarkowska, D.,
1852 Tabata, S., Sandberg, G., and Kakimoto, T. (2006). Roles of Arabidopsis ATP/ADP
1853 isopentenyltransferases and tRNA isopentenyltransferases in cytokinin biosynthesis.
1854 Proc. Natl. Acad. Sci. U. S. A. *103*, 16598–16603. 10.1073/pnas.0603522103.
1855 84. Ren, B., Liang, Y., Deng, Y., Chen, Q., Zhang, J., Yang, X., and Zuo, J. (2009). Genome-

1856 wide comparative analysis of type-A Arabidopsis response regulator genes by
1857 overexpression studies reveals their diverse roles and regulatory mechanisms in
1858 cytokinin signaling. Cell Res. *19*, 1178–1190. 10.1038/cr.2009.88.
1859 85. Ferreira, F.J., and Kieber, J.J. (2005). Cytokinin signaling. Curr. Opin. Plant Biol. *8*, 518–
1860 525. 10.1016/j.pbi.2005.07.013.
1861 86. Kakimoto, T. (2003). Perception and Signal Transduction of Cytokinins. Annu. Rev. Plant
1862 Biol. *54*, 605–627. 10.1146/annurev.arplant.54.031902.134802.
1863 87. Jain, M., Tyagi, A.K., and Khurana, J.P. (2006). Molecular characterization and
1864 differential expression of cytokinin-responsive type-A response regulators in rice (*Oryza*
1865 *sativa*). BMC Plant Biol. *6*, 1. 10.1186/1471-2229-6-1.
1866 88. To, J.P.C., Haberer, G., Ferreira, F.J., Deruère, J., Mason, M.G., Schaller, G.E., Alonso,
1867 J.M., Ecker, J.R., and Kieber, J.J. (2004). Type-A Arabidopsis response regulators are
1868 partially redundant negative regulators of cytokinin signaling. Plant Cell *16*, 658–671.
1869 10.1105/tpc.018978.
1870 89. Kiba, T., Yamada, H., Sato, S., Kato, T., Tabata, S., Yamashino, T., and Mizuno, T.
1871 (2003). The type-A response regulator, ARR15, acts as a negative regulator in the
1872 cytokinin-mediated signal transduction in *Arabidopsis thaliana*. Plant Cell Physiol. *44*,
1873 868–874. 10.1093/pcp/pcg108.
1874 90. Acheampong, A.K., Shanks, C., Cheng, C.Y., Eric Schaller, G., Dagdas, Y., and Kieber,
1875 J.J. (2020). EXO70D isoforms mediate selective autophagic degradation of type-A ARR
1876 proteins to regulate cytokinin sensitivity. Proc. Natl. Acad. Sci. U. S. A. *117*, 27034–
1877 27043. 10.1073/pnas.2013161117.
1878 91. To, J.P.C., Deruère, J., Maxwell, B.B., Morris, V.F., Hutchison, C.E., Ferreira, F.J.,
1879 Schaller, G.E., and Kieber, J.J. (2007). Cytokinin regulates type-A Arabidopsis response
1880 regulator activity and protein stability via two-component phosphorelay. Plant Cell *19*,
1881 3901–3914. 10.1105/tpc.107.052662.
1882 92. Bothma, J.P., Norstad, M.R., Alamos, S., and Garcia, H.G. (2018). LlamaTags: A
1883 Versatile Tool to Image Transcription Factor Dynamics in Live Embryos. Cell *173*, 1810-
1884 1822.e16. 10.1016/j.cell.2018.03.069.
1885 93. Imamura, A., Yoshino, Y., and Mizuno, T. (2001). Cellular Localization of the Signaling
1886 Components of Arabidopsis His-to-Asp Phosphorelay. Biosci. Biotechnol. Biochem. *65*,
1887 2113–2117. 10.1271/bbb.65.2113.
1888 94. Lee, D.J., Kim, S., Ha, Y.M., and Kim, J. (2008). Phosphorylation of Arabidopsis
1889 response regulator 7 (ARR7) at the putative phospho-accepting site is required for ARR7
1890 to act as a negative regulator of cytokinin signaling. Planta *227*, 577–587.
1891 10.1007/s00425-007-0640-x.
1892 95. Buechel, S., Leibfried, A., To, J.P.C., Zhao, Z., Andersen, S.U., Kieber, J.J., and
1893 Lohmann, J.U. (2010). Role of A-type Arabidopsis Response Regulators in meristem
1894 maintenance and regeneration. Eur. J. Cell Biol. *89*, 279–284.
1895 10.1016/j.ejcb.2009.11.016.
1896 96. Xie, M., Chen, H., Huang, L., O'Neil, R.C., Shokhirev, M.N., and Ecker, J.R. (2018). A B-
1897 ARR-mediated cytokinin transcriptional network directs hormone cross-regulation and
1898 shoot development. Nat. Commun. *9*, 1604. 10.1038/s41467-018-03921-6.
1899 97. Mähönen, A.P., Bishopp, A., Higuchi, M., Nieminen, K.M., Kinoshita, K., Törmäkangas,
1900 K., Ikeda, Y., Oka, A., Kakimoto, T., and Helariutta, Y. (2006). Cytokinin signaling and its
1901 inhibitor AHP6 regulate cell fate during vascular development. Science *311*, 94–98.
1902 10.1126/science.1118875.
1903 98. Kieber, J.J., and Schaller, G.E. (2018). Cytokinin signaling in plant development.
1904 Development *145*, dev149344. 10.1242/dev.149344.
1905 99. Hwang, I., Chen, H.C., and Sheen, J. (2002). Two-component signal transduction
1906 pathways in Arabidopsis. Plant Physiol. *129*, 500–515. 10.1104/pp.005504.

1907 100. Feng, J., Wang, C., Chen, Q., Chen, H., Ren, B., Li, X., and Zuo, J. (2013). S-
1908 nitrosylation of phosphotransfer proteins represses cytokinin signaling. Nat. Commun. *4*,
1909 1529. 10.1038/ncomms2541.
1910 101. Zhang, W., To, J.P.C., Cheng, C.Y., Eric Schaller, G., and Kieber, J.J. (2011). Type-A
1911 response regulators are required for proper root apical meristem function through post-
1912 transcriptional regulation of PIN auxin efflux carriers. Plant J. *68*, 1–10. 10.1111/j.1365-
1913 313X.2011.04668.x.
1914 102. Abel, S., Nguyen, M.D., and Theologis, A. (1995). The *PS-IAA4/5-like* Family of Early
1915 Auxin-inducible mRNAs in *Arabidopsis thaliana*. J. Mol. Biol. *251*, 533–549.
1916 10.1006/jmbi.1995.0454.
1917 103. Park, J.Y., Kim, H.J., and Kim, J. (2002). Mutation in domain II of IAA1 confers diverse
1918 auxin-related phenotypes and represses auxin-activated expression of Aux/IAA genes in
1919 steroid regulator-inducible system. Plant J. *32*, 669–683. 10.1046/j.1365-
1920 313X.2002.01459.x.
1921 104. Abel, S., Oeller, P.W., and Theologis, A. (1994). Early auxin-induced genes encode
1922 short-lived nuclear proteins. Proc. Natl. Acad. Sci. U. S. A. *91*, 326–330.
1923 10.1073/pnas.91.1.326.
1924 105. Zenser, N., Ellsmore, A., Leasure, C., and Callis, J. (2001). Auxin modulates the
1925 degradation rate of Aux/IAA proteins. Proc. Natl. Acad. Sci. U. S. A. *98*, 11795–11800.
1926 10.1073/pnas.211312798.
1927 106. Worley, C.K., Zenser, N., Ramos, J., Rouse, D., Leyser, O., Theologis, A., and Callis, J.
1928 (2000). Degradation of Aux/IAA proteins is essential for normal auxin signalling. Plant J.
1929 *21*, 553–562. 10.1046/j.1365-313X.2000.00703.x.
1930 107. Ramos, J.A., Zenser, N., Leyser, O., and Callis, J. (2001). Rapid degradation of
1931 auxin/indoleacetic acid proteins requires conserved amino acids of domain II and is
1932 proteasome dependent. Plant Cell *13*, 2349–2360. 10.1105/tpc.13.10.2349.
1933 108. Figueiredo, M.R.A. de, and Strader, L.C. (2022). Intrinsic and extrinsic regulators of
1934 Aux/IAA protein degradation dynamics. Trends Biochem. Sci. *47*, 865–874.
1935 10.1016/j.tibs.2022.06.004.
1936 109. Liao, C.Y., Smet, W., Brunoud, G., Yoshida, S., Vernoux, T., and Weijers, D. (2015).
1937 Reporters for sensitive and quantitative measurement of auxin response. Nat. Methods
1938 *12*, 207–210. 10.1038/nmeth.3279.
1939 110. Radhakrishnan, S.K., Lee, C.S., Young, P., Beskow, A., Chan, J.Y., and Deshaies, R.J.
1940 (2010). Transcription Factor Nrf1 Mediates the Proteasome Recovery Pathway after
1941 Proteasome Inhibition in Mammalian Cells. Mol. Cell *38*, 17–28.
1942 10.1016/j.molcel.2010.02.029.
1943 111. Gladman, N.P., Marshall, R.S., Lee, K.H., and Vierstra, R.D. (2016). The proteasome
1944 stress regulon is controlled by a pair of NAC transcription factors in arabidopsis. Plant
1945 Cell *28*, 1279–1296. 10.1105/tpc.15.01022.
1946 112. Njomen, E., and Tepe, J.J. (2019). Proteasome Activation as a New Therapeutic
1947 Approach to Target Proteotoxic Disorders. J. Med. Chem. *62*, 6469–6481.
1948 10.1021/acs.jmedchem.9b00101.
1949 113. Anderson, R.T., Bradley, T.A., and Smith, D.M. (2022). Hyperactivation of the
1950 proteasome in Caenorhabditis elegans protects against proteotoxic stress and extends
1951 lifespan. J. Biol. Chem. *298*, 102415. 10.1016/j.jbc.2022.102415.
1952 114. Kandel, R., Jung, J., and Neal, S. (2024). Proteotoxic stress and the ubiquitin proteasome
1953 system. Semin. Cell Dev. Biol. *156*, 107–120. 10.1016/j.semcdb.2023.08.002.
1954 115. Quy, P.N., Kuma, A., Pierres, P., and Mizushima, N. (2013). Proteasome-dependent
1955 activation of mammalian target of rapamycin complex 1 (mTORC1) is essential for
1956 autophagy suppression and muscle remodeling following denervation. J. Biol. Chem. *288*,
1957 1125–1134. 10.1074/jbc.M112.399949.

116. Zhao, J., Zhai, B., Gygi, S.P., and Goldberg, A.L. (2015). MTOR inhibition activates overall protein degradation by the ubiquitin proteasome system as well as by autophagy. Proc. Natl. Acad. Sci. U. S. A. *112*, 15790–15797. 10.1073/pnas.1521919112.
117. Zhang, Y., Nicholatos, J., Dreier, J.R., Ricoult, S.J.H., Widenmaier, S.B., Hotamisligil, G.S., Kwiatkowski, D.J., and Manning, B.D. (2014). Coordinated regulation of protein synthesis and degradation by mTORC1. Nature *513*, 440–443. 10.1038/nature13492.
118. Zhao, J., Garcia, G.A., and Goldberg, A.L. (2016). Control of proteasomal proteolysis by mTOR. Nature *529*, E1–E2. 10.1038/nature16472.
119. Zhang, Y., and Manning, B.D. (2016). Zhang & Manning reply. Nature *529*, E2–E3. 10.1038/nature16473.
120. Rousseau, A., and Bertolotti, A. (2016). An evolutionarily conserved pathway controls proteasome homeostasis. Nature *536*, 184–189. 10.1038/nature18943.
121. Mills, E.W., and Green, R. (2017). Ribosomopathies: There's strength in numbers. Science *358*, eaan2755. 10.1126/science.aan2755.
122. Warren, A.J. (2018). Molecular basis of the human ribosomopathy Shwachman-Diamond syndrome. Adv. Biol. Regul. *67*, 109–127. 10.1016/j.jbior.2017.09.002.
123. Hawer, H., Mendelsohn, B.A., Mayer, K., Kung, A., Malhotra, A., Tuupanen, S., Schleit, J., Brinkmann, U., and Schaffrath, R. (2020). Diphthamide-deficiency syndrome: a novel human developmental disorder and ribosomopathy. Eur. J. Hum. Genet. *28*, 1497–1508. 10.1038/s41431-020-0668-y.
124. Armistead, J., Patel, N., Wu, X., Hemming, R., Chowdhury, B., Basra, G.S., Del Bigio, M.R., Ding, H., and Triggs-Raine, B. (2015). Growth arrest in the ribosomopathy, bowen-conradi syndrome, is due to dramatically reduced cell proliferation and a defect in mitotic progression. Biochim. Biophys. Acta - Mol. Basis Dis. *1852*, 1029–1037. 10.1016/j.bbadis.2015.02.007.
125. Zhou, C., Zang, D., Jin, Y., Wu, H., Liu, Z., Du, J., and Zhang, J. (2011). Mutation in ribosomal protein L21 underlies hereditary hypotrichosis simplex. Hum. Mutat. *32*, 710–714. 10.1002/humu.21503.
126. Dixon, M.J. (1995). Treacher Collins syndrome. J. Med. Genet. *32*, 806–808. 10.1136/jmg.32.10.806.
127. Gazda, H.T., Sheen, M.R., Vlachos, A., Choesmel, V., O'Donohue, M.F., Schneider, H., Darras, N., Hasman, C., Sieff, C.A., Newburger, P.E., et al. (2008). Ribosomal Protein L5 and L11 Mutations Are Associated with Cleft Palate and Abnormal Thumbs in Diamond-Blackfan Anemia Patients. Am. J. Hum. Genet. *83*, 769–780. 10.1016/j.ajhg.2008.11.004.
128. Oliver, E.R., Saunders, T.L., Tarlé, S.A., and Glaser, T. (2004). Ribosomal protein L24 defect in belly spot and tail (*Bst*), a mouse *Minute*. Development *131*, 3907–3920. 10.1242/dev.01268.
129. McGowan, K.A., Li, J.Z., Park, C.Y., Beaudry, V., Tabor, H.K., Sabnis, A.J., Zhang, W., Fuchs, H., De Angelis, M.H., Myers, R.M., et al. (2008). Ribosomal mutations cause p53-mediated dark skin and pleiotropic effects. Nat. Genet. *40*, 963–970. 10.1038/ng.188.
130. Oristian, D.S., Slooíman, L.G., Zhou, X., Wang, L., Farach-Carson, M.C., and Kirn-Safran, C.B. (2009). Ribosomal protein L29/HIP deficiency delays osteogenesis and increases fragility of adult bone in mice. J. Orthop. Res. *27*, 28–35. 10.1002/jor.20706.
131. Uechi, T., Nakajima, Y., Nakao, A., Torihara, H., Chakraborty, A., Inoue, K., and Kenmochi, N. (2006). Ribosomal protein gene knockdown causes developmental defects in zebrafish. PLoS One *1*, e37. 10.1371/journal.pone.0000037.
132. Marygold, S.J., Coelho, C.M.A., and Leevers, S.J. (2005). Genetic analysis of RpL38 and RpL5, two minute genes located in the centric heterochromatin of chromosome 2 of *Drosophila melanogaster*. Genetics *169*, 683–695. 10.1534/genetics.104.034124.
133. Lee, C.C., Tsai, Y.T., Kao, C.W., Lee, L.W., Lai, H.J., Ma, T.H., Chang, Y.S., Yeh, N.H., and Lo, S.J. (2014). Mutation of a Nopp140 gene *dao-5* alters rDNA transcription and

2009 increases germ cell apoptosis in *C. elegans*. Cell Death Dis. *5*, e1158.
2010 10.1038/cddis.2014.114.
2011 134. Ito, T., Kim, G.T., and Shinozaki, K. (2000). Disruption of an Arabidopsis cytoplasmic
2012 ribosomal protein S13-homologous gene by transposon-mediated mutagenesis causes
2013 aberrant growth and development. Plant J. *22*, 257–264. 10.1046/j.1365-
2014 313X.2000.00728.x.
2015 135. Horiguchi, G., Mollá-Morales, A., Pérez-Pérez, J.M., Kojima, K., Robles, P., Ponce, M.R.,
2016 Micol, J.L., and Tsukaya, H. (2011). Differential contributions of ribosomal protein genes
2017 to *Arabidopsis thaliana* leaf development. Plant J. *65*, 724–736. 10.1111/j.1365-
2018 313X.2010.04457.x.
2019 136. Zhao, H., Lü, S., Li, R., Chen, T., Zhang, H., Cui, P., Ding, F., Liu, P., Wang, G., Xia, Y.,
2020 et al. (2015). The Arabidopsis gene *DIG6* encodes a large 60S subunit nuclear export
2021 GTPase 1 that is involved in ribosome biogenesis and affects multiple auxin-regulated
2022 development processes. J. Exp. Bot. *66*, 6863–6875. 10.1093/jxb/erv391.
2023 137. Takagi, M., Absalon, M.J., McLure, K.G., and Kastan, M.B. (2005). Regulation of p53
2024 translation and induction after DNA damage by ribosomal protein L26 and nucleolin. Cell
2025 *123*, 49–63. 10.1016/j.cell.2005.07.034.
2026 138. Deisenroth, C., and Zhang, Y. (2010). Ribosome biogenesis surveillance: Probing the
2027 ribosomal protein-Mdm2-p53 pathway. Oncogene *29*, 4253–4260.
2028 10.1038/onc.2010.189.
2029 139. Warner, J.R., and McIntosh, K.B. (2009). How Common Are Extraribosomal Functions of
2030 Ribosomal Proteins? Mol. Cell *34*, 3–11. 10.1016/j.molcel.2009.03.006.
2031 140. Dutt, S., Narla, A., Lin, K., Mullally, A., Abayasekara, N., Megerdichian, C., Wilson, F.H.,
2032 Currie, T., Khanna-Gupta, A., Berliner, N., et al. (2011). Haploinsufficiency for ribosomal
2033 protein genes causes selective activation of p53 in human erythroid progenitor cells.
2034 Blood *117*, 2567–2576. 10.1182/blood-2010-07-295238.
2035 141. Danilova, N., Sakamoto, K.M., and Lin, S. (2008). Ribosomal protein S19 deficiency in
2036 zebrafish leads to developmental abnormalities and defective erythropoiesis through
2037 activation of p53 protein family. Blood *112*, 5228–5237. 10.1182/blood-2008-01-132290.
2038 142. Girardi, T., Vereecke, S., Sulima, S.O., Khan, Y., Fancello, L., Briggs, J.W., Schwab, C.,
2039 De Beeck, J.O., Verbeeck, J., Royaert, J., et al. (2018). The T-cell leukemia-associated
2040 ribosomal RPL10 R98S mutation enhances JAK-STAT signaling. Leukemia *32*, 809–819.
2041 10.1038/leu.2017.225.
2042 143. Ludwig, L.S., Gazda, H.T., Eng, J.C., Eichhorn, S.W., Thiru, P., Ghazvinian, R., George,
2043 T.I., Gotlib, J.R., Beggs, A.H., Sieff, C.A., et al. (2014). Altered translation of GATA1 in
2044 Diamond-Blackfan anemia. Nat. Med. *20*, 748–753. 10.1038/nm.3557.
2045 144. Khajuria, R.K., Munschauer, M., Ulirsch, J.C., Fiorini, C., Ludwig, L.S., McFarland, S.K.,
2046 Abdulhay, N.J., Specht, H., Keshishian, H., Mani, D.R., et al. (2018). Ribosome Levels
2047 Selectively Regulate Translation and Lineage Commitment in Human Hematopoiesis.
2048 Cell *173*, 90-103.e19. 10.1016/j.cell.2018.02.036.
2049 145. In, K., Zaini, M.A., Müller, C., Warren, A.J., Von Lindern, M., and Calkhoven, C.F. (2016).
2050 Shwachman-Bodian-Diamond syndrome (SBDS) protein deficiency impairs translation re-
2051 initiation from C/EBPα and C/EBPβ mRNAs. Nucleic Acids Res. *44*, 4134–4146.
2052 10.1093/nar/gkw005.
2053 146. Kondrashov, N., Pusic, A., Stumpf, C.R., Shimizu, K., Hsieh, A.C., Xue, S., Ishijima, J.,
2054 Shiroishi, T., and Barna, M. (2011). Ribosome-mediated specificity in Hox mRNA
2055 translation and vertebrate tissue patterning. Cell *145*, 383–397.
2056 10.1016/j.cell.2011.03.028.
2057 147. Deliu, L.P., Turingan, M., Jadir, D., Lee, B., Ghosh, A., and Grewal, S.S. (2022).
2058 Serotonergic neuron ribosomal proteins regulate the neuroendocrine control of
2059 Drosophila development. PLoS Genet. *18*, e1010371. 10.1371/journal.pgen.1010371.

148. Adams, K.W., and Cooper, G.M. (2007). Rapid turnover of Mcl-1 couples translation to cell survival and apoptosis. J. Biol. Chem. *282*, 6192–6200. 10.1074/jbc.M610643200.
149. Truckenbrodt, S., Viplav, A., Jähne, S., Vogts, A., Denker, A., Wildhagen, H., Fornasiero, E.F., and Rizzoli, S.O. (2018). Newly produced synaptic vesicle proteins are preferentially used in synaptic transmission. EMBO J. *37*, e98044. 10.15252/embj.201798044.
150. D'Agostino, I.B., Deruère, J., and Kieber, J.J. (2000). Characterization of the response of the Arabidopsis response regulator gene family to cytokinin. Plant Physiol. *124*, 1706–1717. 10.1104/pp.124.4.1706.
151. Bishopp, A., Help, H., El-Showk, S., Weijers, D., Scheres, B., Friml, J., Benková, E., Mähönen, A.P., and Helariutta, Y. (2011). A mutually inhibitory interaction between auxin and cytokinin specifies vascular pattern in roots. Curr. Biol. *21*, 917–926. 10.1016/j.cub.2011.04.017.
152. Sud, M., Fahy, E., Cotter, D., Azam, K., Vadivelu, I., Burant, C., Edison, A., Fiehn, O., Higashi, R., Nair, K.S., et al. (2016). Metabolomics Workbench: An international repository for metabolomics data and metadata, metabolite standards, protocols, tutorials and training, and analysis tools. Nucleic Acids Res. *44*, D463–D470. 10.1093/nar/gkv1042.
153. Mähönen, A.P., Bonke, M., Kauppinen, L., Riikonen, M., Benfey, P.N., and Helariutta, Y. (2000). A novel two-component hybrid molecule regulates vascular morphogenesis of the Arabidopsis root. Genes Dev. *14*, 2938–2943. 10.1101/gad.189200.
154. Sotta, N., Shantikumar, L., Sakamoto, T., Matsunaga, S., and Fujiwara, T. (2016). TPR5 is involved in directional cell division and is essential for the maintenance of meristem cell organization in *Arabidopsis thaliana*. J. Exp. Bot. *67*, 2401–2411. 10.1093/jxb/erw043.
155. Heisler, M.G., Ohno, C., Das, P., Sieber, P., Reddy, G. V., Long, J.A., and Meyerowitz, E.M. (2005). Patterns of auxin transport and gene expression during primordium development revealed by live imaging of the Arabidopsis inflorescence meristem. Curr. Biol. *15*, 1899–1911. 10.1016/j.cub.2005.09.052.
156. Müller, B., and Sheen, J. (2008). Cytokinin and auxin interaction in root stem-cell specification during early embryogenesis. Nature *453*, 1094–1097. 10.1038/nature06943.
157. Brackmann, K., Qi, J., Gebert, M., Jouannet, V., Schlamp, T., Grünwald, K., Wallner, E.S., Novikova, D.D., Levitsky, V.G., Agustí, J., et al. (2018). Spatial specificity of auxin responses coordinates wood formation. Nat. Commun. *9*, 875. 10.1038/s41467-018-03256-2.
158. Argyros, R.D., Mathews, D.E., Chiang, Y.H., Palmer, C.M., Thibault, D.M., Etheridge, N., Argyros, D.A., Mason, M.G., Kieber, J.J., and Schallera, G.E. (2008). Type B response regulators of Arabidopsis play key roles in cytokinin signaling and plant development. Plant Cell *20*, 2102–2116. 10.1105/tpc.108.059584.
159. Rademacher, E.H., Möller, B., Lokerse, A.S., Llavata-Peris, C.I., Van Den Berg, W., and Weijers, D. (2011). A cellular expression map of the *Arabidopsis AUXIN RESPONSE FACTOR* gene family. Plant J. *68*, 597–606. 10.1111/j.1365-313X.2011.04710.x.
160. Saerens, D., Pellis, M., Loris, R., Pardon, E., Dumoulin, M., Matagne, A., Wyns, L., Muyldermans, S., and Conrath, K. (2005). Identification of a universal VHH framework to graft non-canonical antigen-binding loops of camel single-domain antibodies. J. Mol. Biol. *352*, 597–607. 10.1016/j.jmb.2005.07.038.
161. Fujii, Y., and Kodama, Y. (2015). *In planta* comparative analysis of improved green fluorescent proteins with reference to fluorescence intensity and bimolecular fluorescence complementation ability. Plant Biotechnol. *32*, 81–87. 10.5511/plantbiotechnology.15.0120a.
162. Alamos, S., Reimer, A., Niyogi, K.K., and Garcia, H.G. (2021). Quantitative imaging of RNA polymerase II activity in plants reveals the single-cell basis of tissue-wide transcriptional dynamics. Nat. Plants *7*, 1037–1049. 10.1038/s41477-021-00976-0.

2111 163. Alexa, A., Rahnenführer, J., and Lengauer, T. (2006). Improved scoring of functional
2112 groups from gene expression data by decorrelating GO graph structure. Bioinformatics
2113 *22*, 1600–1607. 10.1093/bioinformatics/btl140.
2114 164. Mustroph, A., Juntawong, P., and Bailey-Serres, J. (2009). Isolation of Plant Polysomal
2115 mRNA by Differential Centrifugation and Ribosome Immunopurification Methods. In
2116 Methods in molecular biology (vol. 553) (Humana Press, a part of Springer
2117 Science+Business Media, LLC), pp. 109–126. 10.1007/978-1-60327-563-7_6.
2118 165. Gao, X., Wan, J., Liu, B., Ma, M., Shen, B., and Qian, S.B. (2015). Quantitative profiling
2119 of initiating ribosomes *in vivo*. Nat. Methods *12*, 147–153. 10.1038/nmeth.3208.
2120 166. Busche, M., Regina Scarpin, M., Hnasko, R., and Brunkard, J.O. (2021). TOR
2121 coordinates nucleotide availability with ribosome biogenesis in plants. Plant Cell *33*,
2122 1615–1632. 10.1093/plcell/koab043.
2123 167. Schindelin, J., Rueden, C.T., Hiner, M.C., and Eliceiri, K.W. (2015). The ImageJ
2124 ecosystem: An open platform for biomedical image analysis. Mol. Reprod. Dev. *82*, 518–
2125 529. 10.1002/mrd.22489.
2126 168. Schindelin, J., Arganda-Carreras, I., Frise, E., Kaynig, V., Longair, M., Pietzsch, T.,
2127 Preibisch, S., Rueden, C., Saalfeld, S., Schmid, B., et al. (2012). Fiji: An open-source
2128 platform for biological-image analysis. Nat. Methods *9*, 676–682. 10.1038/nmeth.2019.
2129 169. de Reuille, P.B., Routier-Kierzkowska, A.L., Kierzkowski, D., Bassel, G.W., Schüpbach,
2130 T., Tauriello, G., Bajpai, N., Strauss, S., Weber, A., Kiss, A., et al. (2015).
2131 MorphoGraphX: A platform for quantifying morphogenesis in 4D. eLife *4*, e05864.
2132 10.7554/eLife.05864.
2133 170. Schäfer, M., Brütting, C., Baldwin, I.T., and Kallenbach, M. (2016). High-throughput
2134 quantification of more than 100 primary- and secondary-metabolites, and phytohormones
2135 by a single solid-phase extraction based sample preparation with analysis by UHPLC-
2136 HESI-MS/MS. Plant Methods *12*, 30. 10.1186/s13007-016-0130-x.
2137 171. Kojima, M., Kamada-Nobusada, T., Komatsu, H., Takei, K., Kuroha, T., Mizutani, M.,
2138 Ashikari, M., Ueguchi-Tanaka, M., Matsuoka, M., Suzuki, K., et al. (2009). Highly
2139 sensitive and high-throughput analysis of plant hormones using ms-probe modification
2140 and liquid chromatographytandem mass spectrometry: An application for hormone
2141 profiling in oryza sativa. Plant Cell Physiol. *50*, 1201–1214. 10.1093/pcp/pcp057.
2142 172. Novák, O., Antoniadi, I., and Ljung, K. (2017). High-resolution cell-type specific analysis
2143 of cytokinins in sorted root cell populations of *Arabidopsis thaliana*. Methods Mol. Biol.
2144 *1497*, 231–248. 10.1007/978-1-4939-6469-7_1.
2145 173. R Core Team (2021). R: A language and environment for statistical computing. R
2146 Foundation for Statistical Computing, Vienna, Austria. URL https://www.R-project.org/.
2147 174. Wickham, H. (2009). ggplot2: Elegant Graphics for Data Analysis R. Gentleman, K.
2148 Hornik, and G. Parmigiani, eds. (Springer) 10.1007/978-0-387-98141-3.
2149 175. Perez-Riverol, Y., Bai, J., Bandla, C., García-Seisdedos, D., Hewapathirana, S.,
2150 Kamatchinathan, S., Kundu, D.J., Prakash, A., Frericks-Zipper, A., Eisenacher, M., et al.
2151 (2022). The PRIDE database resources in 2022: A hub for mass spectrometry-based
2152 proteomics evidences. Nucleic Acids Res. *50*, D543–D552. 10.1093/nar/gkab1038.
2153

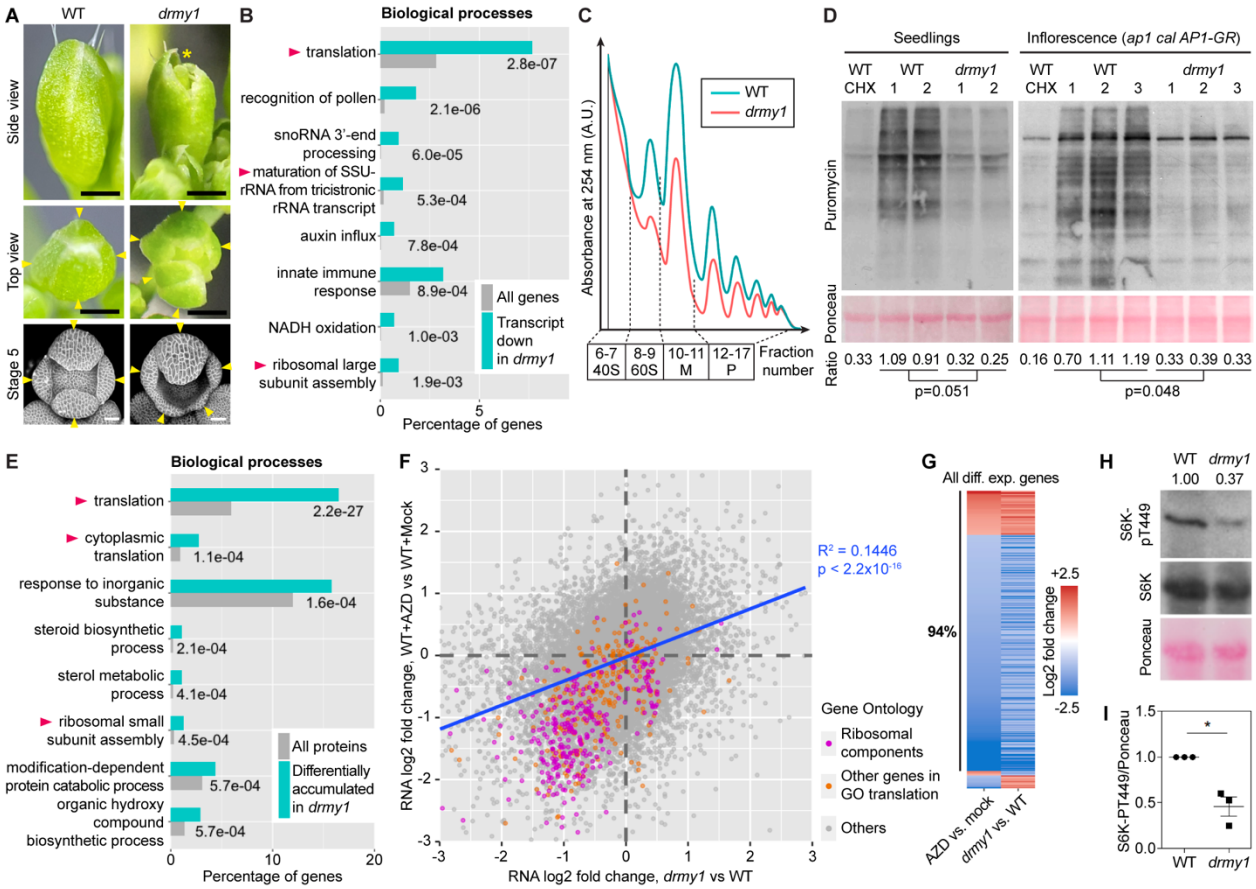

Figure 1. *drmy1* has reduced ribosome abundance, translation rate, and TOR activity.

(A) Top row, stage 12 buds of WT (left) and *drmy1* (right) viewed from the side. Asterisk shows the gap between sepals with petals and carpels exposed. Middle row, stage 12 buds of WT (left) and *drmy1* (right) viewed from the top. Arrowheads point to sepals. Note that the *drmy1* bud has 5 sepals of unequal size and unevenly spaced, exposing the stamens and carpels. Bottom row, stage 5 buds of WT (left) and *drmy1* (right) containing *35S::mCitrine-RCI2A* (plasma membrane marker). Arrowheads point to sepal primordia. Note that the *drmy1* bud has 5 sepal primordia of different sizes. Scale bars are 0.5 mm for stage 12 bud images and 25 µm for stage 5 bud images.

(B) Gene ontology (GO) enrichment of downregulated genes in *drmy1* compared to WT, in the *ap1 cal AP1-GR* background. Shown are the top 8 GO terms and their enrichment p-values. A complete list can be found in Supplemental Dataset 1. Arrowheads highlight terms related to ribosome biogenesis or translation.

(C) Polysomal profiles of WT (blue) and *drmy1* (red) in the *ap1 cal AP1-GR* background, representative of 3 biological replicates each. Additional replicates are in Supplemental Dataset 2. M, monosomes. P, polysomes.

(D) Puromycin labeling of WT vs *drmy1*. Left, WT and *drmy1* seedlings. From left to right: WT pre-treated with CHX, two biological replicates of WT pre-treated with mock, and two biological replicates of *drmy1* pre-treated with mock. All groups were then treated with puromycin. For seedlings to match in size, WT seedlings were 8 days old and *drmy1* seedlings were 10 days old.

Right, WT and *drmy1* inflorescences of induced *ap1 cal AP1-GR* background. From left to right: WT co-treated with puromycin and CHX, three biological replicates of WT treated with puromycin, and three biological replicates of *drmy1* treated with puromycin. In both experiments, RuBisCO large subunit on Ponceau S-stained membrane is shown as a loading control (bottom). Ratio between puromycin and Ponceau S signals, normalized by the mean of WT, is shown on the bottom (p-values are from two-sided Student's t-test).

(E) Gene ontology (GO) enrichment of differentially accumulated proteins in *drmy1* compared to WT, in the *ap1 cal AP1-GR* background. Shown are the top 8 GO terms and their enrichment p-values. A complete list can be found in Supplemental Dataset 1. Arrowheads highlight terms related to ribosome biogenesis or translation.

(F-G) Coherent alteration of gene expression by *drmy1* and AZD-8055 TOR inhibitor treatment. **(F)** Scatterplot of RNA log2 fold change in *drmy1* vs WT (x-axis), and WT+AZD vs WT+Mock (y-axis), in 7-day-old seedlings. Genes are color-coded based on the following categories: genes in "Structural constituents of the ribosome" (GO:0003735) and its offspring terms (magenta); all other genes in "Translation" (GO:0006412) and its offspring terms (orange); all other genes (gray). Blue line shows a linear regression of all points ($R^2 = 0.1446$, $p < 2.2\times10^{-16}$). **(G)** Of the 466 genes that are differentially expressed under both conditions, 439 (94%) are coherently altered by AZD-8055 treatment and the *drmy1* mutation.

(H-I) Phosphorylation of the direct TOR substrate, S6K-pT449, in WT and *drmy1*. **(H)** A representative blot. Top, S6K-pT449. Middle, total S6K protein. Bottom, Ponceau S staining. Ratio between S6K-pT449 signal and Ponceau S signal is shown above the blots. **(I)** Ratio between S6K-pT449 and Ponceau S signals normalized by WT, quantified across in three experiments, shows that TOR activity decreased by half in *drmy1*. (mean ± SD; *, $p<0.05$).

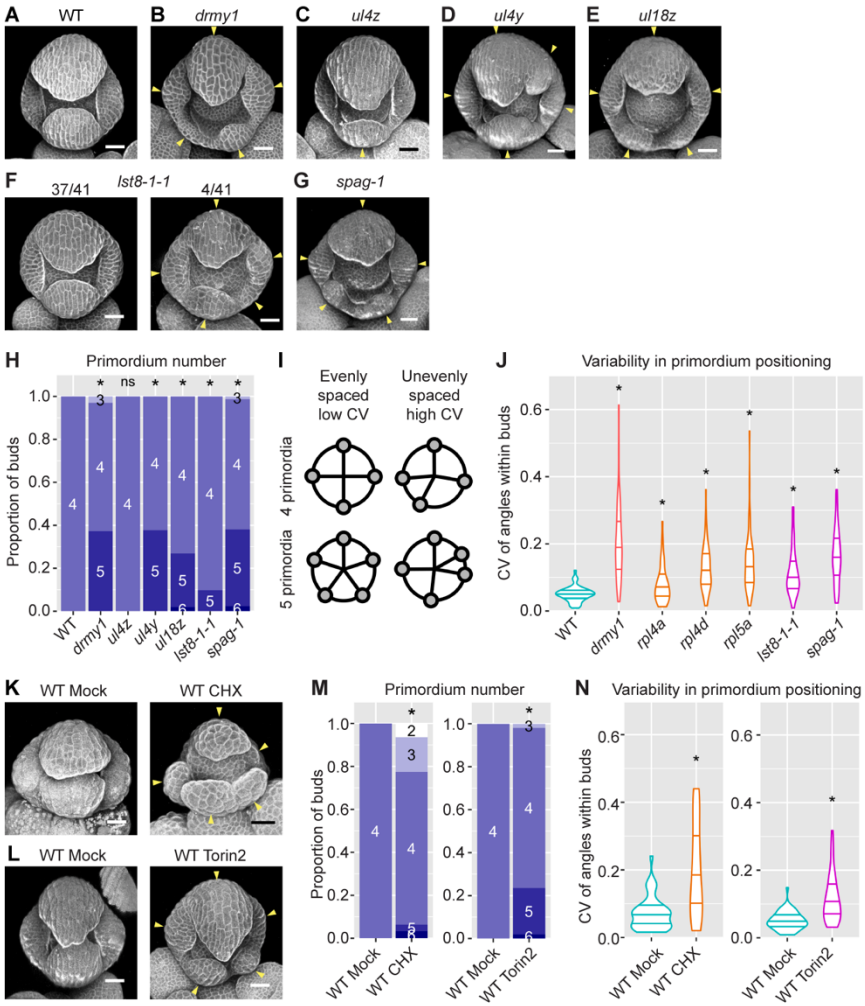

Figure 2. Defects in TOR activity, ribosome, and translation disrupt robust sepal initiation.
(A-G) Representative images of stage 5 buds in WT (A), *drmy1* (B), *ul4z* (C), *ul4y* (D), *ul18z* (E), *lst8-1-1* (F), and *spaghetti-1* (G). Tissue morphology is visualized by either propidium iodide (a cell wall-staining dye) or a plasma membrane marker. Arrowheads indicate sepal primordia that are variable in number, position, and size. Note that *ul4z* flowers always develop four sepal primordia, although of different sizes; *lst8-1-1* occasionally (4/41, 9.8%) develops buds with more than four sepal primordia.
(H) Quantification of sepal primordium number, comparing *drmy1* (n = 67 buds), *ul4z* (n = 52 buds), *ul4y* (n = 53 buds), *ul18z* (n = 52 buds), *lst8-1-1* (n = 41 buds), and *spaghetti-1* (n = 84 buds) with WT (n = 51 buds). Asterisks indicate statistically significant ($p < 0.05$) differences from WT in Fisher's contingency table tests.
(I) Illustration of robust versus variable positioning of sepal primordia. Primordia are considered robustly positioned if they are evenly distributed around the edge of the bud. Within each bud, angles between adjacent primordia with respect to the center of the bud are measured, and coefficient of variation (CV) is calculated. A bud with robustly positioned primordia would have similar angular values and a low CV value. A bud with variably positioned primordia would have very different angular values and a high CV value.

(J) Quantification of variability in primordium positioning (CV) in the same buds as in (H), following illustration in (I). Asterisks indicate statistically significant ($p < 0.05$) differences from WT in Wilcoxon's rank sum tests.
(K) Representative images of buds from *in vitro*-cultured WT inflorescences treated with mock or 2 μM CHX for 9-10 days. Arrowheads indicate sepal primordia that are variable in number, position, and size.
(L) Representative images of buds from WT plants treated with mock or 2 nmol Torin2 for 15 days. Arrowheads indicate sepal primordia that are variable in number, position, and size.
(M-N) Quantification of sepal primordium number (M) and positional variability (N) similar to (H,J), comparing CHX-treated (n = 31 buds), CHX-mock (n = 42 buds), Torin2-treated (n = 51 buds) and Torin2-mock buds (n = 56 buds). Scale bars in all micrographs, 25 μm.

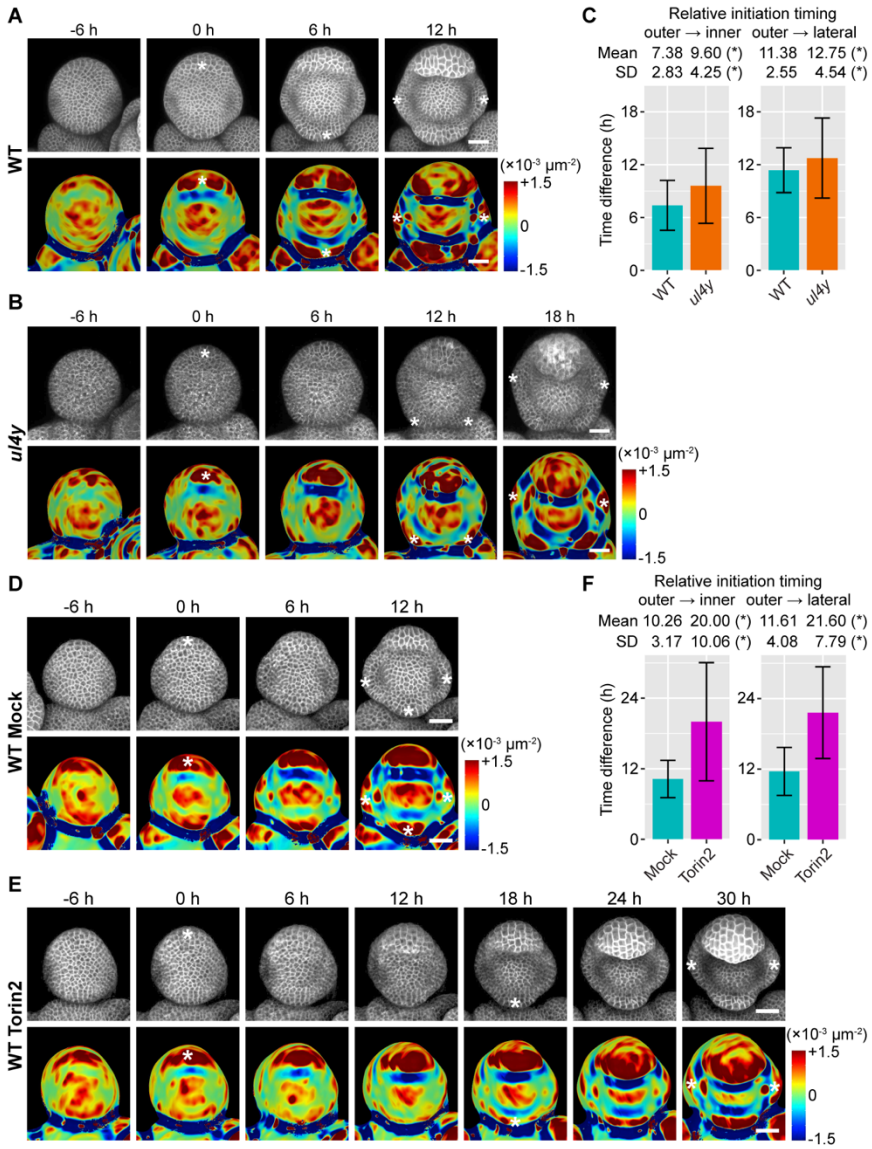

Figure 3. TOR and ribosomal defects cause variability in the timing of sepal initiation.
(A-C) 6h-interval live imaging of the sepal initiation process in WT (A) and *ul4y* (B), which is quantified in (C). n = 48 buds for WT; n = 40 buds for *ul4y*.
(D-F) 6h-interval live imaging of the sepal initiation process in buds from WT plants treated with mock or 2 nmol Torin2 twice a day for 15 days, which is quantified in (F). n = 31 buds for mock; n = 15 buds for Torin2.
In **(A,B,D,E)**, top rows show the *35S::mCitrine-RCI2A* membrane marker, and bottom rows show Gaussian curvature heatmaps of the same image stacks. Asterisks indicate sepal initiation events, defined as a dark red band (primordium with positive curvature) separated from the floral meristem by a dark blue band (boundary with negative curvature) in the heatmap. Scale bars, 25 µm.
In **(C,F)**, the amount of time between outer and inner sepal initiation (left) and between outer and lateral sepal initiation (right) were calculated for each bud. Bar plot shows mean ± SD which is

also shown on top of each plot. Asterisks indicate statistically significant differences ($p < 0.05$) in Wilcoxon's rank sum test (for mean) or Levene's test (for SD).

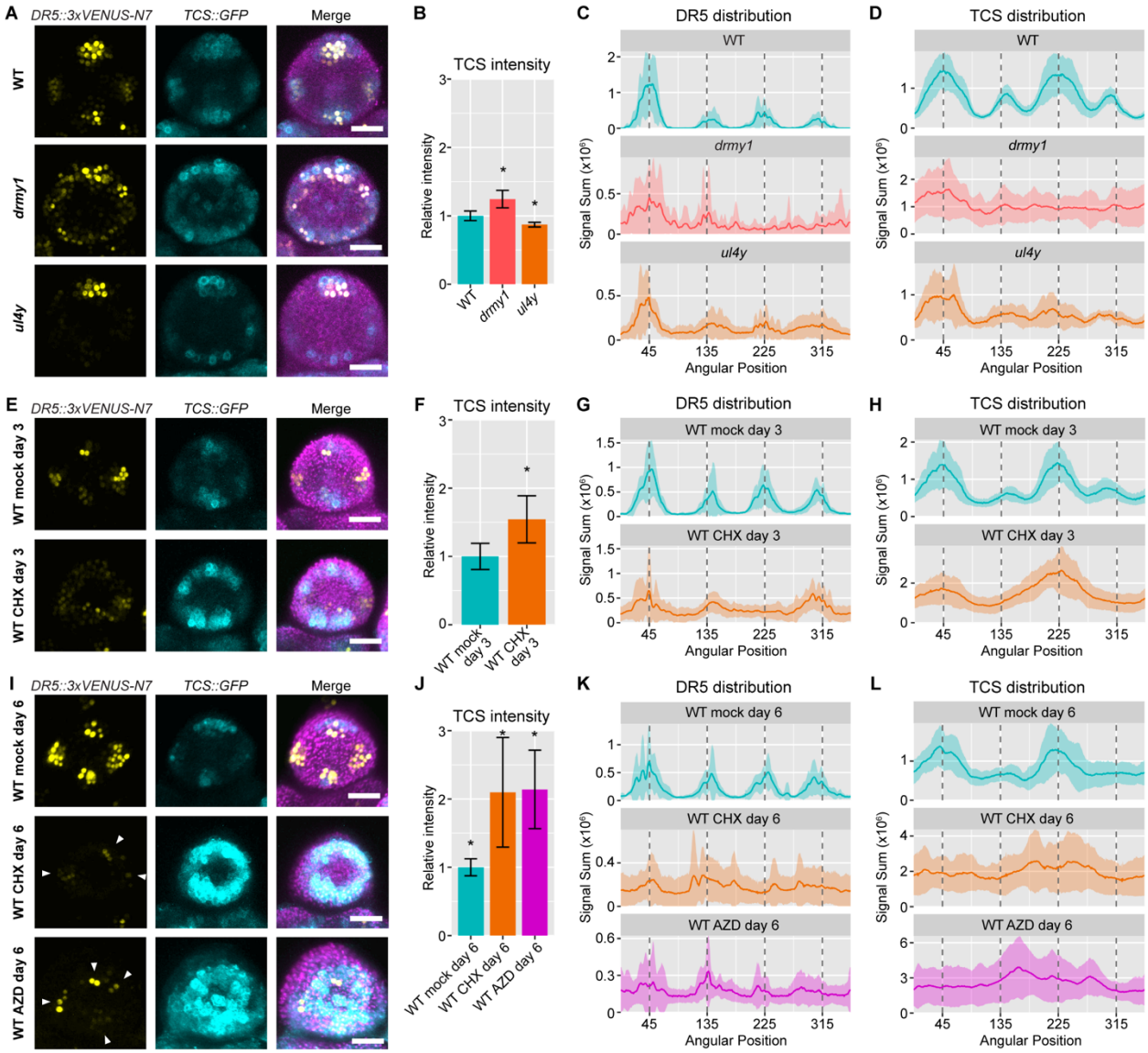

Figure 4. Inhibition of TOR activity and translation cause variability in auxin and cytokinin signaling.

(A-D) The ribosomal mutant *ul4y* loses robustness in auxin and cytokinin signaling. (A) Representative images of late stage 2 buds of WT, *drmy1*, and *ul4y*, showing the auxin signaling reporter *DR5::3xVENUS-N7* in yellow, the cytokinin signaling reporter *TCS::GFP* in cyan, and both merged with Chlorophyll (in WT) or *UBQ10::mCherry-RCI2A* (in *drmy1* and *ul4y*) in magenta. (B) Quantification of TCS intensity (integrated density divided by area) from maximum intensity projection images, normalized to mean of WT. Shown are mean ± SD. Asterisks show statistically significant differences from WT in two-tailed Student's t-tests (*drmy1*, $p = 2.1\times10^{-6}$; *ul4y*, $p = 3.4\times10^{-5}$). (C) Circular histogram of DR5 signal distribution. Each bud was divided into 360 sectors of 1° each. Within each sector, DR5 signal measured in pixel intensity units (0-255 range) was summed. This sum was plotted along the x-axis starting from the sector at 1:30 position (between the incipient outer sepal and incipient right sepal) going counterclockwise. I.e., in WT, the outer

sepal is near 45°, the inner sepal near 225°, and the lateral sepals near 45° and 135° (vertical dotted lines). The mean was plotted as a solid line, and mean ± SD was plotted as a shaded area. (D) Circular histogram of TCS signal distribution. Sample size for (A-D): WT, n = 12 buds; *drmy1*, n = 15 buds; *ul4y*, n = 10 buds.

(E-H) 3 days of translation inhibition causes increased and diffuse cytokinin signaling, and diffuse auxin signaling. (E) Representative images of late stage 2 WT buds treated *in vitro* with mock or 2 μM CHX for 3 days. Shown are *DR5::3xVENUS-N7* in yellow, *TCS::GFP* in cyan, and both merged with Chlorophyll in magenta. (F) Quantification of TCS intensity from maximum intensity projection images, normalized to mean of WT mock day 3. Shown are mean ± SD. Asterisk shows statistically significant difference in a two-tailed Student's t-test ($p = 2.0\times10^{-4}$). (G) Circular histogram of DR5 signal distribution. (H) Circular histogram of TCS signal distribution. Sample size for (E-H): WT mock day 3, n = 10 buds; WT CHX day 3, n = 12 buds.

(I-L) 6 days of TOR or translation inhibition causes increased and diffuse cytokinin signaling, and randomly positioned auxin signaling maxima. (I) Representative images of late stage 2 WT buds treated *in vitro* with mock, 2 μM CHX, or 2 μM AZD for 6 days. Shown are *DR5::3xVENUS-N7* in yellow, *TCS::GFP* in cyan, and both merged with Chlorophyll in magenta. Arrowheads point to randomly positioned auxin maxima. (J) Quantification of TCS intensity from maximum intensity projection images, normalized to mean of WT mock day 6. Shown are mean ± SD. Asterisks show statistically significant differences from mock in two-tailed Student's t-tests (CHX, $p = 1.0\times10^{-3}$; AZD, $p = 1.2\times10^{-4}$). (K) Circular histogram of DR5 signal distribution. (L) Circular histogram of TCS signal distribution. Sample size for (I-L): WT mock day 6, n = 12 buds; WT CHX day 6, n = 11 buds; WT AZD day 6, n = 10 buds. Scale bars in all micrographs, 25 μm.

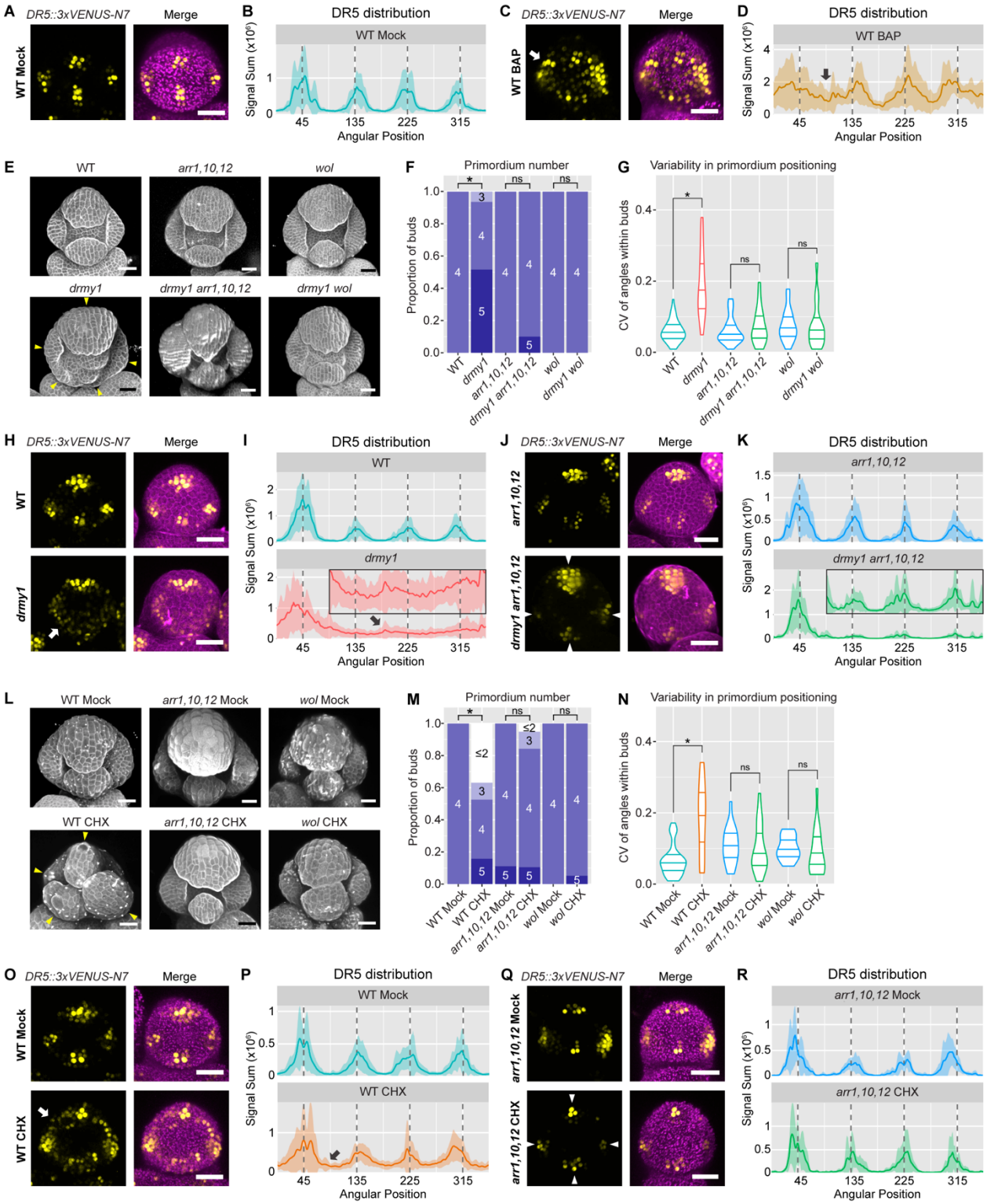

Figure 5. Cytokinin signaling is required for increased variability in auxin signaling and sepal initiation under translation inhibition.

(A-D) Cytokinin treatment makes auxin signaling diffuse. Shown are late stage 2 WT buds under mock (A,B) or 5 µM cytokinin (BAP) treatment (C,D) for 4 days. (A,C) Auxin signaling reporter

DR5 in yellow, and *DR5* merged with Chlorophyll in magenta. (B,D) Circular histograms of the *DR5* signal, showing mean (solid line) and mean ± SD (shaded area). Arrows point to DR5 signal in variable positions. Sample size: WT Mock n = 10, WT BAP n = 10. Also see Zhu et al. (2020), in this reference see Extended Data Figure 7e.

(E-G) Cytokinin signaling is required for variable sepal initiation in *drmy1*. (E) Stage 5 buds. Sepal primordia in *drmy1* are variable (arrowheads), which does not occur in *drmy1 arr1,10,12* and *drmy1 wol* mutants. (F,G) Quantification of sepal primordium number (F) and positional variability (G), comparing WT (n = 58) with *drmy1* (n = 31), *arr1,10,12* (n = 24) with *drmy1 arr1,10,12* (n = 20), and *wol* (n = 36) with *drmy1 wol* (n = 39). Asterisks indicate statistically significant ($p < 0.05$) differences in Fisher's contingency table tests (F) and Wilcoxon's rank sum tests (G) respectively.

(H-K) Cytokinin signaling is required for variable patterning of auxin signaling in *drmy1*. Shown are late stage 2 buds of WT vs *drmy1* (H,I), and *arr1,10,12* vs *drmy1 arr1,10,12* (J,K). (H,J) Auxin signaling reporter *DR5* in yellow, and *DR5* merged with propidium iodide in magenta. Arrows point to diffuse DR5 signal in variable positions of the *drmy1* bud. Arrowheads show four robust DR5 maxima in the *drmy1 arr1,10,12* bud. (I,K) Circular histograms of the *DR5* signal, showing mean (solid line) and mean ± SD (shaded area). For ease of visualization, circular histograms of *drmy1* and *drmy1 arr1,10,12* between 90 and 360 degrees are enlarged and shown as insets (y-axis range 0-0.4). Note the presence of DR5 signal in inter-sepal regions in *drmy1* (black arrow) which is largely suppressed in *drmy1 arr1,10,12*. Sample size: WT n = 19, *drmy1* n = 16, *arr1,10,12* n = 13, *drmy1 arr1,10,12* n = 9.

(L-N) Cytokinin signaling is required for variable sepal initiation under translation inhibition. (L) Stage 6 buds of WT, *arr1,10,12*, and *wol*, treated with Mock or 2 μM CHX for 10 days. WT initiates sepal primordia at variable positions when treated with CHX (arrowheads), which does not occur in *arr1,10,12* and *wol*. (M,N) Quantification of sepal primordium number (M) and positional variability (N), comparing mock and CHX within each genotype. Sample size: WT Mock n = 29, WT CHX n = 19, *arr1,10,12* Mock n = 18, *arr1,10,12* CHX n = 19, *wol* Mock n = 15, *wol* CHX n = 19. Asterisks indicate statistically significant ($p < 0.05$) differences in Fisher's contingency table tests (M) and Wilcoxon's rank sum tests (N) respectively.

(O-R) Cytokinin signaling is required for diffuse auxin signaling under translation inhibition. Shown are late stage 2 buds of WT (O,P) and *arr1,10,12* (Q,R), treated with Mock or 2 μM CHX for 3 days. (O,Q) Auxin signaling reporter *DR5* in yellow, and *DR5* merged with Chlorophyll in magenta. Arrows point to diffuse DR5 signal in variable positions in CHX-treated WT. Arrowheads show four robust DR5 maxima in CHX-treated *arr1,10,12*. (P,R) Circular histograms of the *DR5* signal, showing mean (solid line) and mean ± SD (shaded area). Sample size: WT Mock n = 17, WT CHX n = 18, *arr1,10,12* Mock n = 7, *arr1,10,12* CHX n = 7. Scale bars in all micrographs, 25 μm.

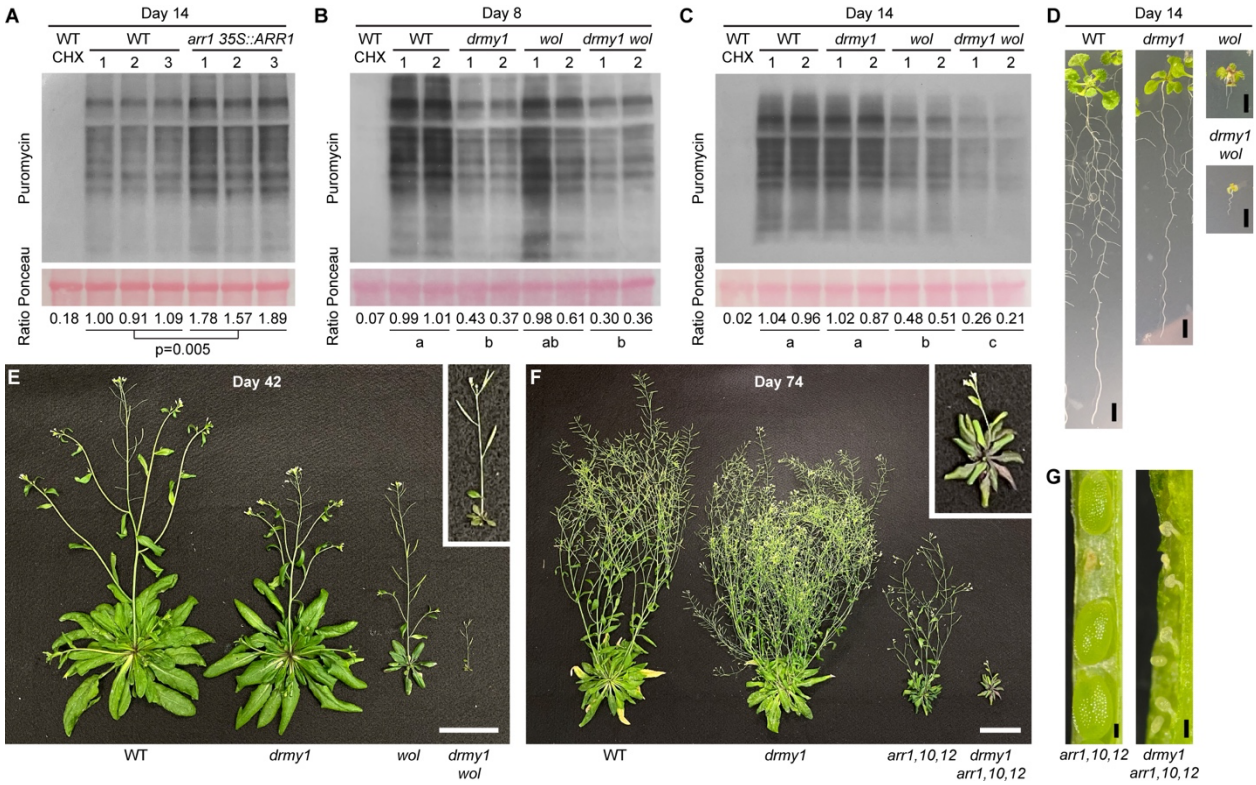

Figure 6. Upregulation of cytokinin signaling is required to maintain translation and fitness in *drmy1*.

(A) Puromycin labeling of WT seedlings with 4 h CHX pre-treatment (control), and three biological replicates each of WT and *arr1 35S::ARR1* seedlings with 4 h mock pre-treatment. All seedlings are 14 days old. RuBisCO large subunit in Ponceau S-stained membrane is shown as a loading control. Signal ratio between puromycin and Ponceau S, normalized to mean of WT, is show on the bottom. P-value is from a two-sided Student's t-test. Also see Karunadasa et al. (2020).

(B,C) Puromycin labeling of WT seedlings with 4 h CHX pre-treatment (control), and two biological replicates of WT, *drmy1*, *wol*, and *drmy1 wol* seedlings with 4 h mock pre-treatment. Seedlings are 8 days old in (B) and 14 days old in (C). RuBisCO large subunit in Ponceau S-stained membrane is shown as a loading control. Letters show compact letter display of a Tukey's all-pair comparison in a one-way ANOVA model.

(D) Representative 14 days old seedling images of WT, *drmy1*, *wol*, and *drmy1 wol* used in (C). Notice that *drmy1 wol* is very small and pale. Scale bars, 5 mm.

(E) Representative aerial part images of 42 days old plants of WT, *drmy1*, *wol*, and *drmy1 wol*. Inset shows the zoomed-in *drmy1 wol* plant, which has a tiny rosette and a short inflorescence. Scale bars, 5 cm. See also Figure S6F.

(F) Representative aerial part images of 74 days old plants of WT, *drmy1*, *arr1*,*10*,*12*, and *drmy1 arr1*,*10*,*12*. Inset shows the zoomed-in *drmy1 arr1*,*10*,*12* plant, which has pale leaves accumulating anthocyanin and a short inflorescence. Scale bars, 5 cm. See also Figure S6E.

(G) Dissected siliques of *arr1,10,12* (left) and *drmy1 arr1,10,12* (right) showing developing seeds. Notice that while *arr1,10,12* occasionally have aborted seeds, all seeds in the *drmy1 arr1,10,12* silique were aborted. Scale bars, 0.2 mm.

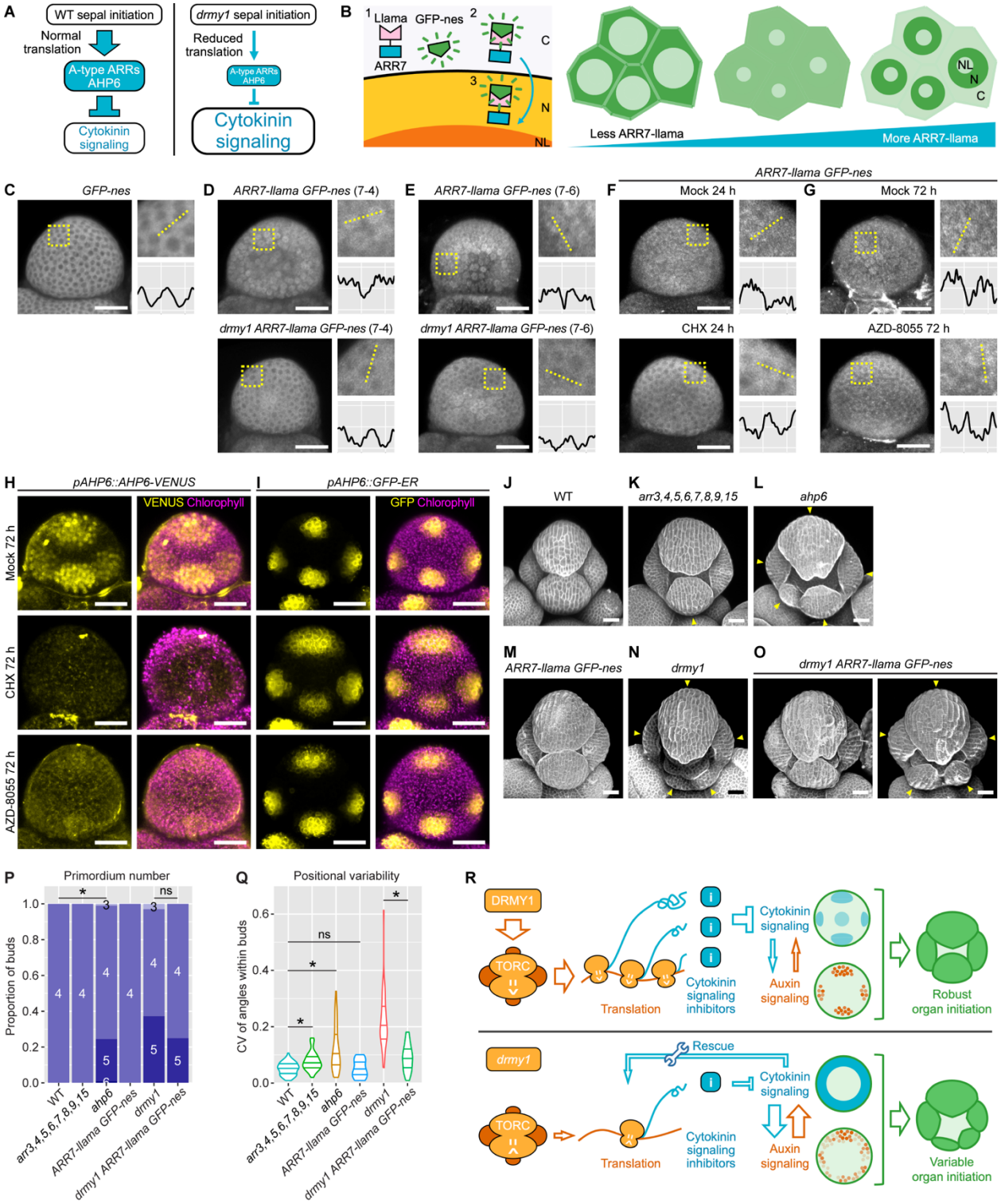

Figure 7. ARR7 and AHP6 protein levels are reduced upon inhibition of TOR and translation. **(A)** The hypothesis. During hormone patterning prior to sepal initiation in the WT floral meristem, A-type ARR and AHP6 proteins are rapidly produced to dampen cytokinin signaling to a normal

level. In *drmy1*, reduced protein synthesis causes reduced levels of these cytokinin signaling inhibitor proteins, resulting in an upregulation of cytokinin signaling.

(B) Illustration of Llama Tag. Plants were co-transformed with *ARR7-llama* (*pARR7::ARR7-linker-llama-ARR7ter*) and *GFP-nes* (*pUBQ10::sfGFP-nes-UBQ3ter*). Without ARR7-llama, GFP localizes to the cytosol due to the nuclear export sequence (nes). ARR7-llama is produced in the cytoplasm, C, and translocates into the nucleus, N. The Llama Tag on ARR7-llama binds to GFP and drags GFP into the nucleus (note that from our observation it is excluded from the nucleolus, NL). Thus, at low ARR7-llama levels, GFP signal is mainly in the cytoplasm. At intermediate ARR7-llama levels, GFP is at comparable levels between the cytoplasm and the nucleus, and no clear pattern can be seen. At high ARR7-llama levels, GFP is mainly seen in the nucleus.

(C) A *GFP-nes* bud showing localization of the GFP signal to the cytoplasm.

(D,E) GFP images of buds from two independent transgenic lines of *ARR7-llama GFP-nes*, 7-4 (D) and 7-6 (E), of WT (top) vs *drmy1* (bottom) genotypes. Images are representative of n = 17 (line 7-4, WT), n = 40 (line 7-4, *drmy1*), n = 9 (line 7-6, WT), and n = 6 (line 7-6, *drmy1*) buds. Note that GFP is more cytoplasm-localized in *drmy1* than WT, indicating reduced ARR7-llama protein level.

(F) GFP images of WT *ARR7-llama GFP-nes* buds treated with mock (top) or 2 μM CHX (bottom) for 24 hours. The mock image is representative of n = 20 buds from three independent lines. The CHX image is representative of n = 19 buds from these same lines.

(G) GFP images of WT *ARR7-llama GFP-nes* buds treated with mock (top) or 2 μM AZD-8055 (bottom) for 72 hours. The mock image is representative of n = 13 buds from two independent lines. The AZD-8055 image is representative of n = 11 buds from these same lines. For (C-G), each image was brightened to reveal subcellular localization patterns of GFP. A square region taken from the image containing 5-10 cells is enlarged and shown on the top right. Within the square, GFP intensity was quantified along the dotted line and plotted on the bottom right. X-axis, pixels (range 0-238). Y-axis, GFP intensity (smoothened by taking the average intensity of 11-pixel neighborhoods; range 90-210 in gray value).

(H-I) Response of the AHP6 protein reporter (H) and transcriptional reporter (I) to mock, CHX, and AZD-8055 treatments for 72 hours. For (H), images are representative of n = 29 (mock), n = 29 (CHX), and n = 34 (AZD-8055) buds in three experiments. For (I), images are representative of n = 11 (mock), n = 9 (CHX), and n = 12 (AZD-8055) buds in two experiments.

(J-Q) Reduction of A-type ARR and AHP6 protein levels contribute to the variability in sepal initiation. (J-O) Stage 5-6 buds of indicated genotype stained with propidium iodide. Arrowheads indicate sepal primordia that are variable in number, position, and/or size. Note that the *arr3,4,5,6,7,8,9,15* bud has an inner sepal that is slightly smaller than its outer sepal and positioned slightly right-skewed (K). The *ahp6* bud develops five sepal primordia of variable sizes and unevenly positioned (L). The *ARR7-llama GFP-nes* constructs partially rescue the *drmy1* phenotype in some buds (O, left) but not others (O, right). (P) Quantification of sepal primordium number. Asterisk indicates statistically significance difference in a Fisher's exact test (WT vs *ahp6*, $p = 3.026\times10^{-7}$; *drmy1* vs *drmy1 ARR7-llama GFP-nes*, p = 0.4389). (Q) Quantification of variability in sepal primordium position. Asterisk indicates statistically significant difference in a Wilcoxon rank sum test (WT vs. arr3,4,5,6,7,8,9,15, $p = 2.948\times10^{-4}$; WT vs *ahp6*, p = 2.137×10^{-}

242 [11]; WT vs *ARR7-llama GFPnes*, p = 1; *drmy1* vs *drmy1 ARR7-llama GFPnes*, p = 1.538×10^{-7}).
243 Data for *drmy1* were reused from Figure 2H, 2J. Data for *ARR7-llama GFP-nes* and *drmy1 ARR7-*
244 *llama GFP-nes* were pooled from two independent lines (7-4 and 7-6). Sample size: WT, n = 78;
245 *arr3,4,5,6,7,8,9,15*, n = 28; *ahp6*, n = 106; *ARR7-llama GFPnes*, n = 16; *drmy1*, n = 67; *drmy1*
246 *ARR7-llama GFP-nes*, n = 20.
247 **(R)** Working model. In WT, DRMY1 maintains TOR activity and translation, which sustains the
248 rapid production of cytokinin signaling inhibitors (ARR7 and AHP6) in response to cytokinin
249 signaling. These inhibitors maintain cytokinin signaling at a normal level, allowing auxin and
250 cytokinin signaling to interact and form robust spatial patterns. Robust patterning of auxin and
251 cytokinin signaling gives rise to robustly initiated sepal primordia. In *drmy1*, due to decreased
252 TOR signaling and translation rate, the meristem cannot rapidly produce cytokinin signaling
253 inhibitor proteins in response to cytokinin signaling. As a result, cytokinin signaling is upregulated,
254 which rescues the translation rate reduction in a homeostatic mechanism. This upregulation of
255 cytokinin signaling disrupts the robust spatial pattern of both cytokinin and auxin signaling, which
256 in turn causes variability in sepal initiation. Scale bars in all micrographs, 25 μm.
257